UNIVERSITY OF CAPE TOWN

MASTER'S DISSERTATION

Single-Fluid Approach to Modeling Dark Matter and Dark Energy

Author:

Vineshree PILLAY

Supervisor:

Prof. Peter DUNSBY

Co-supervisor:

Prof. Orlando LUONGO

A thesis submitted in fulfilment of the requirements

for the degree of Masters dissertation

in the

Cosmology and Gravity Group

Department of Mathematics and Applied Mathematics

5th June 2024

Declaration of Authorship

I, Vineshree PILLAY, hereby declare that the work on which this dissertation is based is my original work (except where acknowledgements indicate otherwise) and that neither the whole work nor any part of it has been, is being, or is to be submitted for another degree in this or any other university.

- I empower the university to reproduce for the purpose of research either the whole or any portion of the contents in any manner whatsoever.
- Where I have consulted the published work of others, this is always clearly attributed.
- Where I have quoted from the work of others, the source is always given. With the exception of such quotations, this dissertation is entirely my own work.
- I have acknowledged all main sources of help.

Signed: Signed by candidate

Date: 15/02/2024

UNIVERSITY OF CAPE TOWN

Abstract

Faculty of Science

Department of Mathematics and Applied Mathematics

Masters dissertation

Single-Fluid Approach to Modeling Dark Matter and Dark Energy

by Vineshree PILLAY

Cosmological observations over the past decades have provided overwhelming evidence for the existence of dark energy, a mysterious and dominant component responsible for the accelerated expansion of the universe. The nature of dark energy remains one of the most intriguing puzzles in modern cosmology. This dissertation presents a comprehensive investigation into the class of Unified Dark Energy Models (UDE), which offer a novel approach to understanding the nature of dark energy by unifying it with other cosmic components, in our case dark matter. The first part of this work reviews the theoretical background and observational evidence for dark energy, highlighting the challenges posed by the cosmological constant and other early models. Next, we present an in-depth analysis of various Unified Dark Energy Models proposed in the literature. The Generalized Chaplygin gas and the Logotropic model. Furthermore, we explore the impact of Unified Dark Energy Models on the large-scale structure of the universe and its evolution at the perturbed level. Following this review we look at a newly proposed equation of state "The Murnaghan equation of state" which accounts for both pressure and matter in the early universe, and exhibits Chaplygin-like behaviour in the later universe. The findings of this study contribute significantly to our understanding of dark energy and its interactions with other cosmic components.

Acknowledgements

The completion of my master's program would not have been possible without the support of the National Astrophysics and Space Science Program (NASSP), especially Prof. Saalih Allie, who made this process seamless and provided me with clarity and reassurance in replying to my sometimes panicked emails. I also thank my academic supervisor, Prof. Peter Dunsby, and co-supervisor, Prof. Orlando Luongo, for their unwavering support and dedication over the past few years. Despite encountering some obstacles along the way, they remained patient with me, for which I am forever grateful. Working with such passionate and caring supervisors has been a pleasure. Additionally, I extend my gratitude to the UCT Cosmology and Gravity group in room 1.10 for their insightful discussions and assistance throughout this journey, even during moments of procrastination. I've been lucky to be surrounded by peers who I can now call my friends.

I would not have been afforded this opportunity without the support from my family, particularly my mom who supported me during my undergraduate studies. To my friends, especially Wanga, for their support in constantly keeping me going and assuring me of my abilities. Finally, I thank my father who spurred on my pursuit for studying astrophysics.

Contents

List of Abbreviations

CMB	**C**osmic **M**icrowave **B**ackground
LHC	**L**arge **H**adron **C**ollider
MOND	**MO**dified **N**ewtonian **D**ynamics
CG	**C**haplygin **G**as
GCG	**G**eneralized **C**haplygin **G**as
FLRW	**F**riedmann **L**emaître **R**obertson **W**alker
GR	**G**eneral **R**elativity
DF	**D**ark **F**luid
DM	**D**ark **M**atter
DE	**D**ark **E**nergy
SC	**S**pherical **C**ollapse model
EoS	**E**quation **o**f **S**tate
LDF	**L**ogotropic **D**ark **F**luid
UDE	**U**nified **D**ark **E**nergy
A-S	**A**nton-**S**chmidt
MDF	**M**urnaghan **D**ark **F**luid
MDE	**M**urnaghan **D**ark **E**nergy
CLASS	the **C**osmic **L**inear **A**nisotropy **S**olving **S**ystem
CAMB	**C**ode for **A**nisotropies in the **M**icrowave **B**ackground

System of Units and Constants

Speed of light	$c = 299792458$ m s^{-1} [1]	1 [2]
Reduced Planck constant	$\hbar = 1.054571817 \times 10^{-34}$ J s [1]	1 [2]
Boltzmann constant	$k_B = 1.380649 \times 10^{-23}$ J K^{-1} [1]	1 [2]
Gravitational constant	$G = 6.67430 \times 10^{-11}$ m^3 g^{-1} s^{-2} [1]	6.7088×10^{-39} (GeV)$^{-2}$
Planck mass	$m_{Pl} = \frac{1}{\sqrt{G}}$	1.2211×10^{19} GeV
Planck length	$l_{Pl} = \frac{1}{m_{Pl}}$	8.1893×10^{-20} (GeV)$^{-1}$
Einsteins gravitational constant	$\kappa = \sqrt{8\pi G}$	4.1057×10^{-19} GeV
Reduced Planck mass	$M_{Pl} = \frac{1}{\kappa}$	2.4357×10^{18} GeV
Dimensionless Hubble constant	$h = 0.674 \pm 0.05$	[3, 4, 5]
Hubble constant	$H_0 = 100h$ km s^{-1} Mpc^{-1}	$2.1332h \times 10^{-42}$ GeV
Conversion Mpc to ly	1 Mpc $= 3.0856 \times 10^{24}$ cm	3.2615×10^6 light years
Conversion fm to GeV	1 fm $= 1 \times 10^{-13}$cm	5.068 (GeV)$^{-1}$
Dimensionless critical density	$\rho_c = \frac{3H_0^2}{8\pi G}$	3.7158×10^{-47}
Dark energy density	$\Omega_{de,0} = 0.679 \pm 0.013$	[3, 5]
Cold dark matter density	$\Omega_{dm,0} = 0.1206 \pm 0.0012$	[3, 5]
Baryon density	$\Omega_{b,0} = 0.02212 \pm 0.00022$	[3, 5]
Matter density	$\Omega_{m,0} = 0.1434 \pm 0.0020$	[3, 5]

Chapter 1

Introduction

Over the past few decades, cosmologists and astrophysicists have made great strides in understanding the fundamental properties that make up our universe. Despite these advancements, two of the most perplexing puzzles in modern cosmology remain: the mystery of dark matter and dark energy. While dark matter is thought to be responsible for the observed gravitational effects on small and large-scale structures, the acceleration of the expansion of the universe is attributed to an unknown force dubbed "dark energy". The introductory chapter that follows discusses the history and motivations behind postulating the existence of dark matter and dark energy, and explores the observational effects produced by these phenomena.

1.1 Background

Gravitational effects are essential in understanding the relationship between structure formation and the space in which it occurs; General Relativity (GR) provides the framework to describe this interplay. Dark matter, an invisible form of matter, is found surrounding both small-scale and large-scale cosmic structures. It forms extended regions known as dark matter halos around galaxies and is also present within cosmic voids. This unexpected gravitational phenomenon has profound implications for our understanding of the universe's structure and evolution. Below, we will explore the observational evidence implying flat rotation curves of galaxies and gravitational lensing on cosmological scales, providing the motivation for dark matter.

In 1933, Fritz Zwicky observed the Coma cluster, specifically the redshift of galaxies and proposed that dark matter might dominate the sum of the mass found in the universe [6]. He deduced that the average velocity was one order of magnitude larger than expected, which would make the system unstable. This observation was confirmed by [7] in their study of spiral galaxies. In a seminal paper, scholars [8, 7] examined the radius where the rotation curve was anticipated to reach its maximum, based on an exponential disk with a scaled fit to the observed 21cm line. They discovered that M33

peaked at a larger radius than anticipated. These findings prompted the conjecture that there must exist some form of non-visible matter that cannot be directly detected, as depicted in Figure 1.1.

One fundamental observation that modern astronomers make is that stars in spiral galaxies follow nearly circular orbits around the galaxy's core, where most of the mass is concentrated. According to Newton's Inverse Square Law [9], the orbital speed of objects decreases as their distance from the center of mass they orbit increases. However, further observations show that the rotation curve of galaxies flattens out as we move away from the center, which contradicts the prediction made by Keplerian motion. This phenomenon, known as flat rotation curves is illustrated in Figure 1.1 and shows the increase/constant in the orbital speed. The increase in orbital speed implies that there is

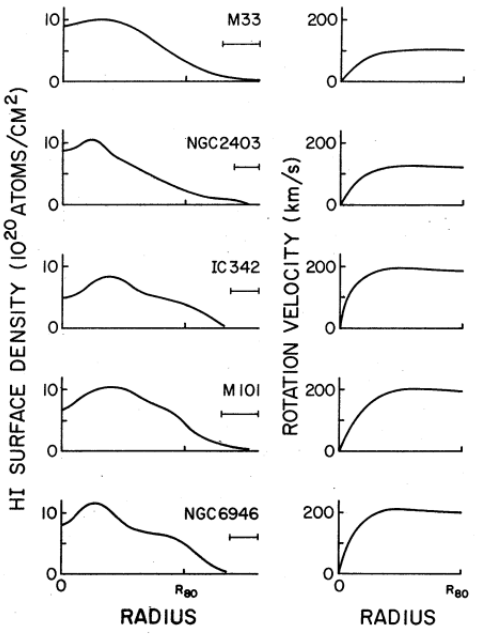

FIGURE 1.1: The rotation curves observed for M33, NGC 2403, IC 342, M101, and NGC 6946 exhibit flat profiles as revealed by 21cm HI observations. Refs. [7] provide the hydrogen surface density profile (on the left) and the rotation curves (on the right) for these five galaxies.

mass feeding this velocity which is roughly proportional to:

$$M \sim \frac{\sigma r^2}{G}, \tag{1.1}$$

where M describes the mass, σ the orbital speed, r the radius from the center of the galaxy and G the gravitational constant. This indicates that the mass is inversely proportional to the gravitational constant and proportional to the orbital speed and radius squared from the center of the galaxy, implying that as we move further from the center, the surrounding mass increases. However, the amount of visible matter present is significantly less than the mass detected through gravitational effects which leads to the postulate of dark matter. Figure 1.2 shows potential dark matter candidates

that may explain the observed flattening of the rotation curve. Research on dark matter is expanding, with astrophysicists and particle physicists working together to uncover the specific species of dark matter that is still unknown in relation to the standard model [10]. Since the 1970s, particle physicists have been actively researching dark matter and developing various methods for its detection, both indirectly and directly. The primary research focuses on neutrinos or particles of similar type [11]. To uncover the truth about dark matter, CERN (European Council for Nuclear Research) has conducted experiments using the LHC (Large Hadron Collider) [12]. The ability to directly measure various types of particles in a controlled experimental environment has been crucial, particularly because astrophysics relies heavily on observation. While CERN primarily focuses on subatomic particles, it does not directly address gravity, which is one of the four fundamental forces[1]. To address this gap, new experiments are being developed to explore gravitation to complete the Standard Model [14].

Dark matter can be categorized as hot or cold, depending on temperature and velocity [15]. Hot dark matter particles were fast-moving in the early universe and continue to be so, while cold dark matter particles were slow-moving in the early universe and maintain a slower pace. In cosmology, cold dark matter is favoured over hot dark matter for several reasons [16]. One reason is its consistency with observations of the hierarchical formation of large-scale structures from small structures. Cold dark matter provides a more plausible explanation for this phenomenon compared to hot dark matter. Additionally, hot dark matter would hinder the growth of small-scale structures like galaxies and galaxy clusters, whereas cold dark matter facilitates their formation [17]. Hot dark matter particles move too fast to be captured by the gravitational pull of small structures, while cold dark matter particles can be trapped, thus promoting structure formation. Hence, in cosmology, cold dark matter is the preferred explanation due to its ability to account for observations of both large-scale and small-scale structure formation.

Another suggested explanation for indirect mass measurements is the Modified Newtonian Dynamics (MOND) theory [18], which alters Newton's laws at various galactic scales to account for discrepancies in energy and mass. At the transitional radius (r) where Keplerian motion is no longer obeyed, and the acceleration drops, the critical acceleration a_0 is defined as shown in Ref. [19]. The point r is therefore defined where,

$$a = \begin{cases} a_{N,} & a \gg a_0, \\ \sqrt{a_N a_0}, & a \ll a_0, \quad \text{where} \quad a_N = \frac{GM}{r^2}. \end{cases} \tag{1.2}$$

For large radii where $F/g = a_N \gg a_0$, Newtonian dynamics holds. However, when $a_0 \to \infty$ and

[1]The four fundamental forces include the Strong, Weak, Electromagnetic, and Gravitational forces, with Gravitation incorporating the concept of Gravitons, which are still hypothetical particles [13]

$G \to 0$, the modification applies at small accelerations $a \ll a_0$. The original formulation of MOND lacks the conservation of momentum, angular momentum, and energy, making its integration into General Relativity (GR) challenging. GR is founded on these fundamental conservation laws, which MOND fails to preserve. Moreover, MOND introduces an acceleration-dependent modification to gravity, contradicting the equivalence principle. Consequently, its compatibility with established science remains uncertain, highlighting the need for a more observationally consistent theory. Therefore, the status of the theory remains a topic of debate [20].

The next unknown in our story is the accelerated expansion of the universe which is attributed to an enigmatic force known as dark energy [21, 22]. This force is referred to as "dark" because it is invisible to telescopes and other astronomical instruments, as it does not interact with light or any other form of electromagnetic radiation. Physicists Saul Perlmutter, Brian Schmidt, and Adam Riess made independent observations of high redshift supernovae, which revealed that these supernovae were receding at a faster rate than expected. This discovery provided evidence for the acceleration of the universe's expansion, challenging the prevailing Einstein de-Sitter model. To account for the late-time expansion, the simplest approach was to introduce the cosmological constant, Λ, which can be incorporated into Einstein's field equations of general relativity to accommodate the effects of dark energy [23]. The cosmological constant represents the energy density of the vacuum of space, exerting a repulsive gravitational force on all matter in the universe and driving it apart at an accelerating rate. This effect becomes increasingly apparent over time, contributing to the observed accelerated expansion of the universe [21, 22]. These suggestions form part of the currently accepted paradigm aiming to describing the cosmos.

To simplify our understanding of these phenomena, scientists [24, 25, 26] have proposed a model that treats dark matter and dark energy as a single "Dark Fluid" (DF) that drives the expansion of the universe and surrounds galaxies.

This dissertation is organized as follows: Chapter 1 provides a review of preliminary concepts that motivate the use of Unified Dark Energy (UDE) models. In Chapter 2, two specific UDE models, namely the Chaplygin gas (CG) model and the Logotropic model, are discussed with the inclusion of how the models behave at the background level. Chapter 3 focuses on reviewing the perturbations of each model, including the justification for specific model parameters and the significance of observational data sets used throughout. Additionally, Chapter 4 introduces a new model called the Murnaghan equation of state, which shares similarities with the generalized Chaplygin gas model. Methods for the statistical analysis of the model introduced in Chapter 4 is presented in Chapter 5, along with common numerical methods used in testing cosmological models. Finally, in Chapter 6, applications and conclusions derived from our analysis are presented, along with commentary on

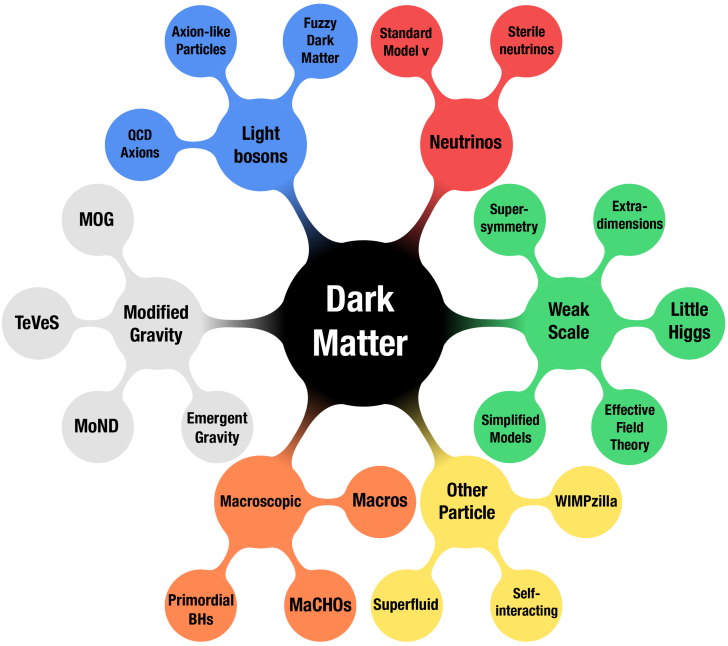

FIGURE 1.2: Figure depicting the diagrammatic representation of the currently proposed candidates for dark matter [10]. Although each of these branches can be explored, this paper will specifically focus on Modified Gravity.

future work following this master's dissertation.

1.2 General relativity

To precisely capture the intricate dynamics of the universe at cosmological scales, a formulation of physics that is independent of coordinate systems is essential. However, Newtonian gravity, which assumes gravity is an instantaneous force acting at a distance, cannot be used to model the evolution of the universe because it does not consider the effects of mass on spacetime geometry. To do this we introduce Einstein's field equations. The connection between matter and the curvature of spacetime can be described using Einstein's field equations [23], given by the expression,

$$G_{\mu\nu} = R_{\mu\nu} - \frac{1}{2} R g_{\mu\nu}. \tag{1.3}$$

In this context, $G_{\mu\nu}$ is known as the Einstein tensor, which characterizes the curvature of spacetime, while $R_{\mu\nu}$ represents the Ricci tensor[2], also referred to as the stress-energy tensor and R the scalar curvature (Ricci scalar). The $g_{\mu\nu}$ term denotes a general metric tensor which satisfies the relation[3]

[2] We use tensors because they represent a fixed relationship between two vectors and are independent of the coordinate system.

[3] where we define $\delta^{\mu}_{\nu} = 1$ for $\mu = \nu$ and $\delta^{\mu}_{\nu} = 0$ for $\mu \neq \nu$, this will be useful later on when we assess perturbations

$g^{\mu\alpha}g_{\alpha\nu} = \delta^{\mu}_{\nu}$. The original formulation of Einstein's field equation includes the $\Lambda g_{\mu\nu}$ term denoting the cosmological constant aimed at describing the late time accelerated expansion of the universe (dark energy term),

$$R_{\mu\nu} - \frac{1}{2}Rg_{\mu\nu} + \Lambda g_{\mu\nu} = 8\pi G T_{\mu\nu}. \tag{1.4}$$

Since we aim to develop a model that does not need separate dark matter and dark energy terms, our system of equations omits the cosmological constant Λ term. The left-hand side of Equation (1.3) pertains to the geometry of spacetime, while the right-hand side describes the energy and momentum of matter components. These matter components can be adjusted based on the specific cosmological model under consideration.

The Ricci tensor describes the local distribution of energy, momentum, and stress within the given spacetime [27]. We can delve deeper into this concept by expanding the term, which is expressed in terms of the Christoffel symbol,

$$\Gamma^{\mu}_{\alpha\beta} = \frac{1}{2}g^{\mu\nu}\left[\frac{\partial g_{\alpha\nu}}{\partial x^{\beta}} + \frac{\partial g_{\beta\nu}}{\partial x^{\alpha}} - \frac{\partial g_{\alpha\beta}}{\partial x^{\nu}}\right]. \tag{1.5}$$

The Christoffel symbol, also known as the connection coefficients or affine connection, facilitates the transformation from one coordinate system to another. Thus the Ricci tensor can be written as,

$$R_{\mu\nu} = \partial_{\alpha}\Gamma^{\alpha}_{\mu\nu} - \partial_{\mu}\Gamma^{\alpha}_{\alpha\nu} + \Gamma^{\alpha}_{\alpha\beta}\Gamma^{\beta}_{\mu\nu} - \Gamma^{\beta}_{\mu\alpha}\Gamma^{\alpha}_{\beta\nu}. \tag{1.6}$$

The Ricci scalar can be obtained by contracting the indices of the Ricci tensor: $R = R_{\mu\nu}g^{\mu\nu}$. Subsequently, the Ricci scalar offers a simple representation of the curvature of spacetime. The Riemann tensor describes the curvature and geometry of spacetime through the second derivative of the Christoffel symbols. The Christoffel symbol is employed to define the concept of parallel transport and is indispensable in general relativity for comprehending the behaviour of matter and energy in curved spacetime. This ties in with the Riemann tensor which is derived from the Christoffel symbols, and describes the curvature of a surface. This form of Einstein's field equation is valid for $c = 1$ which allows us to simplify the dimensions present and thus calculations.

The Einstein-Hilbert action, a mathematical expression within Einstein's theory of general relativity, embodies the principle of least action. This principle posits that the path traversed by a system between two points minimizes the action [28]. The action, which is a functional of the spacetime metric, describes how matter and energy determine the curvature of spacetime. The action includes a term proportional to the Ricci scalar and another term proportional to the square of the Ricci tensor, with a proportionality constant known as the gravitational constant [29]. We can derive Einstein's

equations from the action integral known as the Einstein-Hilbert action and defined as,

$$S = \int d^4x \sqrt{-g} \left(\mathcal{L}_G + \mathcal{L}_M \right), \tag{1.7}$$

where $g = \det\left(g_{\mu\nu}\right)$, $\mathcal{L}_G = \dfrac{1}{16\pi G} R$ describes the Einstein-Hilbert action and $\mathcal{L}_M$ the matter action. The second Lagrangian is related to the energy-momentum tensor via,

$$T_{\mu\nu} = -2\frac{\delta \mathcal{L}_M}{\delta g^{\mu\nu}} + g_{\mu\nu}\mathcal{L}_M. \tag{1.8}$$

By specifying the form of the energy-momentum tensor in a Unified Dark Energy (UDE) model, we can derive the equations of motion for the dark energy field and discern its evolution over time. This facilitates predictions about the universe's behaviour at various epochs and enables comparison of these predictions with observational data. Moreover, the energy-momentum tensor offers a means to assess the validity of different UDE models and to constrain their parameters using observational data.

1.3 The Friedmann model

1.3.1 The Cosmological Principle and observed isotropy

The cosmological principle states that the universe is the same for all observers on large scales. This principle is based on the idea that the universe is statistically isotropic and homogeneous [29]. Isotropy means that the universe has no preferred direction, while homogeneity implies that the universe has no preferred location. These concepts are related, but not equivalent. By definition, the assumption of isotropy and homogeneity in general relativity (GR) ensures symmetry, enabling us to solve equations [27] with less mathematical work. This presumption finds support in observations of the Cosmic Microwave Background (CMB) and the uniform distribution of galaxies across the celestial sphere, with any deviations from isotropy typically measuring around 10^{-5}, as indicated by Ref. [3]. By assuming that we are typical cosmological observers, we can make a priori predictions about the large-scale structure of the universe.

1.3.2 FLRW metric

Conformal time is a time measurement that considers the expansion of the universe. It is determined by dividing the time taken by a photon to travel between two points in an expanding universe by a

specific function of the scale factor denoted a, in terms of redshift is given by,

$$a = \frac{1}{1+z}. \tag{1.9}$$

Understanding this concept is crucial since our derivations will build upon it and facilitate the treatment of perturbation theory. The conversion from cosmic time (t) to conformal time (η) is given by the derivative,

$$\mathrm{d}t = a\mathrm{d}\eta, \tag{1.10}$$

where the background metric can be written in terms of Equation (1.10) as,

$$\mathrm{d}s^2 = g^{(0)}_{\mu\nu}\, \mathrm{d}x^\mu\, \mathrm{d}x^\nu \tag{1.11}$$

where we denote the background with the superscript "0". In these derivations we will be using the Einstein summation convention. We will apply the same assumptions as above, that is, we are dealing with a homogeneous and isotropic universe [30]. The motivation for using the Friedmann–Lemaître–Robertson–Walker (FLRW) metric is that it provides zeroth order solutions and serves as a starting point for more complex models that can explain the universe's smaller-scale structures and phenomena. The general form of the metric is,

$$\mathrm{d}s^2 = \mathrm{d}t^2 - a^2(t)\left\{\mathrm{d}\chi^2 + \Sigma^2(\chi)(\mathrm{d}\theta^2 + \sin^2\theta\,\mathrm{d}\varphi^2)\right\}, \tag{1.12}$$

where χ describes the comoving distance between two points, t the cosmic time and $\Sigma^2(\chi)$,

$$\Sigma^2(\chi) = \begin{cases} \sin^2\chi, & k > 0 \\ \chi^2, & k = 0 \\ \sinh^2\chi & k < 0, \end{cases}$$

and describes the solutions to the spatial line element in comoving coordinates, provided homogeneity and isotropy are maintained, since this ensures spatial isotropy and thus spatial symmetry. The FLRW metric can also be expressed in terms of k, which denotes the spatial curvature[4] by,

$$\mathrm{d}s^2 = \mathrm{d}t^2 - a^2(t)\left\{\frac{\mathrm{d}r^2}{1-kr^2} + r^2(\mathrm{d}\theta^2 + \sin^2\theta\,\mathrm{d}\varphi^2)\right\}, \tag{1.13}$$

[4]See Appendix §A.1 for derivation.

where $k = -1, 0, 1$, and refers to whether the universe is open, flat, or closed, respectively [29]. Our investigation will primarily focus on the flat case where $k = 0$ due to compelling observational motivations. The CMB radiation reveals temperature fluctuations that align with predictions based on a flat geometry and tend to be of the order $\Delta T/T \sim 10^{-5}$. Additionally, Baryon Acoustic Oscillations (BAO) present imprints from sound waves in the early universe, observed through surveys like the Sloan Digital Sky Survey (SDSS), displaying characteristic patterns consistent with a flat geometry. Furthermore, the proposal of dark energy, driven by observations of an accelerated expansion, provides an additional rationale for utilizing a flat geometry. Substituting (1.10) into (1.13), we can express the FLRW metric as,

$$\mathrm{d}s^2 = a^2(\eta)\Big\{ \mathrm{d}\eta^2 - \Big[\mathrm{d}\chi^2 + \Sigma^2(\chi)\Big(\mathrm{d}\theta^2 + \sin^2\theta \ \ \mathrm{d}\varphi^2\Big)\Big]\Big\}. \tag{1.14}$$

The advantage of this is that one can compute the logarithm of the scale factor, thus directly linking it with cosmic time [31]. The derivative of the scale factor can be written in terms of the e-foldings $N = \ln a$ as,

$$\dot{a} = \frac{\mathrm{d}a}{\mathrm{d}t} = \frac{\mathrm{d}a}{a\,\mathrm{d}\eta} = \frac{\mathrm{d}\,\ln a}{\mathrm{d}\eta}.$$

This will prove useful later on when we characterise inflation by the factor e^N. This transformation aids in comparing and quantifying the rate of expansion at a given period of inflation. Referring back to our derivation, the FLRW metric tells us several crucial things about the universe we live in. Firstly, it offers insight into the rate at which the universe is expanding. Secondly, it characterizes the universe's geometry, determining whether it is open, closed, or flat, and elucidating how this configuration influences the behaviour of light and other particles. Thirdly, it enables us to estimate the density of matter and energy, which are essential aspects of the universe's structure, and the scale at which they occur. The FLRW metric in Cartesian coordinates takes the form,

$$\mathrm{d}s^2 = \ \mathrm{d}t^2 - a^2(t)\delta_{ij}\,\mathrm{d}x^i\,\mathrm{d}x^j, \tag{1.15}$$

with non-vanishing Christoffel symbols,

$$\begin{aligned} \Gamma^0_{ij} &= \delta_{ij}\dot{a}a, \\ \Gamma^i_{0j} = \Gamma^i_{j0} &= \delta_{ij}\frac{\dot{a}}{a} = \delta_{ij}H, \end{aligned} \tag{1.16}$$

where components of the Ricci tensor is shown to be,

$$\begin{aligned} R_{00} &= -3\frac{\ddot{a}}{a}, \\ R_{ij} &= \delta_{ij}\left(2\dot{a}^2 + a\ddot{a}\right). \end{aligned} \tag{1.17}$$

From this we can write the Ricci scalar as,

$$R = -R_{00} + \frac{1}{a^2} R_{ii} = 6 \left[\frac{\ddot{a}}{a} + \left(\frac{\dot{a}}{a} \right)^2 \right]. \tag{1.18}$$

Inserting (1.18) into Einstein's field equation (1.3) results in the Einstein tensor shown below. We can compute all the components beginning with the G_{0i} component which will be zero, while the (00) and (ij) components become,

$$G_{00} = 3 \left(\frac{\dot{a}}{a} \right)^2, \tag{1.19a}$$

$$G_{ij} = (-2\ddot{a}a - \dot{a}^2)\delta_{ij}. \tag{1.19b}$$

Thus, for a universe consisting of n fluid components, with a perfect fluid description given by,

$$T^{(n)}_{\mu\nu} = (\rho_n + p_n)\, u_\mu u_\nu + p_n g_{\mu\nu}, \tag{1.20}$$

where ρ_n describes the sum of energy densities[5], p_n describes the pressure for n fluids and u_μ the four-velocity vector. We can then substitute (00) and (ii) components, arriving at,

$$\left(\frac{\dot{a}}{a} \right)^2 = \frac{8\pi G}{3} \rho, \tag{1.21}$$

$$\left(\frac{\dot{a}}{a} \right)^2 + 2\frac{\ddot{a}}{a} = -8\pi G p, \tag{1.22}$$

where Equation (1.21) is the Friedmann equation. We can use (1.21) and (1.22) to obtain the Raychaudhuri equation given by,

$$\frac{\ddot{a}}{a} = -\frac{4\pi G}{3}(\rho + 3p). \tag{1.23}$$

To facilitate accelerated expansion, the condition $p < -\rho/3$ must be met. Building upon our previous discussions and observations, we acknowledge the dominant influence of a negative constant energy in the universe. To provide the simplest explanation, we reintroduce the variable Λ. By incorporating this energy density into the Friedmann equation, we obtain,

$$H^2 = \frac{8\pi G}{3} \left(\rho_m + \rho_r + \rho_\Lambda - \frac{k}{a^2} \right), \tag{1.24}$$

where H is the Hubble parameter, G is the usual gravitational constant as defined previously, ρ_m is the matter energy density, ρ_r is the radiation energy density and ρ_Λ is the vacuum energy density. If

[5]Non-relativistic matter, relativistic particles (radiation) and dark energy

we omit matter, radiation, curvature components and letting $H^2 = (\dot{a}/a)^2$ we arrive at,

$$\left(\frac{\dot{a}}{a}\right) = \frac{\Lambda}{3}, \tag{1.25}$$

with solution,

$$a(t) \sim e^{\sqrt{\Lambda/3}t}. \tag{1.26}$$

This indicates that the vacuum energy by itself would result in an exponential expansion of the universe. The Raychaudhuri equation (1.23) is essential in predicting space-time singularities for given models. When applied to a group of geodesics that either converge or diverge, the Raychaudhuri equation predicts that the expansion of the group will eventually become infinite or negative at some point in the future. As a result, the group will either develop a singularity or approach a singularity in a finite amount of time making it crucial in determining the dynamics of the dark energy component of the universe.

1.3.3 Energy-momentum tensor with perfect fluid description

The approach of considering a single perfect fluid enables us to formulate theories based on a straightforward assumption. This provides a solid foundation for developing cosmological models and serves as a useful testing ground for their refinement. The energy-momentum tensor characterizes the distribution of matter and radiation throughout the universe. In Unified Dark Energy (UDE) models, it is crucial for the total energy of the dark fluid to remain positive, in accordance with the principle that energy cannot be created out of nothing. Departures from these conditions within the energy-momentum tensor of the dark fluid may result in instabilities or other physical inconsistencies in the universe. We describe the fluid using the 4-momentum $p^\mu = mu^\mu$ [29], which provides a comprehensive description of the energy-momentum of a fluid.

The energy-momentum tensor has the following form,

$$T^{\mu\nu} = \begin{pmatrix} \rho & 0 & 0 & 0 \\ 0 & p & 0 & 0 \\ 0 & 0 & p & 0 \\ 0 & 0 & 0 & p \end{pmatrix}. \tag{1.27}$$

We can generalize this expression for the case of matter in motion [28]. The dependence on energy density and pressure goes as,

$$T^{\mu\nu} = (\rho + p)u^\mu u^\nu - p\eta^{\mu\nu}, \tag{1.28}$$

where u^μ is the 4-velocity vector of the form,

$$u^\mu = \mathrm{d}x^\mu / \mathrm{d}\tau = (1,0,0,0). \tag{1.29}$$

To extend expression (1.27) for curved space, we replace the Minkowski space metric $\eta^{\mu\nu}$ with an arbitrary metric $g^{\mu\nu}$ such that $g_{\mu\nu} = \eta_{\mu\nu} = (-1,1,1,1)$. In each region of spacetime, a locally Lorentzian reference frame exists where the metric tensor aligns locally with the Minkowski tensor [30]. Within this frame, the energy-momentum tensor for matter assumes the structure expressed in Equation (1.28). Upon transitioning to an arbitrary reference frame, we obtain,

$$T^{\mu\nu} = (\rho + p)u^\mu u^\nu - p g^{\mu\nu}, \tag{1.30}$$

where ρ denotes the energy density and p represents the pressure. It is important to emphasize that Equation (1.30) is typically applicable under conditions of weak gravity. In scenarios where gravitational effects are strong, the expression for the energy-momentum tensor may include supplementary terms contingent upon the curvature tensor. We can rewrite the energy-momentum tensor in (1.30) in the following way,

$$T^\nu{}_\mu = g^{\nu\alpha}T_{\alpha\mu} = (\rho + p)u^\nu u_\mu - p g^\nu{}_\mu = (\rho + p)u^\nu u_\mu - p\delta^\nu{}_\mu, \tag{1.31}$$

for simplicity. Equation (1.27) and the trace of $T^\mu{}_\nu$ is given by,

$$T \equiv \bar{T}^\mu{}_\mu = \rho - 3p. \tag{1.32}$$

The constant value of the trace reflects the cosmological principle, signifying uniform characteristics across the universe at large scales. Any deviation from this value would disrupt the homogeneity and isotropy of the universe, thereby contravening the cosmological principle. The conservation of the energy-momentum tensor stems from the Bianchi identities [27] via,

$$T^{\mu\nu}_{;\nu} = T^{\mu\nu}_{,\nu} + \Gamma^\mu_{\alpha\beta}T^{\alpha\beta} + \Gamma^\beta_{\alpha\beta}T^{\mu\alpha}, \tag{1.33}$$

where the semi-colon denotes the covariant derivative. The spatial terms do not contribute any useful information, however the $T^{0\nu}_{;\nu}$ term yields the continuity equation,

$$\dot{\rho} + 3H(\rho + p) = 0, \tag{1.34}$$

which will be explored numerically in assessing particular UDE models in Chapter 2.

1.3.4 Equation of state solutions

In general we can express the equation of state (EoS) for the background in terms of density alone. Here, ρ denotes the density and not rest-mass density like the thermodynamic case which will be explored later on. To simplify our calculations we assume our fluid is barotropic, meaning it is only a function of pressure $p(\rho)$. The background parameter w takes the form of a simple linear function given by,

$$p = w\rho. \tag{1.35}$$

By assessing different values of w, we can infer the dominating processes during a particular epoch of cosmological history, and can be summarized,

$$w = \begin{cases} 0 & \text{Pressure-less dust, i.e. baryonic matter and dark matter.} \\ \frac{1}{3} & \text{Radiative particles such as photons or ultra-high relativistic particles.} \\ -1 & \text{Cosmological constant: represents the negative pressure due to expansion.} \end{cases}$$

Returning to the continuity equation (1.34), we can express this in terms of the background w as follows,

$$\dot{\rho} + 3H\rho(1+w) = 0. \tag{1.36}$$

The equation above can be integrated to yield a solution for a perfect fluid with a constant EoS parameter w,

$$\rho = \rho_0 a^{-3(1+w)}, \tag{1.37}$$

where $\rho_0 = \exp(c)$ a positive integration constant. We can express the density ρ for the three cases of w mentioned above, along with their corresponding solutions given by,

$$w = \begin{cases} 0 & \xrightarrow{solution} & \rho_d = \rho_0 a^{-3} \\ \frac{1}{3} & \xrightarrow{solution} & \rho_r = \rho_0 a^{-4} \\ -1 & \xrightarrow{solution} & \rho_\Lambda = C \end{cases} \tag{1.38}$$

where ρ_d describes the pressureless dust era, ρ_r the radiation era and ρ_Λ the solution where C denotes the constant domination of dark energy and dark matter. These solutions aid us in assessing the behaviour of cosmological models with respect to some reference density (ρ_0), typically the critical density (ρ_c) and the scale factor.

1.4 The ΛCDM model

The absence of direct evidence for dark matter or dark energy has motivated us to explore alternative models for structure formation, alongside the well-known ΛCDM model, which assumes a flat geometry ($k = 0$). This opens up the possibility of investigating models that incorporate different geometrical elements. The current pressure in the ΛCDM regime can be expressed as,

$$p = 0, \quad \text{for pressureless matter.} \tag{1.39}$$

We know from above that for background EoS $w = -1$ the result is a positive constant (1.38), thus we require for late time expansion that $\Lambda > 0$. The Friedmann equations with the inclusion of the cosmological constant and curvature is given by,

$$\left(\frac{\dot{a}}{a}\right)^2 = \frac{8\pi G}{3}\rho - \frac{k}{a^2} + \frac{\Lambda}{3}, \tag{1.40a}$$

$$\frac{\ddot{a}}{a} = -\frac{4\pi G}{3}\left(\rho + 3p\right) + \frac{\Lambda}{3}. \tag{1.40b}$$

In line with our previous analysis, we will focus on the scenario of a flat universe ($k = 0$). This choice is supported by observations of the CMB [3] and BAO data, which have provided evidence for a constrained curvature term [32, 33, 34] given by,

$$\Omega_{k,0} = 0.0007 \pm 0.0019, \tag{1.41}$$

suggesting that our universe is approximately flat. With such a tightly constrained bound, there is sufficient evidence to adopt a flat geometry and work with a flat FLRW metric, which greatly simplifies our analytical derivations.

Observational data allows us to test theoretical predictions of the ΛCDM model. The Planck mission of 2018 [5] provides values for cosmological parameters that are particularly useful for these comparisons. We express these parameters in terms of the dimensionless density parameter with a flat geometry $k = 0$ and defined as,

$$\Omega_i = \frac{\rho_i}{\rho_c}, \tag{1.42}$$

where the critical density ρ_c is,

$$\rho_c = \frac{3H^2}{8\pi G}, \tag{1.43}$$

and defined as the total energy content of the universe today. Rewriting the Friedman Equations (1.40) in terms of the dimensionless density parameter, with the inclusion of radiation, matter and

cosmological constant, we arrive at,

$$H^2 = H_0^2 \left[\Omega_{r,0} \left(\frac{a_0}{a} \right)^4 + \Omega_{m,0} \left(\frac{a_0}{a} \right)^3 + \Omega_\Lambda \right]. \tag{1.44}$$

where the scale factor $a_0 = 1$ and refers to the redshift $z = 0$, corresponding to our current day. Three key insights emerge from this analysis. First, the radiation term dominates when a is small, so at early stages of the universe's history. Second, the matter term becomes significant at $a \approx a_0 \Omega_{r,0}/\Omega_{m,0}$, resulting in matter being the dominant form of energy in the universe. Third, the dark energy term Ω_Λ takes over at $a \approx a_0(\Omega_{m,0}/\Omega_\Lambda)^{1/3}$ and beyond, as the universe expands as the scale factor increases, making dark energy the dominant form of energy in the universe. Figure 1.3 illustrates these trends, while Table 1.1 presents observational values for dimensionless density parameters for matter, radiation, and Λ, obtained from the Planck spacecraft mission [5].

$\Omega_b^{(0)}$	$\Omega_m^{(0)}$	$\Omega_r^{(0)}$	$\Omega_\Lambda^{(0)}$	$H_{0[CMB]}$
0.0487	0.315	9.3×10^{-5}	0.6847	67.4 ± 0.5 km s^{-1} Mpc^{-1}

TABLE 1.1: Cosmological parameters from the Planck spacecraft mission [3], where the present content is denoted with superscript $^{(0)}$. These numerical values were used throughout the analysis.

The universe has undergone two phases of accelerated expansion: the inflation period and the expansion driven by dark energy. These periods can be analyzed by examining the time dependence of energy density parameters, as shown in Figure 1.3.

Since observations align with our currently chosen geometry, namely that our current universe is nearly flat, we can set the sum of all present (using subscript "0") content equal to unity,

$$\Omega_{tot} = 1 = \Omega_{r,0} + \Omega_{m,0} + \Omega_{\Lambda,0}. \tag{1.45}$$

We can relate the scale factor with time by solving for the different epochs of energy domination. For a flat universe with only matter the Friedmann equation reduces to,

$$\left[\frac{\dot{a(t)}}{a(t)} \right]^2 = \frac{H_0^2 \Omega_{m,0}}{a^3(t)}, \tag{1.46}$$

resulting in the solution given in Equation (1.47b). We can do the same for the radiation and cosmological constant cases and arrive at solutions givien in Equations (1.47a) and (1.47c) as shown below,

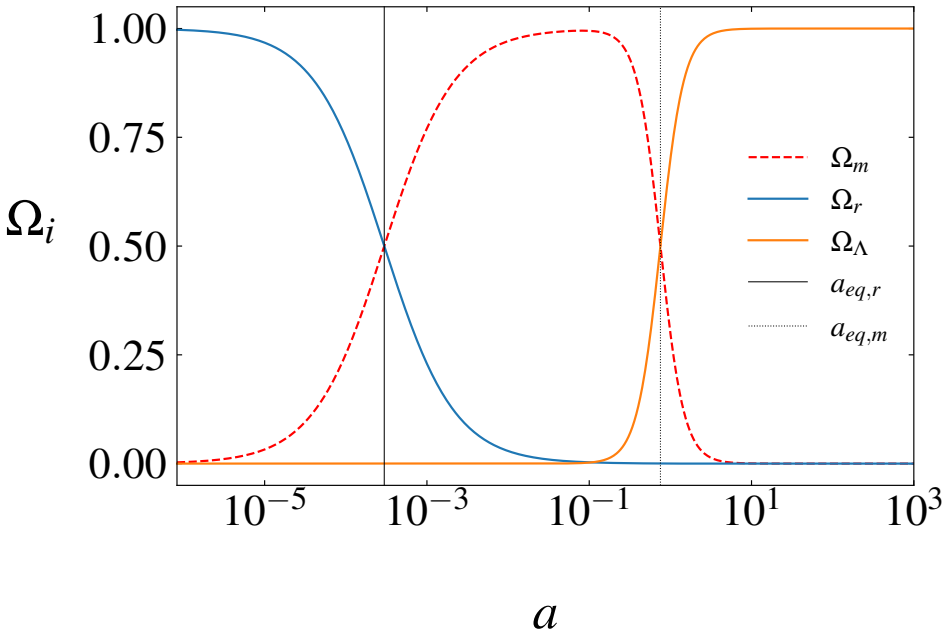

FIGURE 1.3: The energy density parameters for radiation (blue solid line), matter (red dashed line) and cosmological constant (orange solid line). The values used are from the recent Planck mission [3]. The black dashed line represents the matter-radiation equality (1.48a) and the solid black line the matter-dark energy equality (1.48b), the transition period between eras.

$$\text{Radiation-domination} \qquad a(t) \propto t^{1/2}, \tag{1.47a}$$

$$\text{Matter-domination} \qquad a(t) \propto t^{2/3}, \tag{1.47b}$$

$$\text{De Sitter Universe} \qquad a(t) \propto \exp\left[H_0\sqrt{\Omega_\Lambda}t\right]. \tag{1.47c}$$

Between these phases we can also define transitional states by relating cosmic time and redshift via,

$$\text{Matter-radiation equality} \qquad z_{eq,r} \sim \frac{\Omega_m}{\Omega_r}, \tag{1.48a}$$

$$\text{Matter-dark energy equality} \qquad z_{eq,m} \sim \left(\frac{\Omega_\Lambda}{\Omega_m}\right)^{1/3} - 1. \tag{1.48b}$$

We can express these relations in terms of the scale factor via Equation (1.9), which is depicted in Figure 1.3 with the black vertical lines. The concludes our description on the equation of state solutions and how we can use them in assessing the behaviour of different cosmological models against the standard paradigm. In Chapter 2, we will show how we can combine dark energy and dark matter to create a single dark fluid. Before exploring single-fluid cosmologies, it is important to acknowledge certain limitations in the ΛCDM model. Observational data suggests that the universe has experienced two periods of cosmic acceleration, posing new challenges for the ΛCDM model, including

the issue of inflation.

1.4.1 The standard cosmological model

While the ΛCDM model successfully addresses many cosmological observations, it grapples with several unresolved issues. Dark matter and dark energy, introduced to explain phenomena such as galaxy rotation curves and cosmic acceleration, present challenges due to their elusive nature. Anomalies in the cosmic microwave background, uncertainties in structure formation on smaller scales, and lingering questions about cosmic inflation further challenges the model. Despite its successes, the ΛCDM model encounters several persistent challenges, including the Cosmic Coincidence Problem, the σ_8 tension, the Hubble constant tension, the Horizon Problem, and the Magnetic Monopole Problem.

Cosmic coincidence problem Observations indicate that the combined density contribution of matter in the universe is nearly equivalent to the critical density required for a flat universe [35]. Consequently, we would expect to observe a curvature contribution comparable in magnitude to the contribution from matter over the course of cosmic history. However, this is not the case, the energy densities of dark matter and dark energy are of the same order of magnitude at the present epoch.

The σ_8 tension The parameter σ_8 measures the amplitude of matter density fluctuations across scales of about 8 megaparsecs [36]. It holds significant importance in characterizing the universe's structure growth and plays a pivotal role in assessing the parameter S_8 [37],

$$S_8 = \sigma_8 \sqrt{\frac{\Omega_m}{0.3}}. \tag{1.49}$$

The parameter S_8 gauges the extent of matter density fluctuations and hinges on both the quantity of matter in the universe (Ω_m) and the degree of clustering (σ_8). It dictates the clustering pattern of matter and the genesis of cosmic structures. Variations between the observed and predicted σ_8 values within the ΛCDM framework, as highlighted by Ref. [38], imply potential shortcomings in the employed model or systematic errors in the datasets utilized.

Hubble constant H_0 tension The Hubble tension arises from the conflicting outcomes regarding the value of the Hubble constant (H_0) obtained from observations of the Cosmic Microwave Background (CMB) by the *Planck* satellite [3] versus direct measurements conducted by the SH0ES collaboration [39], focusing on nearby celestial objects like Cepheid variable stars and Type Ia supernovae [4]. These methods yield differing values for H_0, with uncertainties ranging from 4σ to 6σ [40]. Ref. [40, 41] provide a comprehensive overview of the current cosmological models proposed to address

one of the most significant tensions in modern cosmology. Unified Dark Energy models represent just one such example.

The Horizon problem The Horizon problem arises due to the homogeneity assumed in the structure of spacetime [42]. This assumption remains applicable only on scales of at least $N < 50$ e-folds, given the current energy density of the universe [3]. As a result, causally disconnected regions can emerge due to the vast distances between them, exceeding the distance light could have traveled since the Big Bang. The resolution to this problem rests on the concept that the entire universe ori-

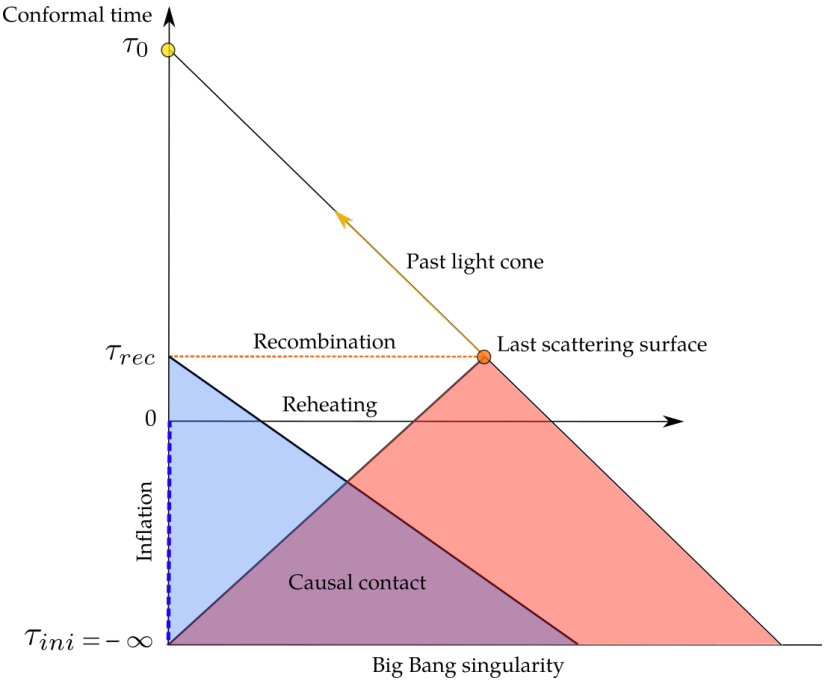

FIGURE 1.4: Conformal diagram indicating how inflation solves the horizon problem. The light cones are at $\pm 45°$, the worldlines of comoving matter are the vertical lines and the particle horizons are the horizontal lines.

ginated from the same causally connected region during the early universe, depicted by the purple region in Figure 1.4. Without inflation, the conformal time would only reach back to τ_0, implying that the distinct regions observed in the CMB today along our past light cone would never have been causally linked. However, with inflation (blue dashed line in Figure 1.4), the conformal time extends to the Big Bang singularity, thereby establishing causal connectivity among these regions along our past light cone.

Magnetic monopole problem In particle physics, the Grand Unified Theory predicts the production of a large number of magnetic monopoles in the early stages of the universe, particularly during the extremely hot period [43]. However, we do not observe this phenomenon. If magnetic monopoles do exist, they are overestimated by Big Bang predictions.

We can modify the potential in our field equation to accommodate the cosmic coincidence problem, and the rarity of magnetic monopoles in the Hot Big Bang model. Therefore, we can still use the ΛCDM model to explain these phenomena since GR includes an initial accelerated expansion period.

1.4.2 The role of dark energy

Dark energy plays a significant role in both General Relativity (GR) and Quantum Field Theory (QFT), often associated with the vacuum energy or cosmological constant. In QFT, the vacuum is not truly empty but is filled with fluctuating fields. These fluctuations can impact the energy density of space, leading to the emergence of a cosmological constant term in Einstein's equations. This term resembles dark energy and contributes to the universe's accelerated expansion. However, the predicted value of vacuum energy density from QFT significantly surpasses the observed value of dark energy by orders of magnitude, giving rise to the cosmological constant problem. We understand that without some form of pressure counteracting gravity, ordinary matter cannot drive the universe's expansion [44]. This realization has led to the introduction of dark energy, often represented by the cosmological constant denoted Λ [45]. Dark energy is conceptualized as a perfect fluid that opposes gravitational effects, exerting negative pressure [46], thereby propelling the universe to expand further.

Two approaches can address the challenge of late-time expansion. One option is to seek direct resolutions to the cosmological constant and coincidence problems. Alternatively, we can explore alternative explanations for late-time acceleration through unified dark energy models, such as Quartessence modeling [47].

1.5 Perturbations in the ΛCDM model

Part of assessing the viability of a particular model is observing the growth of large scale structure as a function of time. Using the methods and assumptions laid out in §1.3, we can show how structures evolve in the universe on smaller scales since this case is not homogeneous. We examine small perturbations around an "unperturbed" background. For this background, denoted as $g^{(0)}_{\mu\nu}$, we analyze relativistic perturbations to the FLRW metric (A.1),

$$g_{\mu\nu} = g^{(0)}_{\mu\nu} + \delta g_{\mu\nu}, \tag{1.50}$$

where $\delta g_{\mu\nu}$ is the perturbed part. Assuming that perturbations arise due to gravitational instabilities[6], in terms of conformal time we can write the background metric as,

$$\mathrm{d}s^2 = g_{\mu\nu}\,\mathrm{d}x^\mu\,\mathrm{d}x^\nu = a^2(\eta)\left[-\mathrm{d}\eta^2 + \delta_{ij}\,\mathrm{d}x^i\,\mathrm{d}x^j + \delta g_{\mu\nu}\,\mathrm{d}x^\mu\,\mathrm{d}x^\nu\right]. \tag{1.51}$$

We now consider the perturbed field equations. Using Einstein's tensor from Equation (1.3) and energy momentum tensor Equation (1.27), we decompose components into the background and perturbed parts,

$$G_{\mu\nu} = G^{(0)}_{\mu\nu} + \delta G_{\mu\nu}, \quad T_{\mu\nu} = T^{(0)}_{\mu\nu} + \delta T_{\mu\nu}, \tag{1.52}$$

where the background and perturbed parts are given by:

$$G^{(0)}_{\mu\nu} = 8\pi G T^{(0)}_{\mu\nu}, \qquad \delta G_{\mu\nu} = 8\pi G \delta T_{\mu\nu}. \tag{1.53}$$

The perturbed Einstein tensor is,

$$\delta G_{\mu\nu} = \delta R_{\mu\nu} - \frac{1}{2}\left(\delta g_{\mu\nu} R + g_{\mu\nu}\delta R\right) \Rightarrow \delta G^{\mu}{}_{\nu} = \delta g^{\mu\alpha} G_{\alpha\nu} + g^{\mu\alpha}\delta G_{\alpha\nu}. \tag{1.54}$$

Distinguishing each component allows us to express the following:

$$\delta R = \delta g^{\mu\alpha} R_{\alpha\mu} + g^{\mu\alpha}\delta R_{\alpha\mu}, \tag{1.55a}$$

$$\delta R_{\mu\nu} = \delta\Gamma^{\alpha}_{\mu\nu,\alpha} - \delta\Gamma^{\alpha}_{\mu\alpha,\nu} + \delta\Gamma^{\alpha}_{\mu\nu}\Gamma^{\beta}_{\alpha\beta} + \Gamma^{\alpha}_{\mu\nu}\delta\Gamma^{\beta}_{\alpha\beta} - \delta\Gamma^{\alpha}_{\mu\beta}\Gamma^{\beta}_{\alpha\nu} - \Gamma^{\alpha}_{\mu\beta}\delta\Gamma^{\beta}_{\alpha\nu}, \tag{1.55b}$$

$$\delta\Gamma^{\mu}_{\nu\lambda} = \frac{1}{2}\delta g^{\mu\alpha}\left(g_{\alpha\nu,\lambda} + g_{\alpha\lambda,\nu} - g_{\nu\lambda,\alpha}\right) + \frac{1}{2}g^{\mu\alpha}\left(\delta g_{\alpha\nu,\lambda} + \delta g_{\alpha\lambda,\nu} - \delta g_{\nu\lambda,\alpha}\right). \tag{1.55c}$$

Recalling the condition that $g_{\nu\alpha}g^{\alpha\mu} = \delta^{\mu}{}_{\nu}$ allows us to drop the quadratic terms, since we only deal with small perturbations. This results in,

$$\delta g^{\mu\nu} = -\delta g_{\alpha\beta} g^{(0)\alpha\mu} g^{(0)\beta\nu}. \tag{1.56}$$

Employing the perfect fluid framework, the energy-momentum tensor incorporates the perturbed components as outlined in Equation (1.31) and can be written as,

$$\delta T^{\mu}_{\nu} = (\delta\rho + \delta p)u^\mu u_\nu + (\rho + p)\left(u^\mu \delta u_\nu + u_\nu \delta u^\mu\right) + \delta p\,\delta^{\mu}_{\nu}, \tag{1.57}$$

[6]Which form overdensities leading to cosmic structures

and introducing the 4-velocity vector denoted by u,

$$u^\mu = u^0(1, v^i), \qquad \text{where} \quad v_i = v^i = \frac{\mathrm{d}x^i}{\mathrm{d}\eta} = \frac{a\,\mathrm{d}x^i}{\mathrm{d}t}, \tag{1.58a}$$

$$u^0 = \frac{\mathrm{d}\eta}{\mathrm{d}t}. \tag{1.58b}$$

By applying the normalization condition for the 4-velocity, we derive the comprehensive expression for u^0 where $g_{\mu\nu}u^\mu u^\nu = -1$ and obtain a similar result to [27], given by,

$$u^0 = \frac{1}{a\sqrt{1-v^2}}\left[1 - \frac{\psi - w_i v^i + \phi v^2 - h_{ij}v^i v^j}{1-v^2}\right], \tag{1.59}$$

where u defines the 4-velocity vector, v the peculiar velocity, a the scale factor, ϕ and ψ spatial scalars and w_i denotes a 3-vector.

By assuming that our fluid is non-relativistic, we can neglect the quadratic terms and focus solely on the linear terms in the perturbed equation which is given by,

$$u^\mu = \left[\frac{1}{a}(1-\psi), \frac{v^i}{a}\right], \tag{1.60a}$$

$$u_\mu = g_{\mu\nu}u^\nu = \left[-a(1+\psi), a\,(v_i + w_i)\right]. \tag{1.60b}$$

The 4-velocity in the background, represented as $u^{\mu(0)} = (1/a, 0, 0, 0)$, leads to the perturbed quantity,

$$\delta u^\mu = \left(-\frac{\psi}{a}, u^i\right), \qquad \delta u_\mu = (-a\psi, u_i), \tag{1.61}$$

resulting in the following components for the perturbed energy-momentum tensor,

$$\begin{aligned} &\delta T^0_0 = -\rho^{(0)}\delta \quad , \quad \delta T^i_0 = -\rho^{(0)}(1+w)v^i \\ &\delta T^0{}_i = \rho^{(0)}(1+w)\,(v_i + w_i) \quad , \quad \delta T^i{}_j = \rho^{(0)}\delta c_s^2 \delta^i_j. \end{aligned} \tag{1.62}$$

The density contrast is defined in terms of perturbed density quantities as,

$$\delta = \frac{\delta\rho}{\rho^{(0)}}, \tag{1.63}$$

with the sound speed and background EoS given by,

$$c_s^2 \equiv \frac{\delta p}{\delta\rho}, \tag{1.64a}$$

$$w = \frac{p^{(0)}}{\rho^{(0)}}, \tag{1.64b}$$

where $\rho^{(0)}$ is the background energy density and δ denotes the linear density perturbation[7]. We denote δ_v the comoving density contrast and that the gauge invariant form equals total matter/comoving gauge. For the ΛCDM case where $c_s^2 = 0$, results in the following for the comoving density contrast

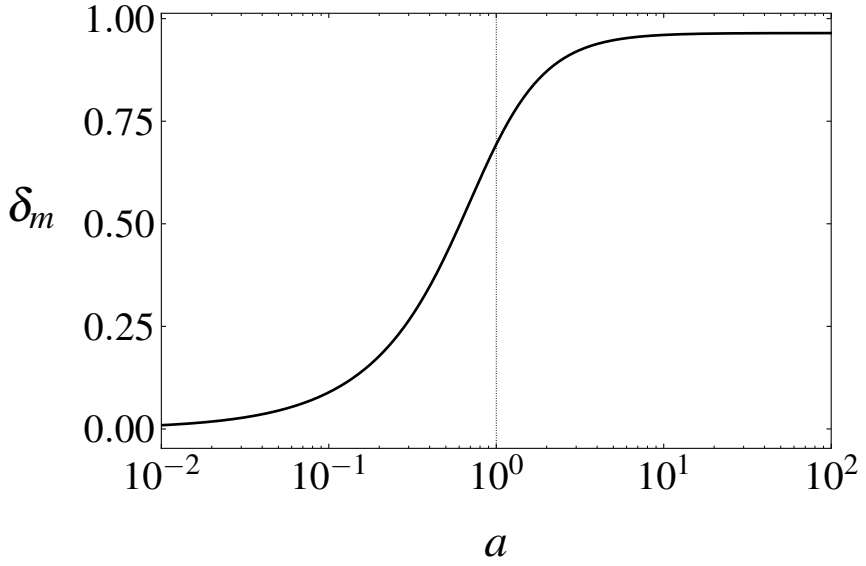

FIGURE 1.5: Linear density contrast, specifically for matter perturbations varying with the scale factor for the ΛCDM model.

for the total matter gauge in terms of e-fold time N,

$$\delta_v'' + \left(2 - \frac{3}{2}\Omega_m\right)\delta_v' - \frac{3}{2}\Omega_m\delta_v = 0 \tag{1.65}$$

Figure 1.5 shows the density contrast of the total matter perturbations in the comoving gauge for the ΛCDM model [8]. High density regions, where the matter density contrast is positive, are more likely to collapse under gravity and form structures like galaxies and clusters. Conversely, low density regions (negative density contrast) tend to expand and become voids. The solution for the matter density contrast case is thus,

$$\delta_m(a) = C_1 a + C_2 a^{-3/2}, \tag{1.66}$$

where C_1 and C_2 are arbitrary constants [48]. From this, we can deduce that over time, the ΛCDM paradigm suggests a phase of increasing growth, characterized by the collapse of regions, followed by a plateau phase indicating a slowdown in growth. One consideration that we have not looked at yet is the dark energy case δ_{de} which we will touch on later in this dissertation. Using the tools outlined above, Chapter 2 will expand on our earlier description and investigate the idea of Unified Dark Energy models/Quartessence [49] within the context of cosmic growth and structure formation.

[7] See Appendix §B.2 for full derivation
[8] Further details on perturbations provided in Chapter 3

Chapter 2

Quartessence

In Chapter 1, we examined the methodologies employed to study the evolution and structure formation of the universe using General Relativity. We investigated the assumptions of homogeneity and isotropy on large scales. However, despite the success of the ΛCDM model in matching observational data, there are still discrepancies between theoretical predictions and observations. One such discrepancy is the presence of dark matter halos surrounding galaxies, which are inferred from the plateau in the velocity rotation curve, as evidenced by the Bullet cluster [50, 51]. Observations of gravitational lensing and X-ray emission of hot gas provide evidence for dark matter, making the Bullet Cluster a crucial point of reference in modern cosmology. Astronomers discovered a significant difference between the distribution of hot gas and dark matter, thus shedding light on the distribution of dark matter halos in galaxy clusters and highlighting the weak interaction of dark matter with other matter.

To tackle this issue, "Quartessence" [52] has been proposed as the union between dark matter and dark energy, termed a "Dark Fluid (DF)", and discussed in Ref. [49]. Quartessence aims to create a unified model explaining the expanding universe and the indirectly observed mass surrounding galaxies known as dark matter halos.

2.1 Unified dark energy models

In this chapter we explore proposed Unified Dark Energy (UDE) models that aim to reconcile the discrepancy between observations and theoretical predictions. The concept of UDE models has been around since the early 1930s, when the existence of an unknown mass was first proposed [53]. Quartessence is a sub-group of k-essence models that offers a promising approach to explain these discoveries. By coupling a scalar field to its kinetic energy, Quartessence aims to arrive at an accelerated expansion of the Universe from a theory that is derived from the action,

$$S = \int \mathrm{d}^4x\sqrt{-g}\left[\frac{1}{2\kappa^2}R + p(\phi, X)\right] + S_m. \tag{2.1}$$

UDE represents a coupled two-fluid system consisting of pressureless dark matter and negative pressure dark energy [48]. The dark sector's background is effectively described as a unified fluid, regardless of its composition (e.g. whether it is comprised of distinct interacting or non-interacting components [54]). The energy density and pressure of this dark fluid can be mathematically expressed as,

$$\rho_{DF} = \rho_{CDM} + \rho_x, \qquad p_{DF} = p_x = w_x(a)\rho_x, \tag{2.2}$$

where the subscript DF describes the Unified Dark Fluid (UDF and UDE used interchangeably throughout), subscript x refers to Dark Energy (DE) and subscript CDM denotes Cold Dark Matter. The total energy density combines the individual energy densities of the dark components, ensuring conservation within the dark sector as a whole. Thus, the unified dark fluid must satisfy the background conservation equation given by,

$$\dot{\rho_{DF}} + 3H[1 + w_{DF}(a)]\rho_{DF} = 0. \tag{2.3}$$

Solving the above equation results in the solution for the general EoS parameter $\rho_{DF}(a)$ and given by,

$$\rho_{DF}(a) = \rho_{DF,0} \exp\left[-3 \int \frac{1 + w_{DF}\left(a'\right)}{a'} \, \mathrm{d}a'\right]. \tag{2.4}$$

Our initial approach involves using the simplest UDE model, which assumes a single perfect fluid with constant negative pressure. The background equation of state for this model is determined using the relation $w = -A/\rho$, where w represents the ratio of pressure to energy density, and A is a positive constant. The Chaplygin gas model replicates this behaviour for certain choices of model parameters [55]. The primary goal is to examine the relationship between pressure and energy density, which will be explored in this chapter. Ultimately, our goal is to identify the UDE model that most accurately matches available observational data and fit/does better than the standard paradigm.

In order to satisfy observational evidence, UDE models must meet certain criteria. Specifically, they must maintain a positive sound speed over time and avoid negative values of α[1] which can result in imaginary sound speeds and phantom regimes. This is important because observations indicate that a significant portion of the universe's energy density has negative pressure. To achieve our goals, we manipulate parameters of density and pressure, using differentiation to determine the sound speed. The most basic UDE model, which is characterised by $p = -A$, adheres to conventional

[1] Where α is introduced from the original Chaplygin has model to increase the degree of freedom.

FLRW equations for background evolution, as shown by,

$$\frac{\dot{a}^2}{a^2} = \frac{8\pi G}{3}\rho, \tag{2.5a}$$

$$\frac{\ddot{a}}{a} = -\frac{4\pi G}{3}(\rho + 3p). \tag{2.5b}$$

It follows that the derivatives of ρ and p yield the expressions,

$$\dot{\rho} = \frac{3}{4\pi G} H \frac{\mathrm{d}H}{\mathrm{d}t}, \tag{2.6a}$$

$$\dot{p} = -\frac{1}{4\pi G}\frac{\mathrm{d}}{\mathrm{d}t}\left(\frac{\ddot{a}}{a} + \frac{1}{2}H^2\right), \tag{2.6b}$$

and since the square of the sound speed can be formulated using the relationship $\dot{p}/\dot{\rho}$ we arrive at,

$$c_s^2 = \frac{1}{3H}\frac{\mathrm{d}}{\mathrm{d}H}\left[H^2\left(q - \frac{1}{3}\right)\right]. \tag{2.7}$$

where we have introduced the deceleration parameter q in terms of sound speed and the Hubble constant, described by,

$$q = \frac{\mathrm{d}}{\mathrm{d}t}\left(\frac{1}{H}\right) - 1. \tag{2.8}$$

Hence, the sign of the square of the sound speed relies on the behaviour of the deceleration parameter q, as defined by Equation (2.8).

When q rapidly shifts towards negative values, the square of the sound speed becomes positive, and vice versa. The rate at which Quartessence transitions from dark matter to dark energy plays a crucial role in determining the pace of q evolution. If this transition happens more rapidly compared to the ΛCDM model, the square of the sound speed will be positive. We notice that the most simple UDE model bares resemblance to the ΛCDM model if we take the pressure to be a negative constant. This will come up again later on.

The evolution of the gravitational field and background in a unified dark fluid is notably affected by the time elapsed between the last scattering surface and the current epoch. Given that the energy density is governed by a single fluid, the sound speed experiences non-zero changes in later stages. This evolutionary shift introduces a sound horizon or Jeans length, which signifies the point at which the dark fluid stops clustering. Consequently, this occurrence alters the evolution of the gravitational potential, leading to the emergence of the Integrated Sachs-Wolfe (ISW) effect [56].

In the ΛCDM model, the ISW effect arises due to the time-varying gravitational potential, causing its decay in later stages when the cosmological constant dominates, as elaborated in Ref. [57]. We will now examine the Chaplygin gas model [24] and the Logotropic model [26, 58] as instances of unified dark energy models. To illustrate their distinct behaviours, we will utilize the previously

defined background and sound speed relations.

2.1.1 The Chaplygin Gas model

The Chaplygin Gas model (CG) is a particular type of UDE model which can describe accelerated expansion without the introduction of exotic matter. Originally formulated to describe steady irrotational flow in aerodynamics [59], the CG model proposes an ideal fluid that accounts for the observed missing energy density and describes the accelerated expansion in cosmology. In this model, we assume the universe is composed of baryonic matter and a dark fluid (DF). The Chaplygin gas model has also been examined within the context of Modified gravity [60, 61], the results of which yielded solutions close to the ΛCDM scenario. To ensure mathematical and observational validity, the model must satisfy multiple criteria as explored by various authors [25, 62, 55]. The CG model is characterized by an EoS, as proposed by [24],

$$p_{CG} = -\frac{A}{\rho_{CG}}. \tag{2.9}$$

The Generalized Chaplygin Gas (GCG) model includes an additional free parameter α that aids in fine tuning the model,

$$p_{GCG} = -\frac{A}{\rho_{GCG}^{\alpha}}, \tag{2.10}$$

where α is constrained between $0 < \alpha \leq 1$ [63]. If $\alpha = 0$ we arrive at the simplest UDE model which exhibits constant negative pressure[2]. Assuming a homogeneous and isotropic state of the universe (FLRW), we can solve the continuity equation,

$$\dot{\rho} + 3H(p + \rho) = 0. \tag{2.11}$$

The analytical solution for the CG energy density, ρ_{CG}, where $\alpha = 1$ and ρ_{GCG} (A.3.1) is shown to have the following form,

$$\rho_C = \sqrt{A + \frac{B}{a^6}} \quad \text{and} \quad \rho_{GCG} = \left[A + \frac{B}{a^{3(1+\alpha)}}\right]^{\frac{1}{1+\alpha}}, \tag{2.12}$$

where B is a positive integration constant. The sound speed for the GCG model is given by,

$$c_s^2 = \frac{\partial p}{\partial \rho} = \frac{\partial}{\partial \rho}\frac{A}{\rho^{\alpha}} = A\alpha\rho^{-(\alpha+1)}, \tag{2.13}$$

[2]See Chapter 1.4 for ΛCDM model.

or in terms of the background as,

$$c_s^2 = -\alpha w \quad \text{where,} \quad w = -A\rho^{-(\alpha+1)}. \tag{2.14}$$

The GCG model performs well for particular positive values of α, as shown by [64], however there exists a limiting value of the order $\sim 10^{-5}$. We can rewrite the density in terms of the present day density denoted ρ_0 by inserting the dimensionless constant A_s,

$$\rho_{GCG} = \rho_0 \left[A_s + (1 - A_s)a^{-3(\alpha+1)}\right]^{(\alpha+1)^{-1}}, \tag{2.15}$$

where $A_s = A/\rho_{GCG,0}^{\alpha+1}$. From this expression we can assess the limiting behaviour of a:

$$\rho_{GCG} \propto \begin{cases} (1 - A_s)^{(\alpha+1)^{-1}} a^{-3} & \text{behaves as matter for } a \ll 1, \\ A_s^{(\alpha+1)^{-1}} & \text{behaves as the cosmological constant for } a \gg 1. \end{cases} \tag{2.16}$$

The restrictions are explored further in Refs. [63, 65, 49, 66]. The GCG model has been shown to be consistent with the observed cosmic expansion and the matter-dominating decelerating phase. Furthermore, it predicts a typical late-time de-Sitter phase of cosmic acceleration. These features provide compelling reasons to further investigate the model. Note that the numerical values used correspond to those cited in §1 and will be employed throughout the analysis to assess all Unified Dark Energy (UDE) models.

2.1.2 The dynamic behaviour of the Chaplygin gas equation of state

The evolution of the background EoS parameter w can be determined by solving the expression in (2.14) numerically, leading to the behaviour as shown in Figure 2.1. The transition from a matter state ($w = 0$) to a vacuum state ($w = -1$) is clearly visible and supports the ΛCDM model. This model predicts the freezing out due to dark energy as the universe expands, which is consistent with current observations. The Raychaudhuri equation, presented in (1.23), provides a condition for an accelerating universe in which $\rho_{GCG} + 3p_{GCG} < 0$, leading to the expansion of the scale factor,

$$a_{acc} > \left(\frac{1 - A}{2A}\right)^{[3(\alpha+1)]^{-1}}. \tag{2.17}$$

According to the Chaplygin gas model, the density never drops below its minimum value of $\rho_m = A^{1/(\alpha+1)}$, regardless of how much the gas expands [67]. When the density reaches this minimum, the EoS parameter becomes -1, resembling the behaviour of the cosmological constant. Additionally, numerical findings suggest the constraint $|\alpha| > 10^{-5}$, as indicated in Refs. [64, 63, 49, 27]. Values

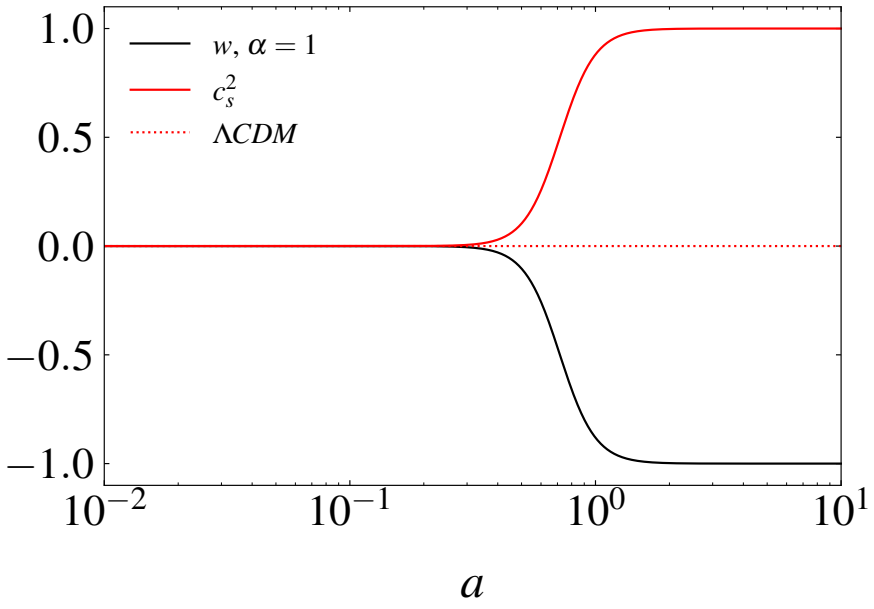

FIGURE 2.1: The background EoS parameter w (solid black line) and sound speed c_s^2 (solid red line) for the CG equation. In terms of the GCG model, this would be the case where $\alpha = 1$. The red dashed line represents the ΛCDM model where $c_s^2 = 0$.

exceeding this results in late time oscillations at the perturbative level. Further details regarding numerical findings from MCMC calculations will be shown in Chapter 4.

2.1.3 Thermodynamics and Logotropic cosmology

To describe thermodynamic systems, we consider a homogeneous and isotropic universe with uniform perfect fluid density ϵ, rest-mass density ρ, and isotropic pressure p. To unify dark matter and dark energy, we introduce a dark fluid and assume a flat universe with $k = 0$ as before. The resulting Friedmann equations are given by [30],

$$\dot{\epsilon} + 3H(\epsilon + p) = 0, \tag{2.18a}$$

$$-\frac{4\pi G}{3}(\epsilon + 3p) = \frac{\ddot{a}}{a}, \tag{2.18b}$$

$$\frac{8\pi G}{3}\epsilon = \left(\frac{\dot{a}}{a}\right)^2 = H^2, \tag{2.18c}$$

where the derivative is with respect to cosmic time, the scale factor denoted $a(t)$, and the Hubble parameter. The continuity equation, represented by (2.18a), can be derived from the first law of thermodynamics[3]. The acceleration of the universe is determined by the second derivative of the scale factor as indicated by (2.18b). The Hubble parameter, on the other hand, is related to the velocity of the expansion of the universe and the energy density, as shown in (2.18c). We can use the deceleration

[3]For a complete derivation, refer to Appendix §A.3.2

parameter (q), which reflects the rate of expansion, as one of the cosmological parameters,

$$q(t) = -\frac{\ddot{a}a}{\dot{a}^2}. \tag{2.19}$$

We typically consider two cases: $q > 0$ (the deceleration of expansion) and $q < 0$ (the acceleration). For a flat universe with EoS $p = \epsilon w$, we can can express the deceleration parameter via the Raychaudhuri equation (1.22) as,

$$q = \frac{1}{2}(1 + 3w). \tag{2.20}$$

If the deceleration parameter is constant, the universe will display different types of expansion. For $q > 0$, the universe will experience decelerating expansion, while $q < 0$ corresponds to a constant rate of expansion. An accelerating power-law expansion is observed when $-1 < q < 0$, while exponential expansion (de Sitter expansion) occurs at $q = -1$. Super-exponential expansion is observed when $q < -1$.

Revisiting our conservation equations, we encounter the first law of thermodynamics, as presented in Ref. [68],

$$\mathrm{d}\left(\frac{\epsilon}{\rho}\right) = -p\,\mathrm{d}\left(\frac{1}{\rho}\right) + T\,\mathrm{d}\left(\frac{s}{\rho}\right), \tag{2.21}$$

where the density $\rho = nm$ is in terms of the number density denoted n and mass density m. As usual, s refers to the entropy. For perfect fluids we assume adiabatic evolution therefore we can set $T = 0$ [30], such that the derivative $\mathrm{d}(s/\rho) = 0$. Equation 2.21 thus reduces to,

$$\mathrm{d}\epsilon = \left(\frac{\epsilon + p}{\rho}\right)\,\mathrm{d}\rho. \tag{2.22}$$

Given an EoS, we can establish a relationship between energy density and rest mass density. The First Law of Thermodynamics and the continuity equation are both conservation formulations that seek to determine density, lending consistency to cosmological theory. In the Friedmann model, entropy is also conserved, enabling the first law of thermodynamics or the continuity equation to evaluate specific equations of state. Simplification of the calculation can be achieved by expressing Equation (2.22) as a first-order linear differential equation given by,

$$\frac{\mathrm{d}\epsilon}{\mathrm{d}\rho} - \frac{\epsilon}{\rho} = \frac{p(\rho)}{\rho}, \tag{2.23}$$

and using variation of parameters we obtain an expression for the total energy density given by,

$$\epsilon = \rho + \rho\int^{\rho} \frac{p(\rho')}{\rho'^2}\,\mathrm{d}\rho' = \rho + u(\rho), \tag{2.24}$$

where $u(\rho)$ can be understood as an internal energy density [68]. The energy density (ϵ) is defined as the sum of the positive rest-mass density (ρ) and the internal energy. Although the rest-mass density is always positive, this is not true for the internal energy [69] which can be either. We note importantly that the total energy ϵ is always positive, which will have significance later on. The solution for the rest-mass density is determined by the integration of the continuity equation,

$$\rho = \frac{\rho_0}{a^3}, \tag{2.25}$$

where ρ_0 refers to the current value ($a_0 = 1$) of the rest-mass density for a particular dark fluid. Substituting this solution into (2.24) we arrive at,

$$\epsilon = \frac{\rho_0}{a^3} + u\left(\frac{\rho_0}{a^3}\right) = \epsilon_m + \epsilon_{\mathrm{DF}}, \tag{2.26}$$

where ϵ_m is the rest mass energy term mimicking CDM and ϵ_{DF} our dark fluid.[4]

In this review, we will investigate two variations of the logotropic model: the pure logotropic case, derived from the hydrodynamical equilibrium equation [68], and the more comprehensive form, derived from Anton-Schmidt fluids [26]. The aim is to establish a unified dark energy model, similar to the Chaplygin gas model, that can account for observational data. As a starting point, we consider the hydrodynamic equation of Ref. [68],

$$\nabla p + \rho \nabla \Phi = 0, \tag{2.27}$$

which assumes that dark matter halos are well-described by Newtonian gravity. The pressure for a polytropic relation [70] is given by,

$$p = K\rho^{\gamma}, \quad \gamma = 1 + \frac{1}{n}, \tag{2.28}$$

where the polytropic constant K may be positive or negative, and the polytropic index γ is arbitrary as shown in [58]. Substituting in the polytropic pressure (2.28) and taking the partial derivative with respect to ρ, we arrive at,

$$\begin{aligned} \nabla(K\rho^{\gamma}) + \rho\nabla\Phi &= 0, \\ \frac{\partial}{\partial\rho}\left(K\rho^{\gamma}\right) + \rho\nabla\Phi = K\frac{\partial}{\partial\rho}(\rho^{\gamma})\nabla\rho + \rho\nabla\Phi &= 0, \end{aligned} \tag{2.29}$$

[4] Appendix A.3.3 for full derivation.

where

$$\frac{\partial}{\partial\rho}(\rho^{\gamma}) = \gamma\rho^{\gamma-1}. \tag{2.30}$$

The condition of hydrostatic equilibrium in equation (2.27) becomes,

$$K\gamma\rho^{\gamma-1}\nabla\rho + \rho\nabla\Phi = 0, \tag{2.31}$$

where we have assumed that $A = K\gamma$ is finite and γ approaches zero, as demonstrated in Ref. [71], which further leads to,

$$A\rho^{-1}\nabla\rho + \rho\nabla\Phi = A\frac{\nabla\rho}{\rho} + \rho\nabla\Phi = 0. \tag{2.32}$$

Since both Equations (2.32) and (2.27) are equal to zero, we can equate them, resulting in,

$$\begin{aligned} \nabla p + \rho\nabla\Phi &= A\frac{\nabla\rho}{\rho} + \rho\nabla\Phi, \\ \int \nabla p \, \mathrm{d}p &= \int A\frac{\nabla\rho}{\rho} \, \mathrm{d}\rho, \\ p &= A\ln\rho + C, \end{aligned} \tag{2.33}$$

where ρ is a function of scale factor. To ensure that pressure forces counteract gravitational attraction, we can treat A as a logotropic temperature and impose the constraint that it is positive. It should be noted that the constant C is arbitrary and leads to the pure logotropic equation given by,

$$p = A\ln\rho = A\ln\left(\frac{\rho}{\rho_{\star}}\right), \tag{2.34}$$

where $\rho_{\star}$ is a reference density. The determination of the sound speed and background EoS for the pure logotropic scenario is achieved by employing the density relation given in Equation (2.24), resulting in an expression for the total energy density,

$$\epsilon = \rho_{\star}\exp\left\{\frac{p}{A}\right\} - p - A. \tag{2.35}$$

2.1.4 Anton-Schmidt's equation of state

We can extend the scope of the logotropic scenario by incorporating Anton-Schmidt's equation of state (EoS), originally formulated for crystalline solids. Originating from solid state physics, this EoS delineates the pressure and is utilized to characterize the deformation of crystalline solids under isotropic stress, as detailed in Ref. [26]. In the paper by authors [72], they introduce the Anton-Schmidt EoS with a small non-negligible pressure term. This consideration bypasses the need to introduce a dark energy term manually. The model expands upon the logotropic dark fluids whereby

we can show that,

$$p(V) = -\beta \left(\frac{V}{V_0}\right)^{-\frac{1}{6}-\gamma_G} \ln\left(\frac{V}{V_0}\right), \tag{2.36}$$

where β is the bulk modulus at V_0, $p(V)$ is the pressure, V is the volume and γ_G is the Grüneisen parameter. This can be thought of as a generalisation of general logotropic models. To adapt the equation presented in (2.36) for cosmological applications, we express the volume in relation to mass density, considering that $V \propto \rho^{-1}$. We can also let $n = -\frac{1}{6} - \gamma_G$ and $\rho_\star$ correspond to the equilibrium volume V_0 which indicates the limit when the pressure vanishes as shown in [73]. Assuming the universe is filled with a single dark fluid this will yield a barotropic EoS. Following the same notation used for the pure logotropic case, this results in the form,

$$p_{A-S}(\rho) = A \left(\frac{\rho}{\rho_*}\right)^{-n} \ln\left(\frac{\rho}{\rho_*}\right), \tag{2.37}$$

where the index n depends on the absolute temperature T of the environment [74], ρ_* is the reference density [72] and $A \propto \beta$. The background EoS where $n \neq 0$, and using the relation $w = p/\rho$, results in,

$$w(\rho) = A \left(\frac{\rho^{-n-1}}{\rho_*^{-n}}\right) \ln\left(\frac{\rho}{\rho_*}\right). \tag{2.38}$$

Later on we will show the generalized logotropic case using Equation (2.37) for varying free parameters n and B. For simplicity we only assess the linear perturbations for the pure logotropic case.

2.1.5 Evolution of the original logotropic model

To demonstrate how the UDE model behaves with respect to the scale factor, we examine both the background EoS and the square of the sound speed. Imposing a positive sound speed satisfying $c_s^2 < 1$ ensures the viability of our model and places constraints on the free parameters. We define the sound speed as,

$$c_s^2 \equiv \frac{\delta p}{\delta \rho}, \tag{2.39}$$

where we simplify the sound speed by assuming our fluid is barotropic[5], and conveniently incorporate the scale factor a by saying,

$$c_s^2 = \frac{\mathrm{d}p}{\mathrm{d}\rho} = \frac{\dot{p}}{\dot{\rho}} = \left(\frac{\partial p}{\partial a}\right)\left(\frac{\partial a}{\partial \rho}\right). \tag{2.40}$$

Using the expression in Equation (2.40) we arrive at,

$$c_s^2 = \frac{A}{\rho(a) - 1}, \tag{2.41}$$

[5]This is only valid if p, even when perturbed only depends on ρ alone [27].

indicating a hyperbolic behaviour, meaning the values for the free parameters will be highly constrained for phantom and real cases. We let the scale factor for the turning point of sound speed to be denoted by a_M, similar to [68]. The background evolution of the EoS parameter can be derived using the usual expression $w = p/\epsilon$, resulting in,

$$w = \frac{\rho_\star}{\rho} \exp\left\{\frac{p}{A}\right\} - \frac{p}{\epsilon}. \tag{2.42}$$

Figure 2.2 demonstrates a distinct behaviour compared to the relation for the CG EoS, highlighting

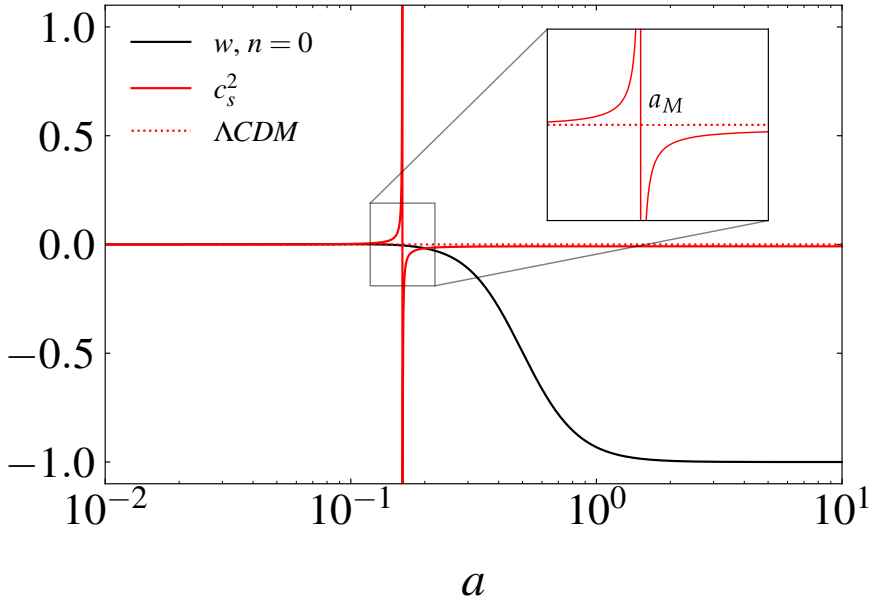

FIGURE 2.2: The EoS parameter w (solid black line) and sound speed for the pure Logotropic model where $n = 0$ (red solid line). For the ΛCDM case, $c_s^2 = 0$ and denoted by the red dashed line

the importance of constraints on the free parameters. Specifically, the sign of A determines the sound speed, as $A \geq 0$ would lead to imaginary sound speeds $c_s^2 \leq 0$. This reinforces the interpretation of A as temperature, as discussed in Ref. [58]. Notably, Figure 2.2 indicates that the sound speed rate of change is constrained by the scale factor at the turning point a_M. For $a < a_M$, the rate of change is real (normal), while for $a > a_M$ (the phantom regime), it is imaginary. We also observe that the model meets the causal and classical instability conditions, given that the sound speed range is bounded by $0 \leq c_s^2 \leq 1$ [75]. These conditions ensure consistency with special relativity laws and the constant value for the speed of light.

The framework established in Chapter 1 serves as the foundation for our derivations. In Chapter 2, we provided an overview of previously explored UDE models. Our current focus is to assess the temporal evolution of perturbations of these models and ascertain their potential contribution to gravitational instability, a precursor to structure formation. Our ultimate goal is to compare these

findings with the well-established ΛCDM model. Chapter 3 introduces linear and non-linear perturbation theory, enabling us to examine the evolutionary dynamics of cosmic structures.

Chapter 3

Perturbation theory

To ensure consistency in our analysis of the GCG and Logotropic models, we follow the methodologies outlined in Chapter 1. This chapter focuses on the ΛCDM model, which describes a homogeneous and isotropic universe using the FLRW metric. While the ΛCDM model is suitable for large scales, it is important to investigate small perturbations to account for the formation and evolution of cosmic structures over time. In Chapter 2, we introduced UDE models that unify dark matter and dark energy. To understand the evolution of these models and their equations of state, we employ perturbation theory, as discussed in §1.5 for the linear case.

3.1 Linear and non-linear evolution for UDE models

Perturbation theory serves as a fundamental framework in cosmology, offering insights into the formation of cosmic structures. It operates on the premise of an early universe that is nearly uniform, a concept supported by the presence of minor anisotropies in the Cosmic Microwave Background (CMB). These initial small perturbations, influenced by self-gravity, undergo evolution to give rise to nonlinear structures [72]. Often referred to as the "seeds" of cosmic structure, these perturbations are predicted by the inflation scenario and exhibit significant agreement with observational data [45].

We seek a generalized method of assessing the perturbations at the background level, leading to the use of second-order perturbations where instead, we do not linearize the Euler and Poisson equation as was done in the case of Newtonian dynamics in §1.5. Instead we can derive the full equation which remains identical to Newtonian laws except for dust. Following the expression derived in Equation (1.65) which can be rewritten using (B.36) and defining the conformal Hubble quantity as $\mathcal{H} = Ha$ to better describe gravitational instability in structure formation. The following describes the sub-horizon [27] equation for a single pressureless fluid as,

$$\delta'' + \mathcal{H}\delta' - \frac{3}{2}\mathcal{H}^2\delta = 0, \tag{3.1}$$

which allows us to derive an expression for the rate of growth δ in terms of the e-folds $N = \ln a$,

$$\frac{\mathrm{d}^2\delta}{\mathrm{d}N^2} + \left(1 + \frac{\mathcal{H}'}{\mathcal{H}}\right)\frac{\mathrm{d}\delta}{\mathrm{d}N} - \frac{3}{2}\Omega_m\delta = \frac{4}{3}\frac{1}{1+\delta}\left(\frac{\mathrm{d}\delta}{\mathrm{d}N}\right)^2 + \frac{3}{2}\Omega_m\delta^2, \tag{3.2}$$

where the left side of the equation is linearized, following a similar approach as described in §1.5. However, the right side introduces new non-linear terms. The rate of growth δ also incorporates a spatial component, which will be valuable for the subsequent explanations. Since it is unclear whether all variants of UDE models perform linearly, it is important to employ a method of assessment using less stringent constraints in terms of linearity. This transitions us to the discourse on the Spherical Collapse Model.

3.1.1 Spherical Collapse model

The goal of this dissertation is to assess the suitability of a specific equation of state (EoS) for describing the evolution of structure in the universe. However, it is important to recognize that linearity may not always hold true. To overcome this limitation, a generalized approach is necessary that can account for structure formation regardless of linearity. The Spherical Collapse model (SC) [76, 77] is a semi-analytical model derived from General Relativity by assuming negligible shear [78]. In order to achieve this, we will utilize Equation (3.2), which represents the density contrast in spherical perturbations.

Authors [77, 48] have demonstrated that the SC model accurately reproduces the non-linear evolution of the Pseudo-Newtonian approach proposed in Ref. [79]. This model allows for the analysis of a multifluid system while preserving the parameterization of the EoS. By starting with the continuity equation for a specific EoS, $p_i = w_i\rho_i$, the SC model enables the calculation of perturbation evolution in the universe.

For a given spherical region with radius r and uniform density ρ_{ci}, we postulate that this region will either collapse under its own gravitational attraction or expand at a rate surpassing the average Hubble flow, leading to the formation of a void [48]. Expressing our system in terms of the spherical region denoted by the subscript ci, we have the EoS $p_{ci} = w_{ci}\rho_{ci}$, accompanied by a distinct continuity equation given by,

$$\dot{\rho}_i + 3H\rho_i(1 + w_i) = 0. \tag{3.3}$$

We note that $w_i \neq w_{ci}$ since these values describe different regions within the sphere. By defining the difference between the background as $\delta w_i \equiv w_{ci} - w_i$, we establish a relationship with the effective

sound speed, as $c^2_{\rm eff} = \delta p_i/\delta\rho_i$ (where $c^2_{\rm eff} \neq c^2_s$), thus,

$$\delta w_i = \frac{\delta\rho_i}{\rho_i + \delta\rho_i}(c^2_{\rm eff} - w_i), \tag{3.4}$$

and serves as an indicator of pressure perturbations. The presence of a perturbation, denoted δ, is necessary for the existence of the factor $c^2_{\rm eff}$, whereas c^2_s is an inherent characteristic of fluid thermodynamics. Furthermore, in a perturbed system the critical determinant of the dynamical behaviour in the perturbed region is described by the ratio $c^2_{\rm eff} = \delta p/\delta\rho$, rather than $c^2_s = \partial p/\partial\rho$ [80] as shown in Chapter 2.

For the SC model, we assume the EoS remains the same both inside and outside the sphere, implying $\delta w_i = 0$ and thus, $w_i = w_{ci}$. Consequently, Equation (3.4) simplifies to $c^2_{\rm eff} = w_i$. This simplification allows us to express the second Friedmann equation for the spherical region as follows;

$$\begin{aligned} \frac{\ddot{a}}{a} &= -\frac{4\pi G}{3}\left(\rho + 3p\right), \\ \frac{\ddot{r}}{r} &= -\frac{4\pi G}{3}\left(\rho_c + 3p_c\right), \end{aligned} \tag{3.5}$$

where the density (ρ) and pressure (p) represent the total contributions from all fluids, whereas in Equation (3.3), they pertain to individual fluids. To define the density contrast for a specific fluid with subscript i, we can express it as,

$$\delta_i + 1 = \frac{\rho_{ci}}{\rho_i}. \tag{3.6}$$

Taking the time derivative of δ_i and using Equations (3.3) and (3.5) we arrive at,

$$\dot{\delta}_i = 3(1+\delta_i)(H-h)(1+w_i), \tag{3.7}$$

where the local Hubble flow is denoted by $h = \dot{r}/r$. Differentiating with respect to time and substituting the background for the spherical region from Equation (3.2), results in the non-linear evolution of δ_i given by,

$$\begin{aligned} &\ddot{\delta}_i + \left(2H - \frac{\dot{w}_i}{1+w_i}\right)\dot{\delta}_i - 4\pi G\left(1+w_i\right)\left(1+\delta_i\right)\sum_j \rho_j\delta_j\left(1+3w_j\right) \\ &\quad = \left[\frac{4+3w_i}{3\left(1+w_i\right)}\right]\frac{\dot{\delta}_i^2}{1+\delta_i}, \end{aligned} \tag{3.8}$$

which is explicitly written in terms of the background only. We show this is equivalent to the Pseudo-Newtonian perturbations for a pressureless fluid in §3.1.2 below.

3.1.2 Pseudo-Newtonian perturbations

In reference to [48], a comparative analysis is presented between the SC model and the Pseudo-Newtonian (PN) model [79] with the aim of establishing the equivalence of the linear and non-linear regimes under the condition that $c_s^2 = w$ and $\vec{\nabla}\delta_i = 0$. This equivalence implies that the EoS remains consistent both inside and outside the sphere in terms of the Lagrangian framework. The derivation presented by Ref. [79] serves as a reference for this analysis beginning with expressions for density, velocity and gravitational potential,

$$\begin{aligned}
&\frac{\partial \rho_i}{\partial t} + \vec{\nabla}_r \cdot (\vec{u}_i \rho_i) + p_i \vec{\nabla}_r \cdot \vec{u}_i = 0, \\
&\frac{\partial \vec{u}_i}{\partial t} + \left(\vec{u}_i \cdot \vec{\nabla}_r\right) \vec{u}_i = -\vec{\nabla}_r \Phi - \frac{\vec{\nabla}_r p_i}{\rho_i + p_i}, \\
&\nabla_r^2 \Phi = 4\pi G \sum_j \left(\rho_j + 3p_j\right),
\end{aligned} \tag{3.9}$$

where ρ_i, p_i, u_i, and Φ represent the density, pressure, velocity, and Newtonian gravitational potential, respectively, for a perfect fluid. The equations presented above provide generalized forms of the continuity equation and Euler's equation, which are applicable to each individual fluid species denoted by subscript i. Furthermore, these equations encompass the modified Poisson equation, which applies to the cumulative sum of all fluid species. Cosmological perturbations arise when we consider heterogeneous deviations from the background quantities [48], given by,

$$\begin{aligned}
\rho_i &= \rho_{0_i}(t) + \delta\rho_i(\vec{x}, t), \\
p_i &= p_{0_i}(t) + \delta p_i(\vec{x}, t), \\
\vec{u}_i &= \vec{u}_{0_i}(t) + \vec{v}_i(\vec{x}, t), \\
\Phi &= \Phi_0(t) + \phi(\vec{x}, t).
\end{aligned} \tag{3.10}$$

By introducing comoving coordinates $\vec{x} = \vec{r}/a$ and utilizing $\vec{\nabla}$ as the gradient operator with respect to $\vec{x}$, along with the definition $\delta_i = \delta\rho_i/\rho_{0i}$, we can express the perturbed equations similarly to [79] as,

$$\dot{\delta}_i + 3H\left(c_{\text{eff},i}^2 - w_i\right)\delta_i = -\left[1 + w_i + \left(1 + c_{\text{eff},i}^2\right)\delta_i\right]\frac{\vec{\nabla}\cdot\vec{v}_i}{a} - \frac{\vec{v}_i \cdot \vec{\nabla}\delta_i}{a}, \tag{3.11}$$

$$\dot{\vec{v}}_i + H\vec{v}_i + \frac{\vec{v}_i \cdot \vec{\nabla}}{a}\vec{v}_i = -\frac{\vec{\nabla}\phi}{a} - \frac{c_{\text{eff},i}^2 \vec{\nabla}\delta}{a\left[1 + w_i + \left(1 + c_{\text{eff},i}^2\right)\delta_i\right]}, \tag{3.12}$$

$$\frac{\nabla^2\phi}{a^2} = 4\pi G \sum_j \rho_{0_j}\delta_j\left(1 + 3c_{\text{eff},j}^2\right), \tag{3.13}$$

where c^2_{eff} is the effective sound speed for each fluid and is only a function of time. As mentioned in Ref. [79], the PN equations offer a limited approximation during the turnaround phase, particularly when the spherical region diverges from the Hubble flow. However, given our primary focus on the evolution of large-scale structures, this approximation is adequate. Now, let us proceed to define the variables involved in our analysis to arrive at expression (3.17),

$$\theta_i \equiv \vec{\nabla} \cdot \vec{v}_i, \tag{3.14}$$

$$C_i \equiv a^{-1} \vec{\nabla} \cdot \left[\left(\vec{v}_i \cdot \vec{\nabla} \right) \vec{v}_i \right], \tag{3.15}$$

$$f_i \equiv \vec{\nabla} \cdot \left[\frac{\vec{\nabla}\phi}{a} + \frac{c^2_{\text{eff},i} \vec{\nabla}\delta_i}{a\left(1 + w_i + \delta_i + c^2_{\text{eff},i}\delta_i\right)} \right]. \tag{3.16}$$

where we have defined variables θ_i, C_i and f_i. Taking the divergence of (3.12) yields,

$$\dot{\theta}_i + H\theta_i + C_i = -f_i. \tag{3.17}$$

We also define new variables A_i and B_i that will prove useful later on, described by,

$$A_i \equiv 3H \left(c^2_{\text{eff},i} - w_i \right) \delta_i, \tag{3.18a}$$

$$B_i \equiv 1 + w_i + \left(1 + c^2_{\text{eff},i} \right) \delta_i. \tag{3.18b}$$

Thus, we can rewrite (3.11) as,

$$\dot{\delta}_i + A_i + \frac{\theta_i}{a} B_i = 0. \tag{3.19}$$

Taking the partial derivative of Equation (3.19) with respect to time and utilizing (3.17) to eliminate $\dot{\theta}_i$, as well as (3.19) to eliminate θ_i, we arrive at the following expression,

$$\ddot{\delta}_i + \dot{A}_i + \left(A_i + \dot{\delta}_i \right) \left(2H - \frac{\dot{B}_i}{B_i} \right) - \frac{B_i}{a} \left(f_i + C_i \right) = 0. \tag{3.20}$$

This formulation applies to both linear and non-linear regimes making it suitable for determining the evolution of a cosmological model with equation of state dependent on density. To ensure the effectiveness of this approach, we assume the absence of non-gravitational interaction between dark energy (DE) and dark matter (DM), and that the total energy of both DE and DM within the collapsed region remains constant [81]. These approaches offer the advantage of allowing us to characterize the Dark Fluid (DF) using two functions: the background EoS parameter (w) and the effective sound speed (c^2_{eff}), as noted in [77]. Moreover, the nonlinear differential equations governing the growth of spherically symmetric perturbations in fluids, assuming an arbitrary time-dependent EoS, are found

to be,

$$\ddot{\delta}_{\mathrm{m}} + 2H\dot{\delta}_{\mathrm{m}} - \frac{4\dot{\delta}_{\mathrm{m}}^2}{3\left(1+\delta_{\mathrm{m}}\right)} = \frac{3H^2}{2}\left(1+\delta_{\mathrm{m}}\right)\left[\Omega_{\mathrm{m}}\delta_{\mathrm{m}} + \Omega_{\mathrm{de}}\delta_{\mathrm{de}}\left(1+3w_{\mathrm{de}}\right)\right] \tag{3.21}$$

$$\ddot{\delta}_{\mathrm{de}} + \left(2H - \frac{\dot{w}_{\mathrm{de}}}{1+w_{\mathrm{de}}}\right)\dot{\delta}_{\mathrm{de}} - \left[\frac{4+3w_{\mathrm{de}}}{3\left(1+w_{\mathrm{de}}\right)}\right]\frac{\dot{\delta}_{\mathrm{de}}^2}{1+\delta_{\mathrm{de}}} = \frac{3H^2}{2}\left(1+w_{\mathrm{de}}\right)\left(1+\delta_{\mathrm{de}}\right)\left[\Omega_{\mathrm{m}}\delta_{\mathrm{m}} + \Omega_{\mathrm{de}}\delta_{\mathrm{de}}\left(1+3w_{\mathrm{de}}\right)\right], \tag{3.22}$$

where δ_m denotes the matter density contrast and δ_{de} is the dark energy density contrast component (where both are considered non-relativistic). This confirms that the SC model is consistent with the Pseudo-Newtonian approach and can be used for the assessment of perturbations in the linear and non-linear regime. In addition to utilizing the density contrast δ parameter to quantify perturbation progression, the growth index as defined below, can also serve as a valuable indicator for evaluating structural growth.

3.2 The Growth Index

The growth index (γ) tracks how quickly structures in the universe expand over time [28] and provides insights into the interplay between cosmic expansion, the growth of cosmic structures, and the properties of dark energy. In the linear regime, where gravitational collapse has not yet become dominant, it describes the rate of evolution of density perturbations. In other terms, it measures the expansion of cosmological structure. The rate of growth for matter perturbations δ_m, describes how the amplitude of matter density fluctuations evolves over time in the linear domain [82], and demonstrates how it is connected to the growth index. The growth index is described as the logarithmic derivative of the linear growth factor with respect to the logarithm of the scale factor, or,

$$f \equiv \frac{d\ln\delta}{d\ln a} \approx \Omega_m^{\gamma}(a), \tag{3.23}$$

where δ_m is the linear growth factor and a is the usual scale factor. The value of γ for the ΛCDM model is approximately $\gamma_{\Lambda CDM} \approx 6/11 \sim 0.55$. Knowing the numerical value for the background model allows us to test different models against this value, as we demonstrate in the following chapters. We emphasize the significance of the function f in quantifying the growth of matter density fluctuations in the universe. Using expression (1.65) from Chapter 1.5, we can compute the behaviour of the growth factor f for the ΛCDM model as shown in Figure 3.1, where the effective matter density is defined as,

$$\Omega_m(a) = \frac{\rho_m(a)}{\rho_m(a) + \rho_{de}(a)}. \tag{3.24}$$

Figure 3.1 illustrates the fluctuation of matter density with respect to the scale factor in the ΛCDM

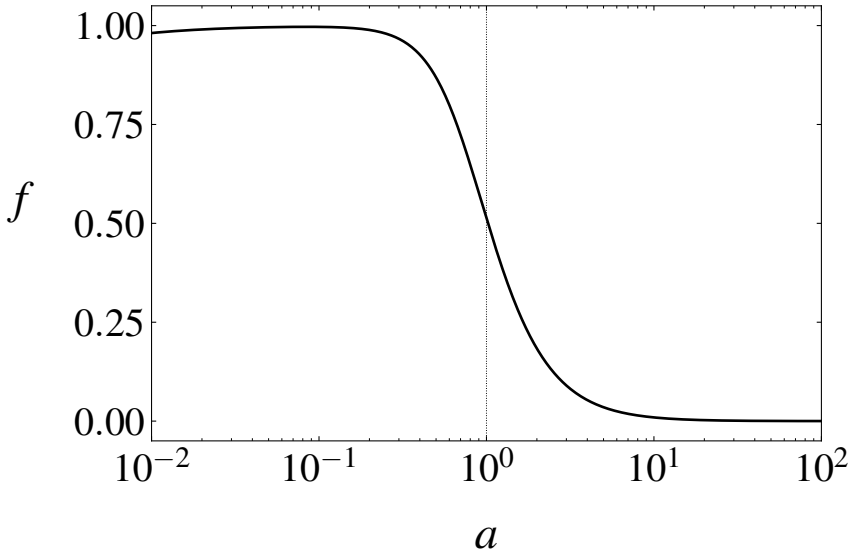

FIGURE 3.1: The growth factor f, as given by Equation (3.23), plotted against the scale factor a for the ΛCDM model.

model. With no comparison models, the function simply states that at early times, the model has a value close to unity, since normalized quantities are used throughout. As we progress to our current day ($a = 1$)/future cosmology, f decrease to zero. Depending on the cosmological model, we may have peaks and troughs, indicating accelerated or slowed structure formation. A steeper slope may indicate faster growth, while a shallower slope suggests slower growth. Analyzing the changes in slope can reveal epochs of significant influence, such as radiation domination, matter domination, or the onset of dark energy domination. Overall the relationship between the growth factor f and time, indicates crucial information regarding the rate of structure formation, along with transitional epochs.

We may test several cosmological theories and evaluate their predictions against data by measuring the growth index and comparing it to the ΛCDM behaviour. For instance, we can place restrictions on the characteristics of dark energy, such as its EoS or its clustering behaviour [83], by monitoring the growth rate of cosmic structures. The underlying nature of the cosmos and its long-term evolution can then be better understood as a result of this. As an example, the case for the ωCDM, a generalization of the ΛCDM model with constant EoS is,

$$\gamma_{\omega CDM} = \frac{3\,(w-1)}{6w-5}, \tag{3.25}$$

for the full derivation see Appendix §B.3. For the ΛCDM model where $c_s^2 = 0$ and background EoS $w = -1$, results in the theoretical index value,

$$\gamma_{\Lambda CDM} \approx \frac{6}{11}. \tag{3.26}$$

We can derive the numerical result by using the priors $c_s^2 = w = 0$ as shown in Figure 3.2, which coincides with the value in expression (3.26) as shown in Figure 3.2.

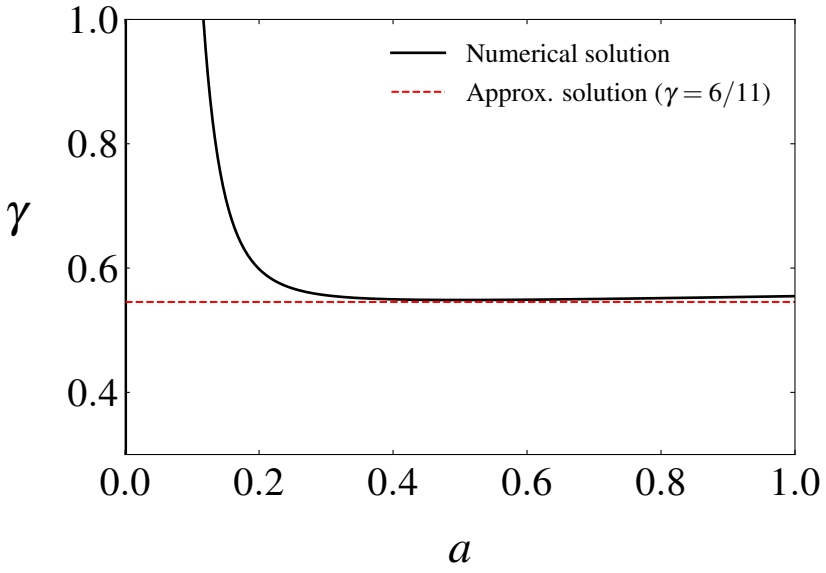

FIGURE 3.2: The numerically obtained solution using the results from Figure 3.1 in the case of ΛCDM ($\Omega_{m,0} = 0.3$) (black solid line) along with the corresponding approximate result with $\gamma = 6/11$ when we allow $c_s^2 = w = 0$ (red dashed line) [84].

The case for the non-zero sound speed (denoting $c_s^2 = s$ for simplicity), we arrive at,

$$\gamma = \frac{3(1+6s)(1-\omega)}{5+6(s-\omega)}, \tag{3.27}$$

which will become useful later on when we assess the rate of growth of each UDE model.

Understanding the perturbations of UDE models is essential for assessing their viability in describing the structure evolution in our universe. As the behaviour of these models may not always be linear, a generalized approach is required to determine the non-linear evolution of these perturbations. The SC model provides a powerful tool to study these perturbations. By applying the SC model to UDE models, we can gain insights into their ability to reproduce the observed structure formation in the universe and compare them with other well-established models, such as the ΛCDM model. Ultimately, understanding the behaviour of unified dark energy models is crucial for advancing our understanding of the universe's evolution and improving our ability to make accurate predictions about its future.

3.3 UDE linear perturbations

3.3.1 GCG perturbations

The GCG EoS as discussed in Chapter 2.1.2 relates pressure and density and allows for variation with the inclusion of the free parameter α constrained between $0 \leq \alpha \leq 1$ with positive constant A [63], expressed Equation (2.10) where p_{GCG} denotes the pressure and $\rho_{GCG} = \rho_{de} + \rho_{dm}$ represents the density of the Generalized Chaplygin gas [85]. Setting $\alpha = 1$ allows us to return to the original CG scenario. When $\alpha = 0$, we obtain a constant negative EoS, which closely resembles the ΛCDM scenario. Using the continuity equation/conservation equation as shown in §2.1.2, we arrive at an analytical solution for density given by,

$$\rho_{GCG} = \rho_{GCG,0} \left[A_s + (1 - A_s) a^{-3(1+\alpha)} \right]^{\frac{1}{1+\alpha}}, \tag{3.28}$$

where $\rho_{GCG,0}$ denotes the current day density, a the scale factor and $A_s = A/\rho_{GCG,0}^{1+\alpha}$ a dimensionless parameter. Note that we can also write A_s in terms of the effective total matter density [86] by expressing the energy density in terms of the dimensionless energy density,

$$A_s = 1 - \left(\frac{\Omega_m - \Omega_b}{1 - \Omega_b} \right)^{1+\alpha}. \tag{3.29}$$

In Figure 3.3, we can see the effect the free parameter α has on the density. A negative value of α was chosen to demonstrate that the density remains well behaved, however as we will see later on this does not hold true when assessing w and c_s^2. Negative values of α are usually excluded due to their tendency to cause instabilities, resulting in imaginary sound speeds. We can however deduce that the greater the value of α, the closer we approach the current day density represented by the solid black line.

We further define the background EoS w for the GCG model as the ratio of pressure and density,

$$w_{GCG} = -\frac{A_s}{A_s + (1 - A_s) a^{-3(1+\alpha)}}. \tag{3.30}$$

The GCG EoS parameter at the present time ($a_0 = 1$) is thus $w_{GCG,0} = -A_s$. During the Universe's expansion, the GCG model shifts from an initial matter-dominated phase ($w_{GCG} \sim 0$) to a subsequent state dominated by dark energy. Over time, it tends towards a cosmological constant scenario ($w_{GCG} \sim -1$), as demonstrated in §2.1.2 for the CG case. The resulting expression for the Hubble parameter near the present epoch is thus given by,

$$H^2 = H_0^2 \left[\Omega_{m,0} a^{-3} + \Omega_{GCG,0} \left[A_s + (1 - A_s) a^{-3(1+\alpha)} \right]^{\frac{1}{1+\alpha}} \right], \tag{3.31}$$

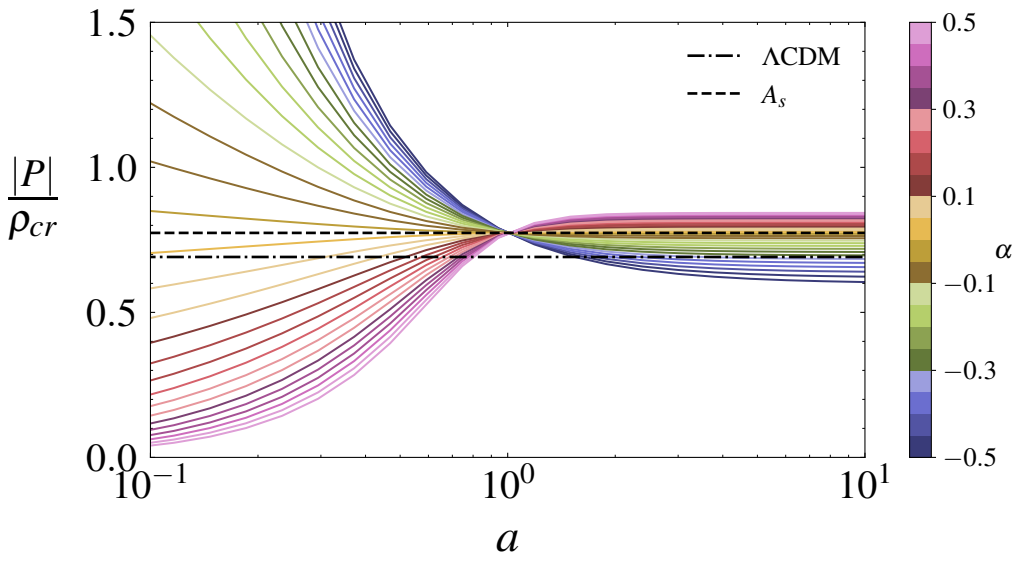

FIGURE 3.3: The pressure as it varies with the scale factor a across different values of the free parameter $-0.5 \leq \alpha \leq 0.5$, illustrating the effects of varying α compared to the ΛCDM model (represented by the black dash-dotted horizontal line).

where we consider a standard dust-like dark matter component and a component of the Generalized Chaplygin Gas (GCG) with present densities denoted by $\Omega_{m,0}$ and $\Omega_{GCG,0}$, respectively. We have neglected radiation since its contribution is negligible to the total energy density around the current epoch [65]. In Chapter 2 we discussed the significance of the sound speed in assessing the rate of evolution of specific models, which is given by Equation (1.64a). In the case of the GCG equation, this yields the expression for a barotropic fluid [87],

$$c^2_{s,GCG} = \frac{\mathrm{d}p}{\mathrm{d}\rho} = \alpha \frac{A}{\rho^{1+\alpha}_{GCG}} = -\alpha w_{GCG}. \tag{3.32}$$

As we approach the limit $z \gg 1$, both the EoS parameter w and the sound speed c_s^2 tend toward zero, indicating that the sound speed remains significantly lower than unity during the early matter-dominated epoch. However, it gradually increases as this era comes to an end. Since $w < 0$ from Equation (3.30), c_s^2 is positive for $\alpha > 0$ and negative for $\alpha < 0$. In order to grow via gravitational instability, the GCG equation follows the condition [64],

$$|c_s^2| \lesssim \frac{3}{2}\left(\frac{aH}{k}\right)^2. \tag{3.33}$$

If the condition is not met, oscillations become evident in the perturbations due to the predominance of the pressure term $(kc_s^2/a)^2$ in Equation (B.33)[1], when compared to the term $3H^2/2$. In the event of a violation of this condition with $c_s^2 < 0$, the perturbations undergo violent instabilities, exhibiting

[1]Refer to Appendix B.2 for the derivation of matter perturbations in the Newtonian gauge

exponential growth, as demonstrated b Ref. [64]. This results in a limitation on the free parameter α,

$$|\alpha| \lesssim 10^{-5}, \tag{3.34}$$

where perturbations are amplified for $\alpha \lesssim -10^{-5}$ since the sound speed is negative. For $\alpha \gtrsim 10^{-5}$, perturbations exhibit rapid oscillations as shown by [87]. Compared to the ΛCDM model, both cases are drastically different. We can resolve this issue by adding a non-adiabatic sound speed [27] that allows c_s to vanish. For the purposes of this investigation, we choose relativity large values for α thus we wont encounter these problems when we perturb the background.

In addition to the adiabatic sound speed, assuming we have perturbations, i.e. $c^2_{\text{eff}} \neq 0$, we can define the effective sound speed for the GCG EoS as,

$$c^2_{\text{eff},GCG} = \frac{\delta p}{\delta \rho} = w_{GCG} \frac{(1+\delta)^{-\alpha} - 1}{\delta}. \tag{3.35}$$

This demonstrates that the effective sound speed, determined by w and δ, depends on the background and the collapsed region. Additionally, it indicates that larger values of δ will result in smaller values of c^2_{eff}, which aligns with the expected behaviour for a GCG clump (where $\delta \gg 1$, $w \sim 0$, $c_s^2 \sim 0$ [80]). Furthermore, taking the limit as $\delta \to 0$ we show that $c^2_{\text{eff}} \to c_s^2$ as expected [88]. In this dissertation, we will adopt the assumption $\delta \gg 1$ and consider the effective sound speed to be equal to the background EoS. This is selected because the SC model shares similarities with the Pseudo-Newtonian approach when analyzing the nonlinear evolution of perturbations involving both dark matter and dark energy [48].

In the case of GCG model following a matter-like evolution, the value of α becomes irrelevant, and the squared sound speed $c^2_{s,GCG}$ is approximately 0. Yet, as we transition towards a cosmological constant, where $w_{GCG} \to -1$, the square of the sound speed is constrained by the parameter α.

Ref.	A_s		α		Data set
[89]	0.642	$+0.097$ -0.093	-0.1688	$+0.1456$ -0.2143	CMB + CC
[89]	0.730	$+0.047$ -0.047	$+0.0181$	$+0.1029$ -0.2129	CMB + JLA
[89]	0.727	$+0.040$ -0.039	-0.0156	$+0.982$ -0.1380	CMB + JLA + CC
[85]	0.7475	$+0.0556$ -0.0539	-0.0250	$+0.1760$ -0.1326	CMB + BAO + SNIa
[90]	0.76	$+0.026$ -0.039	$+0.033$	$+0.066$ -0.0071	CMB + BAO + SNIa + $H(z)$ + BBN
[91]	0.774	$+0.022$ -0.022	$+0.096$	$+0.059$ -0.074	CMB + BAO + SNIa + $H(z)$ + BBN

TABLE 3.1: Constrained values of A_s and α at 1σ confidence region obtained from previous works [91].

The constraints on the parameters A_s and α were first studied by [92]. For the original CG EoS, A_s was found to lie within the range of 0.66 to 1. However, for the GCG with $\alpha = 0.5$, A_s was limited to 0.62 to 1, and for $\alpha = 2$, the range was 0.75 to 1. Further investigations into these parameters were performed using statistical techniques [93]. Refinements to the free parameters were made, as demonstrated by [89, 85, 90, 91]. The value of A_s was established to lie within 0.549 and 0.796 at the 1σ level, as summarized in Table 3.1.

On the other hand, the values of α are less constrained and can vary depending on the dataset used. Initially, it was assumed that $0 \leq \alpha \leq 1$, but the literature in Table 3.1 illustrates that α can also be negative, influenced by different datasets and the inclusion of non-linearities.

Using the latest value of $A_s = 0.774$ reported in [91], and considering the constrained range of α ($-0.1688 \leq \alpha \leq 0.096$ from Table 3.1), we explore the impact of varying α on the background EoS and sound speed. However, for physical consistency, we restrict α to the range $0 < \alpha < 1$ to avoid imaginary sound speeds when $\alpha < 0$, even though the background behaviour remains well-behaved under such conditions. Figure 3.4 (left) illustrates the dependency of the GCG EoS parameter w_{GCG} on different values of α. A larger α results in a more rapid transition from $w_{GCG} \sim 0$ to $w_{GCG} \sim -1$, permitting the GCG model to accommodate both dark matter and dark energy, at least in terms of the background behaviour. Additionally, Figure 3.4 shows that models entering an accelerated epoch earlier undergo a faster transition [57]. The effect of the sign of α on the sound speed is demonstrated in Figure 3.4 (right), where $\alpha = -0.1$ leads to imaginary sound speeds. Smaller values of α correspond to smaller sound speeds.

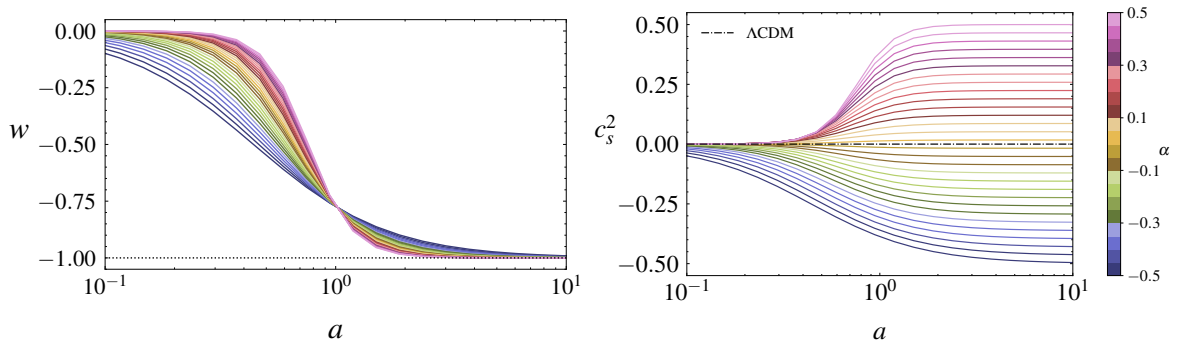

FIGURE 3.4: The background EoS (left) and the square of the sound speed (right) for the GCG EoS plotted against the scale factor, with $A_s = 0.774$ [91]. The range of $-0.5 \leq \alpha \leq 0.5$ is considered.

With the necessary functions in place to evaluate perturbations, we can now return to the previously introduced SC model and apply it to the GCG EoS for the three values of α used in Figure 3.4. Following the initial conditions laid out in [80], and working in the linear regime, our perturbations

for the matter and DE components can be characterized by [48],

$$\ddot{\delta}_{\rm m} + 2H\dot{\delta}_{\rm m} = \frac{3H^2}{2}\left[\Omega_{\rm m}\delta_{\rm m} + \Omega_{\rm de}\delta_{\rm de}\left(1+3w_{\rm de}\right)\right], \tag{3.36a}$$

$$\ddot{\delta}_{\rm de} + \left(2H - \frac{\dot{w}_{\rm de}}{1+w_{\rm de}}\right)\dot{\delta}_{\rm de} = \frac{3H^2}{2}\left(1+w_{\rm de}\right)\left[\Omega_{\rm m}\delta_{\rm m} + \Omega_{\rm de}\delta_{\rm de}\left(1+3w_{\rm de}\right)\right], \tag{3.36b}$$

where we have neglected the non-linear terms from Equations (3.21) and (3.22) up until the limit as shown in Ref. [94]. Since we are only working with the background, we will only assess Equation (3.36a). By transitioning from cosmic time denoted by a dot to conformal time denoted by primes, the derivative with respect to e-foldings, denoted $N = \ln a$, simplifies the linear differential equation to,

$$\delta'' + \left(2 + \frac{H'}{H}\right)\delta' - \frac{3}{2}\Omega_m(a)\delta = 0. \tag{3.37}$$

Inserting Equation (3.31) for H, H' and $\Omega_m(a)$ from Equation (3.24), similarly to Ref. [95] we arrive at expression (3.37). Figure 3.5 illustrates that in the linear regime, the GCG model exhibits a slower

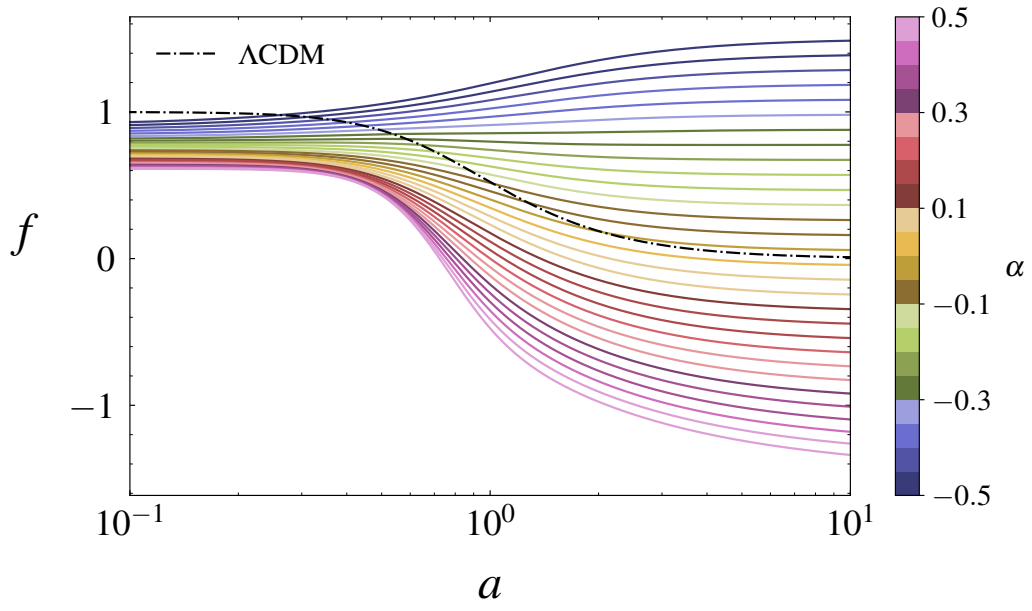

FIGURE 3.5: Linear density growth, specifically for matter perturbations scaled by a for the ΛCDM model (black dashed line) and the GCG EoS for $-0.5 \leq \alpha \leq 0.5$.

growth rate compared to the ΛCDM model. The sign for α plays an important role since we head into negative growth factors which are deemed nonphysical and deviate significantly from our base comparison. While many studies use the power spectrum for such comparisons with the standard model, for simplicity, we will focus on the matter density contrast. It is important to clarify whether we allow the GCG fluid to cluster. In this dissertation, we assume that the only clustering component is matter, implying $\delta_{de} = 0$. For future works we can remove this assumption to assess the non-linear regime, i.e. the DE case. Figure 3.6 shows the growth factor varying with the scale factor compared to

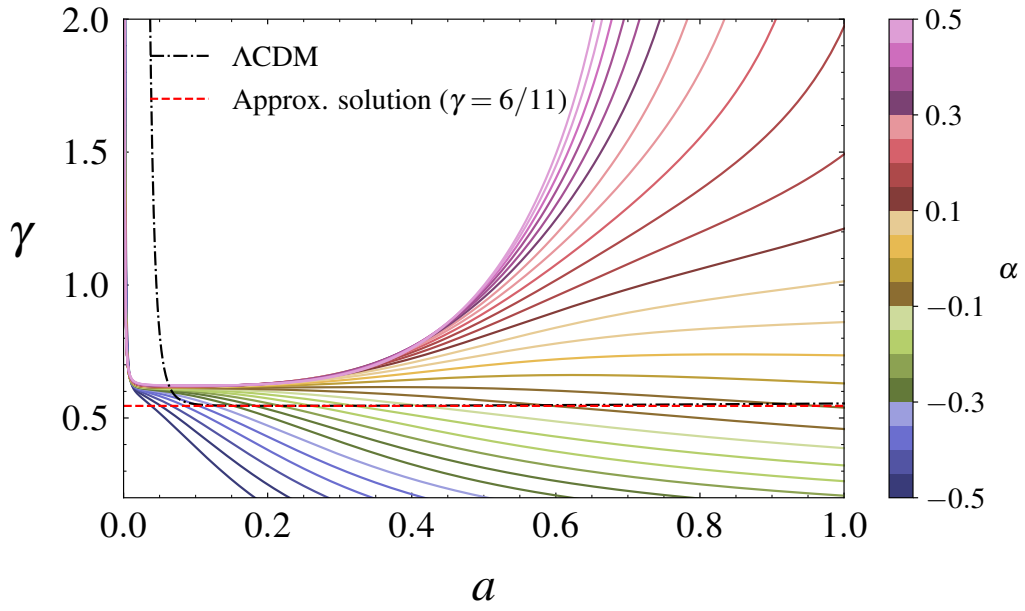

FIGURE 3.6: The growth factor γ plotted against the scale factor a for the ΛCDM model (black dashed line) and the GCG EoS for $-0.5 \leq \alpha \leq 0.5$.

the ΛCDM scenario. The model is relatively well behaved and aligns with the value for the ΛCDM model for a range $0 \leq \alpha < 0.1$. This is useful as it serves as an initial test in comparing models without the bias of observational data sets. The pressure plays a critical role in the GCG model, significantly influencing structure formation during the matter era. Successful structure formation, especially in the linear perturbations regime, requires effective pressure suppression. However, to account for late-time cosmic acceleration, a negative pressure becomes necessary. Satisfying both of these demands simultaneously presents a challenge within the GCG model [27].

3.3.2 Anton-Schmidt's equation of state and the Logotropic model

The Anton-Schmidt equation of state (A-S EoS), as discussed in §2.1.4, can be categorized into four distinct scenarios [73, 72]. For simplicity, we will focus on the case where the parameters n and γ are unrestricted. The specific EoS, which we will refer to throughout our analysis, is provided in [72] and given by,

$$p_{A-S} = A \left(\frac{\rho}{\rho_*}\right)^{-n} \ln\left(\frac{\rho}{\rho_*}\right). \tag{3.38}$$

The A-S EoS (3.38) consists of the positive free parameter A, which represents a Logotropic temperature [58], the reference density ρ_*, and the number density n. In the special case where $n = 0$, the equation reduces to the pure Logotropic scenario described in §A.3.3. To derive the density, we employ the first law of thermodynamics as discussed in §2.1.3. Substituting the EoS (3.38) into Equation

(2.24), we obtain the total density parameter given by,

$$\epsilon = \rho + \frac{3A}{(n+1)}\left(\frac{\rho_{m,0}}{\rho_*}\right)^{-n} a^{3n}\ln a - \frac{A}{(n+1)}\left(\frac{\rho_{m,0}}{\rho_*}\right)^{-n} a^{3n}\left[\ln\left(\frac{\rho_{m,0}}{\rho_*}\right) + \frac{1}{(n+1)}\right]. \tag{3.39}$$

In this method, the first term represents a pressure-less fluid akin to matter, while the second term incorporates pressure effects and can be understood as the dark energy component. Thus, this approach aims to unify dark matter and dark energy into a single dark fluid. However, for the sake of comparison with the conventional scenario, where matter and dark energy are treated as separate fluids, we revert to Equation (2.26) to describe the total energy density as,

$$\epsilon = \epsilon_m + \epsilon_{de}, \tag{3.40}$$

where the full derivation can be found in Appendix A.3.3,

$$\epsilon = \epsilon_{m,0}a^{-3} + \frac{3A}{(n+1)}\left(\frac{\rho_{m,0}}{\rho_*}\right)^{-n} a^{3n}\ln a + \epsilon_{de,0}a^{3n}. \tag{3.41}$$

To compute the background parameter $w = p/\epsilon$ based on the Logotropic temperature, we reorganize Equations (3.38) and (3.41) to be expressed in terms of the dimensionless parameter B, defined as[2],

$$B = \frac{A}{n+1}\left(\frac{\rho_{m,0}}{\rho_*}\right)^{-n}\frac{1}{\epsilon_c\Omega_{de,0}}, \tag{3.42}$$

where the normalized density parameters Ω_i can be written as,

$$\Omega_{m,0} \equiv \frac{\epsilon_{m,0}}{\epsilon_c}, \tag{3.43a}$$

$$\Omega_{de,0} \equiv \frac{\epsilon_{de,0}}{\epsilon_c}, \tag{3.43b}$$

where ϵ_c corresponds to the critical density ($a_0 = 1$). Additionally, it is worth noting that this formulation fulfills the condition $\Omega_{de,0} = 1 - \Omega_{m,0}$, where $\Omega_{de,0}$ represents the dark energy density parameter and $\Omega_{m,0}$ represents the matter density parameter.

Having decomposed the contributions from dark energy and matter, we can express the EoS as $w_{de} = p_{de}/\epsilon_{de}$ for the dark energy component and $w = p/\epsilon$ for the total contribution. Consequently,

[2]This is purely for convenience and similarly performed by Ref. [72]

the pressure and density can also be expressed in terms of dimensionless parameter B as,

$$p = -\epsilon_c \left(1 - \Omega_{m,0}\right) \left[B + (n+1)(1 + 3B \ln a)\right] a^{3n}, \tag{3.44a}$$

$$\epsilon = \Omega_{m,0} a^{-3} \epsilon_c + \left(1 - \Omega_{m,0}\right) \left(1 + 3B \ln a\right) a^{3n} \epsilon_c. \tag{3.44b}$$

Thus for the background EoS we obtain,

$$w = -\frac{\left(1 - \Omega_{m,0}\right) \left[B + (n+1)(1 + 3B \ln a)\right] a^{3n}}{\Omega_{m,0} a^{-3} + \left(1 - \Omega_{m,0}\right) \left(1 + 3B \ln a\right) a^{3n}}. \tag{3.45}$$

For the epoch where matter is negligible in comparison to DE, we can simplify the pressure in Equations (3.44a) and (3.44b) to,

$$p_{de} = -\epsilon_c \left(1 - \Omega_{m,0}\right) \left[B + (n+1)(1 + 3B \ln a)\right] a^{3n}, \tag{3.46a}$$

$$\epsilon_{de} = \epsilon_c \left(1 - \Omega_{m,0}\right) \left(1 + 3B \ln a\right) a^{3n}. \tag{3.46b}$$

Thus for the background DE we arrive at,

$$w_{de} = -\frac{B}{\left(1 + 3B \ln a\right)} - (n+1). \tag{3.47}$$

The determination of the sound speed is essential for understanding the early formation of structures in the universe [96]. To calculate the value, we adopt a similar approach to the GCG derivation discussed in Chapter 2 by utilizing Equation (2.40), which is applicable to an adiabatic fluid[3],

$$c_s^2 = \frac{\partial p}{\partial a} \left(\frac{\partial \rho}{\partial a}\right)^{-1} = \frac{\left(1 - \Omega_{m,0}\right)}{\Omega_{m,0}} a^{3(n+1)} \left[B(1 + 2n) + n(n+1)(1 + 3B \ln a)\right]. \tag{3.48}$$

3.3.3 The importance of B

In Chapter 2.1.3, we examined the pure Logotropic case were $n = 0$ in the A-S model. However, by introducing two additional free parameters, B and n, which can potentially vary with the scale factor, we gain flexibility in selecting optimal values for these parameters based on previous studies. Before we proceed to discuss specific numerical values, it is worth highlighting the significance of the Planck density in relation to B. In the general Logotropic Dark Fluid (LDF), the parameters A and n are both free, with A representing the minimum energy density that depends on B [58]. In [69] they interpret B as a dimensionless Logotropic temperature and demonstrate how it bares resemblance to

[3]For the full derivation of $p, p_{de}, w, w_{de}, c_s^2$ see §A.3.3

the ratio between the Planck density ρ_{Pl} and the cosmological density ρ_Λ given by,

$$\frac{\rho_{Pl}}{\rho_\Lambda} \sim 10^{123}, \tag{3.49}$$

this underlies the cosmological constant problem discussed in Chapter 1. Equation (3.49) describes the disproportionate order of magnitude between cosmological observations and predictions from particle physics and quantum field theory. Incorporating this value enables us to address the discrepancies by including it in defined dimensionless constants. Thus, we can express B as,

$$B \simeq \frac{1}{\ln\left(\frac{\rho_{Pl}}{\rho_\Lambda}\right)} \simeq \frac{1}{123\ln(10)}. \tag{3.50}$$

Using the latest values from [3] we can determine a more precise value given by,

$$A = B\rho_{de,0}c^2, \tag{3.51}$$

where $\rho_{de,0} = (1-\Omega_{m,0})\rho_c = 6.72 \times 10^{-24}\text{gm}^{-3}$ [68] at present time. Using the relation in Equation (2.26) we obtain a ratio for the Planck density and dark energy density,

$$\frac{\rho_{Pl}}{\rho_{de}} = \frac{\Omega_{m,0}}{(1-\Omega_{m,0})}\exp\left\{1+\frac{1}{B}\right\}. \tag{3.52}$$

We can extract values for ρ_{de}, ρ_{Pl}, and $\Omega_{m,0}$ from [5] to calculate the following,

$$B_{pl} = \left[\ln\left(\frac{(1-\Omega_{m,0})}{\Omega_{m0}}\frac{\rho_{Pl}}{\rho_{de}}\right) - 1\right]^{-1} = 3.53 \times 10^{-3}. \tag{3.53}$$

The identification of the value for B with the Planck density ρ_{Pl} [58, 68] potentially eliminates its status as a free parameter. Part of this investigation will be to determine the effect the parameter B has on the perturbations and the background.

The utilization of the variable B, as indicated in Equation (3.42), becomes crucial in deriving an equivalent value and expression for more generalized equations of state. This reconciliation between the A-S EoS and LDF ensures their mutual consistency. In a comprehensive MCMC analysis conducted by Boshkayev et al. (2021) [73], four distinct Anton-Schmidt equations of state, incorporating free parameters n and γ, were thoroughly examined. We will touch on these finding as well as compare the viability of introducing more free parameters in attempting to reproduce and remedy present day values and problems.

Capozziello et al. (2017) [72] first introduced the Anton-Schmidt's EoS as a cosmological model

by providing further generalization of the Logotropic model. Building upon this, Boshkayev et al. (2019) [74] expanded the class of Logotropic fluids by considering the Anton-Schmidt EoS as a more general form and comparing the effect varying n and γ (Grüneisen parameter) has. They investigated a universe governed by a single fluid, where the pressure evolves based on a logarithmic EoS. Following this definition, four classes of Logotropic models emerged, (where Model I and II are the A-S gases), to assess the viability against observational data and the current ΛCDM model [73]. In the first case, the parameter n is assumed to be constant throughout cosmic evolution, making it a free parameter of the model. This represents the simplest A-S scenario, where the temperature of the Universe has a minimal influence on the fluid's evolution. In the second case, they fix $n = -1$, resulting in negligible temperature effects and removing n as a free parameter from the model. These two approaches correspond to the extreme cases of the more general Logotropic models discussed as a third case where $n = 0$ (the pure Logotropic framework). Lastly, they introduce a new Logotropic model formulation as a further case, assuming a specific scenario for the pressure. This case attempts to resolve the negative sound speed issue by removing the constant temperature approximation on n, however it was found that further investigation was needed to determine how the Grüneisen parameter depends on temperature. Subsequently, in Ref. [97], the authors explored the different findings from [73] and discovered that further generalizations of the logarithmic EoS results in decreased statistical predictability.

In Ref. [75], they investigated generalized Logotropic models, introducing specific cases for A_i in which A can vary with respect to i. To maintain consistency among these works, we adopt the EoS presented in [75],

$$p = \sum_{i=0}^{N} A_i \ln^i \left(\frac{\rho}{\rho_*} \right), \tag{3.54}$$

where ρ_* is reference density. In [97], a different approach is taken where the parameter A is fixed as a constant, and only n is varied resulting in the equation,

$$p = A \ln^n \left(\frac{\rho_m}{\rho_{Pl}} \right), \tag{3.55}$$

with Planck density ρ_{Pl} as the reference density and n being a real parameter. The study conducted in [97] reveals that both the original Logotropic model and its generalized versions do not provide strong statistical evidence against the ΛCDM scenario. The pure Logotropic model, in particular, exhibits greater predictability compared to the Anton-Schmidt model. The generalized versions of the pure Logotropic model show minimal deviation from experimental expectations, particularly regarding the free coefficients. As a result, these models exhibit degeneracy with the concordance paradigm. It was concluded in Ref. [97] that the original Logotropic model [58, 69] has an equal

number of parameters as the ΛCDM model if we identify ρ_* with the Planck density. At the large-scale cosmological background level, the model behaves similarly to the ΛCDM model for about 25 billion years into the future. However, it potentially addresses certain issues encountered by the ΛCDM model, such as the core-cusp problem, universal surface density, and the Tully-Fisher relation, particularly concerning dark matter halos at small scales. This makes it an intriguing alternative to the ΛCDM model. However, it faces a disadvantage: although the squared speed of sound is positive during the relevant period, it increases over time and becomes excessively large in the present epoch, posing challenges at the perturbative level [98, 99].

Reference	n		Data set
[72]	-0.147	$+0.113$ -0.107	OHD + JLASNeIa + BAO
[73]	$+0.004$	$+0.015$ -0.009	SNeIa + OHD
[97]	-0.492	$+0.621$ -0.751	SNeIa + OHD + σ_8

TABLE 3.2: Free parameter n for different data sets. References only refer to the value for n since we are comparing the hydrodynamical Logotropic case with the more general thermodynamical Anton-Schmidt EoS.

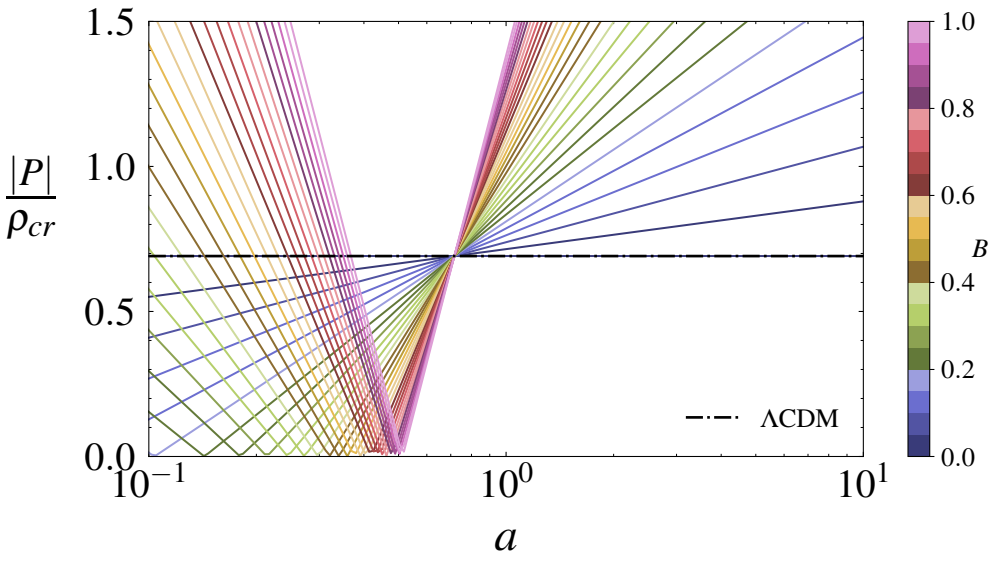

FIGURE 3.7: The pressure is depicted across various values of the free parameter B as the scale factor a changes, showing how different values of B affect the pressure's sign compared to the ΛCDM model (shown by the black horizontal line).

In Table 3.2, the only free parameter is n, as B can be fixed as a constant through analytical calculations. This reduces the statistical uncertainty associated with determining the MCMC parameterization. Following the concluding remarks by [73], we choose the original Logotropic model[4], where dark matter and baryons are disentangled. This choice is further justified by the conclusion stated

[4] modified $n = 0$, model IV in [73]

in [73] that Logotropic models perform better than Anton-Schmidt variants, and the case for $n = -1$ is completely ruled out as shown in [100]. The study demonstrated that Logotropic models exhibit less stability compared to the standard cosmological paradigm, and there is no statistical advantage in utilizing a Logotropic and/or A-S universe over the ΛCDM, ωCDM, and CPL scenarios. Thus we can assess the background for the original Logotropic model given by,

$$p = A \ln\left(\frac{\rho_m}{\rho_{Pl}}\right), \tag{3.56}$$

and compare the scenario where we take the rest mass density of the LDF, denoted ρ_{DF} [75],

$$p = A \ln\left(\frac{\rho_{DF}}{\rho_{Pl}}\right), \tag{3.57}$$

where A is a new fundamental constant and ρ_{Pl} is the Planck density resulting in a dimensionless term inside the logarithm. This EoS provides the unification of DM and DE [75, 99], however this introduces a new problem in that we can no longer use the relation in Equation (3.51) which allows us to relate the Planck density and critical density via the dimensionless variable B in Equation (3.53). Going back to the original formulation of the Logotropic model (3.56), where $\epsilon = \epsilon_m$, the energy density is given by,

$$\epsilon = \epsilon_{dm} - A\left[1 + \ln\left(\frac{\epsilon_m}{\rho_{Pl}}\right)\right], \tag{3.58}$$

where the first term is the DM term and the second term is the DE. In terms of the scale factor this gives us pressure in the form,

$$p = -A\left(1 + \frac{1}{B} + 3\ln a\right), \tag{3.59}$$

and resulting density given by,

$$\epsilon = \frac{\Omega_{m,0}\epsilon_{cr}}{a^3} + A\left(\frac{1}{B} + 3\ln a\right), \tag{3.60}$$

where ϵ_{cr} is the critical density ($a = 1$). This coincides with the same expression in Equation (3.51). We note that $A > 0$, and since $A = B\epsilon_{cr} = 3.53 \times 10^{-3}\epsilon_{cr}$ [68], the pressure and density become,

$$p = -(1 - \Omega_{m,0})\epsilon_{cr}(B + 1 + 3B\ln a), \tag{3.61a}$$

$$\epsilon = \frac{\Omega_{m,0}\epsilon_{cr}}{a^3} + \epsilon_{cr}(1 - \Omega_{m,0})(1 + 3B\ln a). \tag{3.61b}$$

Figure 3.7 presents the plot of energy density ϵ with respect to the free parameter B, illustrating how it evolves over time. Notably, as B increases, the universe begins to deviate from the ΛCDM case represented by the black line. Initially, for all values of B, the energy density starts at infinity.

However, it gradually decreases with the expansion of the scale factor a, reaching a minimum, and then exhibits an increase for specific values $0 < B \leq 1.0$. Comparing these results with those in [75], it becomes evident that the magnitude of B significantly influences the energy density during the evolution of the Universe. Consequently, it is crucial to set B sufficiently small to replicate the behaviour of the ΛCDM model, thereby relating it conveniently to the Planck density [69].

Taking the ratio of pressure and total energy density results in,

$$w = \frac{p}{\epsilon} = -\frac{\left(1-\Omega_{m,0}\right)\left(1+B+3B\ln a\right)}{\Omega_{m,0}a^{-3}+\left(1-\Omega_{m,0}\right)\left(1+3B\ln a\right)}, \tag{3.62}$$

with the dimensionless speed of sound given by [99],

$$c_s^2 = p'(\epsilon) = \frac{B}{\epsilon/\epsilon_{cr}-1}. \tag{3.63}$$

We can also write the sound speed in terms of dimensionless density $\Omega_{m,0}$ provided $B \neq 0$ (in which case $c_s^2 = 0$ at all times) as,

$$c_s^2 = \left(\frac{\Omega_{m,0}}{B\left(1-\Omega_{m,0}\right)}a^{-3}-1\right)^{-1}. \tag{3.64}$$

To explore the impact of parameter B on the background, we investigate its relationship by considering a range of values: $0 \leq B \leq 1$ (depicted in Figure 3.7). In the plot depicted right of Figure 3.8, it can be observed that the sound speed deviates at scale factor $a_{(w=-1)}$, showing positive values for scale factor $a < a_{(w=-1)}$ and negative values for scale factor $a > a_{(w=-1)}$. This divergence occurs only for models where $B < \Omega_{m,0}/(1-\Omega_{m,0})$, specifically limited to $a > 1$. Consequently, the Logotropic fluid model proves to be effective throughout the present time, ensuring a continuous evolution of the sound speed. By analyzing the influence of the order of magnitude of B on the background (see Figure 3.8), we can gain valuable insights from this analysis.

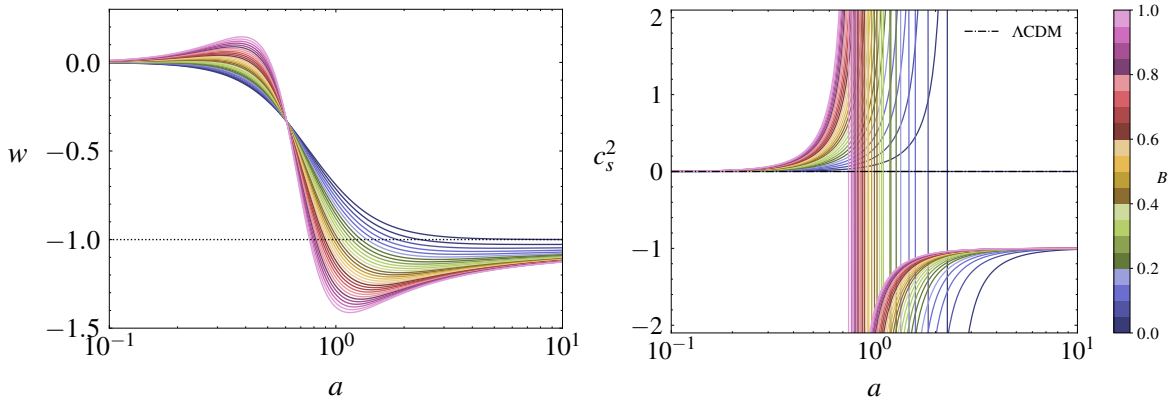

FIGURE 3.8: The background EoS w (left) and the squared of the sound speed c_s^2 (right) of the Logotropic EoS varying with the scale factor a, with varying free parameter $0 \leq B \leq 1.0$.

The Logotropic model demonstrates remarkable consistency with observations, achieved by introducing a parameter B that allows it to precisely recover the ΛCDM model when B is set to 0, as illustrated in Figure 3.8 [69]. Notably, what distinguishes this theory is that B deviates from the conventional concept of a free parameter found in other cosmological models, which often involve multiple free parameters. Instead, B is determined by well-defined physical considerations, effectively acting as a fundamental constant with a fixed value of $B = 3.53 \times 10^{-3}$. The significance of defining B in Equation (3.50) lies in its role in addressing the disparity between the energy density predicted by particle physics and the observational results from cosmological measurements. With this definition, one can interpret B as the inverse dimensionless Logotropic temperature, defining a new cosmological constant that shares similar orders of magnitude with theoretical predictions. Furthermore, the slight yet non-zero value of B corresponds to the non-zero value of the Planck constant $\hbar$, suggesting potential involvement of quantum mechanics in the realm of DM and DE on a cosmological scale.

We can assess the growth of structures by looking at how δ evolves. Following the procedure in §3.1.1 we can determine how the background evolves with the scale factor using the following Equation,

$$\delta'' + (A\delta)' + \left[\left(2 + \frac{H'}{H}\right) - \frac{B'}{B}\right]\left(\delta' + A\delta\right) - Bf\delta = 0, \tag{3.65}$$

where,

$$A = 3(c_s^2 - w), \qquad B = 1 + w, \qquad f = \frac{3}{2}(1 + 3c_s^2)\Omega_m(a) \tag{3.66}$$

There are two free parameters in Equation (3.65), the sound speed which we will denote $c_s^2 = s$ for simplicity and the background EoS w. Following a similar procedure to [73] we allow the clustering component be due to matter, and set $w = 0$, while we leave the adiabatic sound to be applied to the whole model. This simplifies our expression to,

$$\delta'' + 3(s\delta)' + \left(2 + \frac{H'}{H}\right)\left(\delta' + 3s\delta\right) - \frac{3}{2}(1 + 3s)\Omega_m(a)\delta = 0, \tag{3.67}$$

where we can express the term H'/H in terms of the barotropic index given by,

$$\frac{H'}{H} = -\frac{3}{2}(w + 1). \tag{3.68}$$

Note that the Hubble rate in terms of observational dimensionless constraints Ω_i from Equation (3.61b) yields the equation,

$$H^2 = H_0^2\left[\Omega_{m,0}a^{-3} + \Omega_{DE,0}(1 + 3B\ln a)\right] \tag{3.69}$$

where $\Omega_{DE,0} = 1 - \Omega_{m,0}$ represents the present-day density parameter values for matter and DE, respectively. [69]. In Figure 3.9, we observe the density contrast for the Logotropic Dark Fluid (LDF)

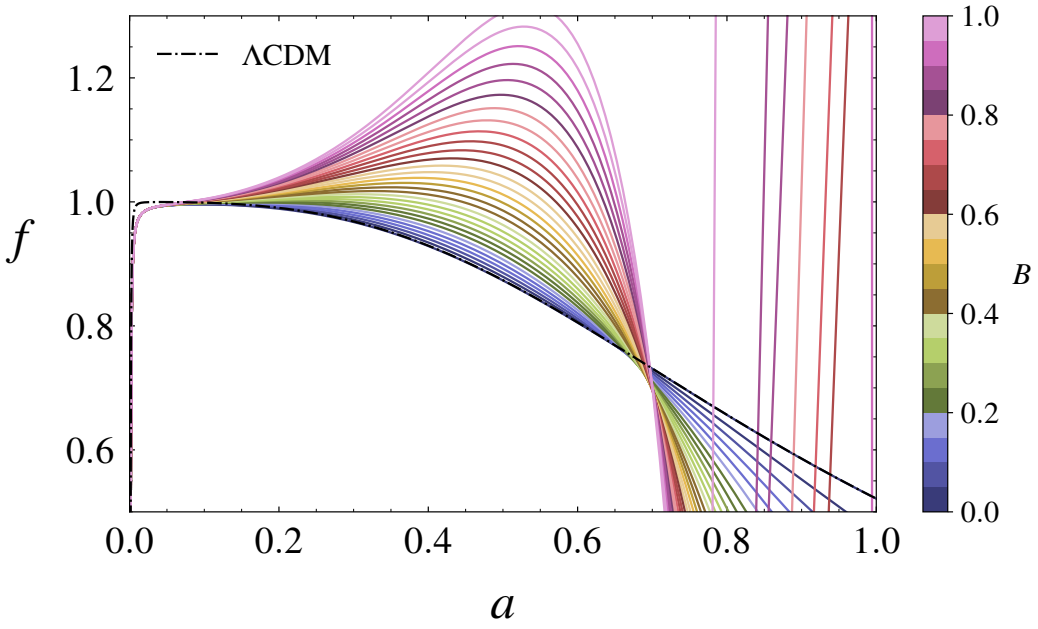

FIGURE 3.9: Growth factor f varying with the scale factor for the ΛCDM model (black line) and original Logotropic EoS with range of values between $0 \leq B \leq 1$ with fixed reference density given by the Planck density.

model across varying values of B, with a fixed reference density given by the Planck density,

$$\rho_{Pl} = \frac{m_{Pl}}{l_{Pl}^3} = \frac{m_{Pl}}{\left(\frac{1}{m_{Pl}}\right)^3} = (m_{Pl})^4 = 2.2223 \times 10^{76} \quad \text{GeV}^4. \tag{3.70}$$

Despite $B = 0$ (blue line) being expected to reproduce the ΛCDM model, it deviates from it at the perturbative level, while still preserving the general behaviour. In Figure 3.9 we clearly observe how smaller values of B affect the growth of structures. On the other hand, the large value $B = 1$ exhibits significant deviations from the ΛCDM model, reinforcing the need for B to be sufficiently small, aligning with the findings in Ref. [69]. Remarkably, the order of magnitude of $B \sim 10^{-3}$ corresponds to the derived value of B using the Planck density which is virtually indistinguishable compared to $B = 0$ according to Figure 3.9.

The following was done to explore the impact of the order of magnitude of B has at the background level of the Logotropic EoS. Initially, we examined small values of B, which successfully replicated certain characteristics observed in the ΛCDM model, such as freezing out towards late times. However, perturbing the background (as shown in Figure 3.9) led to a different scenario. Additionally, for non-zero values of B, specifically $B = 3.53 \times 10^{-3}$, derived from the Planck density, we demonstrate the behaviour through the background and sound speed, as shown in Figure 3.10. This aids in addressing the nature of a non-zero B.

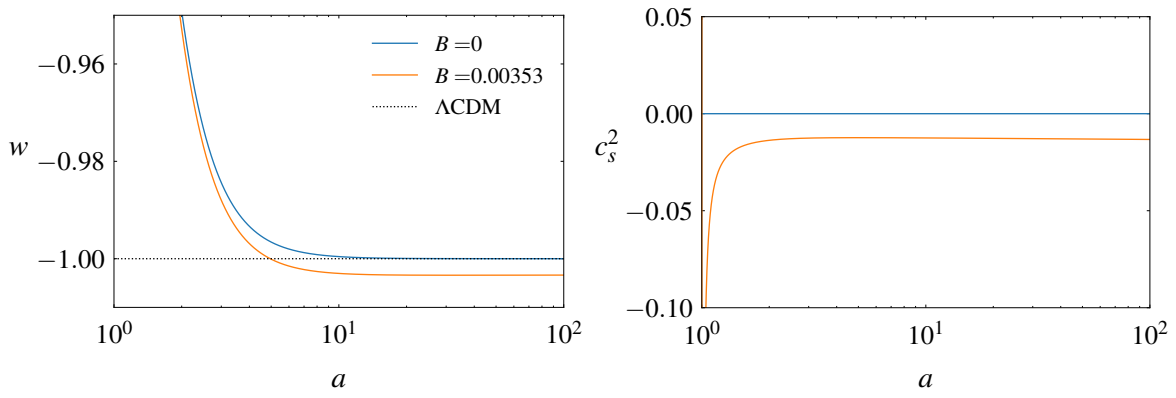

FIGURE 3.10: The left plot displays the EoS parameter w, while the right plot shows the squared sound speed c_s^2 of the Logotropic EoS plotted against the scale factor a. Two scenarios are considered: $B = 0$ (blue line) and $B = 3.35 \times 10^{-3}$ (orange line). The reference density is defined by the Planck density in Equation (3.70).

Figure 3.10 (left) illustrates the evolution of the background EoS parameter w over the range of $a = 10^0 - 10^2$. Remarkably, in the Logotropic model, w remains near 0 for small values of a, gradually decreases, and falls below -1 at $a \approx 5$. It reaches its minimum at $w_{\text{min}} = -1.0035$ when $a = 1$. In the future evolution of the Logotropic Universe, a unique phantom flip signature emerges, an effect not present in the ΛCDM model. In Figure 3.10 (right), we observe the evolution of the sound speed within the range of $a = 10^0 - 10^2$. The behaviour resembles the typical Logotropic pattern, with negative sound speeds as we approach the present day $a = 1$. Despite the constant B being sufficiently small, it fails to address the issue of negative sound speed. In comparison to the standard approach, the Logotropic model does not offer any advantages, especially since perturbations become unstable due to the inherent nature of negative sound speed, seemingly present in Logotropic models in general.

Compared to the GCG EoS, generalizations of the Logotropic model offers significantly greater breadth. It presents a multitude of options for free parameters, allowing for the inclusion of various observational constants and additional parameters. As a result, the model assumes a critical role in elucidating observational phenomena that are often attributed to dark energy and dark matter. Notably, it can account for the accelerated expansion of the universe and the formation of dark matter halos. However, the further we generalization, the less statistical rigor we have compared to the standard approach [97]. Note that when we switch from dimensionless variable B for the Logotropic case, we omit any inclusion density ρ_{de} which differs to the GCG case where we still include the critical density in deriving the background w.

In Chapter 4, we will explore a potential UDE model, the Murnaghan equation of state, which has not been explored extensively in the literature. This topic remains largely unexamined within the realm of cosmology.

Chapter 4

A new UDE model

We now introduce a new Unified Dark Energy (UDE) model, specifically the Murnaghan EoS [101]. Initially developed in solid-state physics, we adapt this novel EoS for cosmological contexts to assess its capability in replicating observational outcomes against a ΛCDM background. The quest for new UDE models persists due to the shortcomings of existing models like the Generalized Chaplygin Gas (GCG) and Logotropic models, which exhibit deficiencies at the perturbative level, emphasizing the necessity to continue our exploration for more viable alternatives.

4.1 The Murnaghan equation of state

The Murnaghan equation of state, named after physicist Francis D. Murnaghan, is an empirical model widely used to describe the relationship between the pressure, volume, and energy of a material [101]. It is derived from three derivative relations, including expressions for pressure, bulk modulus, and its derivative at constant pressure, given by,

$$p = -\left(\frac{\partial U}{\partial V}\right)_S, \tag{4.1a}$$

$$K = -V\left(\frac{\partial p}{\partial V}\right)_T, \tag{4.1b}$$

$$K' = \left(\frac{\partial K}{\partial p}\right)_T, \tag{4.1c}$$

where p denotes the pressure, U denotes the internal energy, V denotes the volume, K denotes the bulk modulus and K' the pressure derivative of the bulk modulus at constant temperature. For constant K' we choose to assign a linear dependence of the bulk modulus on the pressure which allows the specification for one bulk modulus and derivative represented by K_0 and K_0' shown below,

$$K = K_0 + pK_0'. \tag{4.2}$$

The resulting pressure relation, derived in Appendix A.4, is given by:

$$p(V) = \frac{K_0}{K_0'}\left[\left(\frac{V}{V_0}\right)^{-K_0'} - 1\right], \tag{4.3}$$

where V denotes volume, K, K_0 are proportionality constants, and V_0 is the equilibrium volume. The equation is crucial for understanding pressure behaviour, especially in the context of a negative pressure universe when $V \leq V_0$.

The Murnaghan EoS, based on Murnaghan's theory of finite strain [101], describes the volume-pressure relationship in solids. It reflects the empirical observation that a solid becomes more resistant to compression as it is compressed [101]. This equation is frequently used to fit experimental data and to compute the thermodynamic properties of materials under high temperature and pressure conditions. It has been successfully applied to a wide range of materials, such as metals, semiconductors, and minerals [102]. In particular, the model is used to perform a regression on a data set, from which one obtains the values of the coefficients of K_0 and K_0'. Knowing the temperature, one can then derive the volume, density, and bulk modulus for any pressure.

In the context of a fluid modeled by the Murnaghan EoS, the entire universe can be represented with a single dark counterpart. This approach involves matter fueling cosmic acceleration, given by the negative EoS in (4.3). Two limiting cases of this equation reveal critical volumes where pressure coexists with matter,

$$\begin{cases} \lim_{V \gg V_0} p(V) & = \dfrac{K_0}{K_0'}\left(\dfrac{V}{V_0}\right)^{-K_0'}, \\ \lim_{V \ll V_0} p(V) & = -\dfrac{K_0}{K_0'}. \end{cases} \tag{4.4}$$

A critical volume exists where matter pressure supersedes the case when $p =$ constant. This implies that both matter and pressure coexist during the early stages of the universe or when we reach this critical volume. In contrast to the ΛCDM model, where two distinct fluids exist, with Λ dominating over matter at late times and driving the universe's expansion, our approach involves a single perfect fluid with a unified EoS capable of accelerating the universe. This approach introduces the concept that, during early/intermediate times, matter possesses pressure, as opposed to the current paradigm which assumes a pressureless case. This is the novelty of the Murnaghan EoS. To assess the EoS within the context of time evolution, we look at the extreme cases where,

Case 1: $V < V_0$. Where we have a matter dominated phase. However, instead of the pressureless case where $p = 0$, we instead have a constant term containing matter and pressure $p(V) = -\dfrac{K_0}{K_0'}$, a matter-like fluid with pressure.

Case 2: $V = V_0$. We call this the transition period where our pressure becomes $p(V) = 0$, the case for the standard model paradigm.

Case 3: $V > V_0$. We transition from $p(V) =$ constant to $p < 0$ in which dark energy dominates corresponding to to a de-Sitter phase capable of accelerating the universe today. We can express this as $p(V) = \frac{K_0}{K_0'}\left(\frac{V}{V_0}\right)^{-K_0'}$.

Using the notation established in the framework of LDE models [58], we relate the volume to the mass density as $V \propto \rho^{-1}$ and reformulate Equation (4.3) for the cosmological context, leading to the following expression,

$$p(\rho) = -\frac{A}{\alpha}\left[\left(\frac{\rho}{\rho_*}\right)^{-\alpha} - 1\right], \tag{4.5}$$

where A and α are positive constants[1] and ρ_* the normalized density, different from the critical density ρ_{cr}. To induce negative pressure, we incorporate a minus sign at the start of our pressure expression. It is noteworthy that in later stages, the system's behaviour closely resembles that of the Chaplygin Gas (CG) EoS, as described in [55], and expressed as,

$$p(\rho) = -\frac{A}{\alpha}\left(\frac{1}{\rho^{\alpha}}\right), \tag{4.6}$$

where we allow our reference density to tend toward unity, $\rho_\star \to 1$. Allowing $A/\alpha = A_s$ to be a positive constant equivalent to the GCG parameter, we arrive at the same expression derived in §2.1.1,

$$p(\rho) = -\frac{A_s}{\rho^{\alpha}}. \tag{4.7}$$

The GCG model is characterized by $0 < \alpha \leq 1$ with a positive constant A_s. Setting $\alpha = 1$ leads to the original Chaplygin gas model introduced by Ref. [59]. For the purposes of consistency, we use the same constraints on α as an initial test. For the Murnaghan model, provided that the density value is significantly large i.e. $\rho \gg 1$, the pressure p stabilizes at a constant value. Consequently, the pressure can be expressed as,

$$p \sim \frac{A}{\alpha}. \tag{4.8}$$

Unlike previous UDE models such as the Chaplygin gas model, which only considers the early and late phases of the universe, the Murnaghan EoS accounts for both pressure and matter in the early universe, and exhibits Chaplygin-like behaviour in the later universe. A formal solution can be obtained by using the first law of thermodynamics as shown below since the original EoS is derived from continuum dynamics.

[1] We choose positive values for A and α since at late times the EoS resembles the Generalized Chaplygin Gas model, thus we follow a similar methodology to remain consistent with previous literature.

By applying the techniques outlined in §2.1.3 and replacing Equation (4.5) into Equation (2.24), assuming positive constants A and α, and a prescribed EoS in the form $p(\rho)$, we can express the total energy density as,

$$\epsilon = \rho c^2 + \rho \int^{\rho} \frac{p(\rho')}{\rho^{2'}} d\rho' = \rho + u(\rho), \tag{4.9}$$

where ρ denotes the rest-mass density, different to the GCG formulation. Equation (4.9) depicts the energy density as consisting of two components: the rest mass energy term $\rho c^2 \propto a^{-3}$, representing dark matter and being positive, and an internal energy term ($u(\rho)$) with a density dependence, resembling dark energy [68]. Since the total energy density is always positive, the internal energy density does not contribute linearly to ρ.

Following the approach detailed in [72], we adhere to a background cosmological model where the connection between the energy density and the scale factor for a specific barotropic fluid [103] (see Appendix A.2) is described by the continuity equation,

$$\dot{\epsilon} + 3\frac{\dot{a}}{a}(\epsilon + p) = 0, \tag{4.10}$$

by integrating the first law of thermodynamics (2.21) with the continuity equation in terms of ϵ, we have an expression that allows us to derive the energy density for our UDE model,

$$\dot{\rho} + 3\frac{\dot{a}}{a}\rho = 0. \tag{4.11}$$

This equation retains its exactness when a fluid is at constant temperature or behaves as a single perfect fluid. Crucially, it does not depend on the specific EoS, denoted by $p(\rho)$. This equation essentially represents the conservation of rest-mass density, and integrating it provides the evolution of the rest mass density given by,

$$\rho_m(a) = \rho_{m,0}\left(\frac{a_0}{a}\right)^3, \tag{4.12}$$

where $\rho_{m,0}$ is the current value of the rest-mass density given by $\rho_{m,0} = 3H_0^2\Omega_{m0}/(8\pi G)$ and $a_0 = 1$ the present day value [58]. Thus, the EoS (4.5) can be expressed as,

$$p(\rho) = -\frac{A}{\alpha}\left[\left(\frac{\rho_{m,0}a^{-3}}{\rho_*}\right)^{-\alpha} - 1\right]. \tag{4.13}$$

Inserting Equation (4.12) into Equation (4.9), we obtain the total energy density,

$$\epsilon = \rho_{m,0}\left(\frac{a_0}{a}\right)^3 + u\left[\rho_{m,0}\left(\frac{a_0}{a}\right)^3\right]. \tag{4.14}$$

Now, inserting EoS (4.5) into the expression for the first law of thermodynamics results in the total energy density for our Murnaghan Dark Fluid model (MDF), [2]

$$\epsilon_M = \rho_{m,0} a^{-3} + \frac{A}{\alpha}\left[\frac{1}{1+\alpha}\left(\frac{\rho_{m,0}a^{-3}}{\rho_\star}\right)^{-\alpha} - 1\right]. \tag{4.15}$$

The first term, representing a pressureless fluid, resembles matter, whereas the subsequent term, originating from pressure effects, can be viewed as the dark energy component. Consequently, this methodology aims to merge dark matter and dark energy into a unified dark fluid. To compare this outcome with the conventional ΛCDM model, we treat matter and dark energy as distinct fluids and express the total density as,

$$\epsilon = \epsilon_m + \epsilon_{de} = \rho_M, \tag{4.16}$$

where ρ_M denotes the sum of matter and dark fluid components. We can assess the density in two ways, either in terms of the total or in terms of the the internal energy term that mimics a "new fluid", our Murnaghan Dark Fluid (MDF). Using the density relation in Equation(4.12), we can express the pressureless fluid (dark matter) and corresponding dark energy term as,

$$\epsilon_m = \rho_{m,0} a^{-3} = \rho_m(a), \tag{4.17}$$

$$\epsilon_{de} = \frac{A}{\alpha}\left[\frac{1}{1+\alpha}\left(\frac{\rho_{m,0}}{\rho_\star}\right)^{-\alpha} a^{3\alpha} - 1\right]. \tag{4.18}$$

For current times we use the subscript "0" for $z = 0$ ($a_0 = 1$). Defining the normalized density parameters as,

$$\Omega_{m,0} = \frac{\epsilon_{m,0}}{\epsilon_{c,0}}, \tag{4.19}$$

$$\Omega_{de,0} = \frac{\epsilon_{de,0}}{\epsilon_{c,0}} = 1 - \Omega_{m,0}, \tag{4.20}$$

where $\epsilon_{c,0} \equiv 3H_0^2 c^2/(8\pi G)$ is the present critical density. We can write the Friedmann equation as,

$$H^2 = H_0^2\left(\frac{\epsilon_m}{\epsilon_{c,0}} + \frac{\epsilon_{de}}{\epsilon_{c,0}}\right), \tag{4.21}$$

$$= H_0^2\left\{\frac{\Omega_{m,0}}{a^3} + \frac{A(1-\Omega_{m,0})}{\alpha}\left[\frac{1}{1+\alpha}\left(\frac{\rho_{m,0}}{\rho_\star}\right)^{-\alpha} a^{3\alpha} - 1\right]\right\}. \tag{4.22}$$

As discussed in [72], a new parameter "B" was introduced for convenience and referred to as the Logotropic temperature. However, it is important to note that this is applicable primarily under the

[2] Appendix §A.3.4 for full derivation

constraint that $K_0 \approx 0$[3] Focusing our study on just the dark energy component, we can determine the background EoS given using the relation $w_{de} = p_{de}/\epsilon_{de}$ which can be written as,

$$w_{de} = \frac{\alpha}{(\alpha+1)\left(\frac{\rho_{m,0}}{\rho_*}\right)^{\alpha} - 1} - 1, \tag{4.24}$$

where the full solution for the background is simply,

$$w = \frac{p}{\rho} = -\frac{A}{\alpha\rho}\left[\left(\frac{\rho}{\rho_\star}\right)^{-\alpha} - 1\right]. \tag{4.25}$$

The choice of fluid type, whether adiabatic or barotropic, determines how the model evolves [103]. In the context of the MDF, the adiabatic and barotropic sound speeds are equivalent, thus

$$c^2_{s,a} = \frac{\partial p}{\partial \rho} = \frac{\mathrm{d}p(\rho)}{\mathrm{d}\rho}, \tag{4.26}$$

resulting in an expression for sound speed given by,

$$c^2_{s,M} = \frac{\mathrm{d}p(\rho)}{\mathrm{d}\rho} = \frac{A}{\rho_M}\left(\frac{\rho_M}{\rho_\star}\right)^{-\alpha}, \tag{4.27}$$

where ρ_M refers to the Murnaghan energy density in Equation (4.15).

4.1.1 Solution to the continuity equation

In the paper [104], the authors assess the large-scale dynamics of the Murnaghan EoS using the continuity equation; however, no analytical solution is attainable. This led to the utilization of the methods outlined in the previous section, which involved employing the first law of thermodynamics to solve for the energy density. Nevertheless, by constraining the model parameters A, α, and $\rho_\star$, we can obtain insightful solutions. The following section summarizes the assumptions made to arrive at these analytical expressions for pressure.

[3] Note the definition given by [72],

$$B_{\log} \equiv \left[\ln\left(\frac{\rho_\star}{\rho_{m,0}}\right) - 1\right]^{-1}. \tag{4.23}$$

1. **ΛCDM-like evolution**. Allowing $z \approx 0$ and thus $a_0 \approx 1$. Letting $\rho \approx \rho_c$, we arrive at the pressure and density expression given by,

$$p \approx -A_\star \ln\left(\frac{\rho_\star}{\rho_c}\right) < 0, \tag{4.28}$$

$$\rho(z) \approx \rho_c \left(\Omega_{DF} + \frac{p}{\rho_c}\right) a^{-3} - p, \tag{4.29}$$

where $\Omega_{DF} \approx \rho/\rho_c$ is the dark fluid density parameter. The solution is degenerate with the ΛCDM as required.

2. **Logotropic-like solution**. Letting K_0 be constant or weakly related to p results in the derivative of $K_0' \approx 0$. Using the relation in Equation (4.1b), we arrive at the solution $p = -K_0 \ln(V/V_0)$. Letting $K_0 \to A_\star$, $V_0 \to \rho_\star$, $V \to \rho$ we arrive at a form for pressure in terms of the logarithm, given by,

$$p \approx -A_\star \ln\left(\frac{\rho}{\rho_\star}\right) < 0, \tag{4.30}$$

which holds for all ρ unlike the previous case which only holds for $\rho = \rho_c$. This expression is exact in form for the A-S EoS when $n = 0$ [72]. In terms of the total matter density, solving for the first law of thermodynamics results in the density expression given by,

$$\epsilon(a) = \rho_m(a) - A_\star \left\{1 + \ln\left[\frac{\rho_m(a)}{\rho_\star}\right]\right\} = \rho_m(a) + \rho_c\left(1 - \Omega_{m,0}\right)\left(1 + 3B\ln a\right), \tag{4.31}$$

where we defined the free parameters as,

$$B \equiv \left[\ln\left(\frac{\rho_\star}{\rho_{m,0}}\right) - 1\right]^{-1}, \tag{4.32a}$$

$$A_\star \equiv B\rho_c\Omega_\Lambda. \tag{4.32b}$$

Following the works of [68], the reference density $\rho_\star$ is identified with the Planck density $\rho_{Pl} = c^5/(\hbar G^2)$ where c is the speed of light, $\hbar$ the reduced Planck constant and G the gravitational constant. They denote this the "GL1" case. "GL2" is defined as the original case without removing $\rho_\star$ and B. Both these cases are assessed in terms of their background quantities.

3. **GCG-like behaviour**. Assuming the bulk modulus is $K_0 \ll K_0' p$, the Murnaghan EoS can be expressed as,

$$p \approx \frac{K_0}{K_0'}\left(\frac{V}{V_0}\right)^{-K_0'}. \tag{4.33}$$

Letting $K_0 \to A_c\rho_\star$, $K_0' \to -\alpha$, $V_0 \to \rho_\star$ and $V \to \rho$, the GCG-like EoS in the cosmological regime can be written as,

$$p = -A_c\rho_\star \left(\frac{\rho}{\rho_\star}\right)^{-\alpha}. \tag{4.34}$$

Solving the continuity equation results in,

$$\rho_{DF}(a) = \rho_{DF,0}\left[A_s + (1-A_s)a^{-3(\alpha+1)}\right]^{\frac{1}{\alpha+1}}, \tag{4.35}$$

where we have redefined the constant A_s to be equivalent to the original GCG formulation,

$$A_s \equiv A_c\left[\frac{\rho_\star}{\rho(a_0)}\right]^{1+\alpha}, \tag{4.36a}$$

$$A_\star \equiv \alpha A_c\rho_\star. \tag{4.36b}$$

Note that we can express A_s exactly as in Equation (3.29). Additionally, numerically derived values are not used, as A_s is approximately equal to $(1-\Omega_{m0})$.

4.1.2 Priors on model parameters

Building upon the works by Ref. [104] which sought to identify prior model parameters through constraints on the continuity equation, we employ this as an initial evaluation to determine the numerical values for our free parameters A, α, and $\rho_\star$.

Additionally, we leverage the deceleration parameter as a prior for our model. The deceleration parameter for a spatially flat universe comprising a single component with the form given by $p = wp$ can be expressed as,

$$q = -\frac{\ddot{a}}{aH^2} = \frac{1}{2}(1+3w). \tag{4.37}$$

The current deceleration and jerk parameters can be written in terms of the e-foldings $N = -\ln(1+z)$ as,

$$q_0 = -\frac{1}{H^2}\left\{\frac{1}{2}\frac{d\left(H^2\right)}{dN} + H^2\right\}\Bigg|_{N=0}, \tag{4.38a}$$

$$j_0 = \left\{\frac{1}{2H^2}\frac{d^2\left(H^2\right)}{dN^2} + \frac{3}{2H^2}\frac{d\left(H^2\right)}{dN} + 1\right\}\Bigg|_{N=0}. \tag{4.38b}$$

The bounds found by [104] are given by,

$$\bar{\alpha} = 0.03^{+0.22}_{-0.17}, \tag{4.39a}$$

$$\bar{\rho}_\star = \rho_{Pl}, \tag{4.39b}$$

$$\bar{A}_\star = \left(1.07^{+0.05}_{-0.05}\right) \times 10^{-5}\rho_{cr}. \tag{4.39c}$$

The extensive range of values for α affords us the opportunity to scrutinize the impact of α variability on the background EoS and sound speed, as elucidated in the subsequent discussion.

4.1.3 Evolution of the Murnaghan equation of state

To ensure alignment with observations of large-scale structure, the sound speed should tend towards zero and avoid assuming negative values to prevent instability. Negative sound speeds contribute to nonphysical perturbations on small scales, thereby significantly altering the late-time history of structure formation.

In the Generalized Chaplygin Gas (GCG) model, the parameter α is constrained to the range $0 \leq \alpha \leq 1$. Likewise, for the Murnaghan EoS, α must be positive to ensure negative pressures throughout time. Employing the values for $A_\star$, α, and ρ_* in (4.39), we can generate plots depicting the sound speed and background EoS, as illustrated in Figure 4.1.

The Murnaghan EoS presents a compelling feature as it begins with characteristics akin to pressureless Cold Dark Matter (CDM), signified by $w \approx 0$ and $c_s^2 \approx 0$, in the early stages. Over time, it gradually converges towards behaviour resembling the cosmological constant, particularly evident for small values of $\alpha < 0.014$. The top panel in Figure 4.1 visually captures this transition from a dust-dominated epoch to the cosmological constant regime, consistent with the ΛCDM model.

Contrasting this behaviour with the Murnaghan Dark Energy (MDE) model across various α values, we observe deviations above or below $w = -1$. This preliminary analysis indicates that α is constrained within the range $0.014 \sim 0.022$. The bottom plot depicting the sound speed in Figure 4.1 reveals a positive-defined sound speed for any α value within the chosen range. This stands in contrast to the ΛCDM case, where the sound speed remains zero throughout. These findings provide a foundation for testable assessments regarding the evolution of matter perturbations over time, as explored in subsequent §4.2. Note, the numerical values (§1) used are consistent with those used for the previous UDE models, thus allowing for comparison.

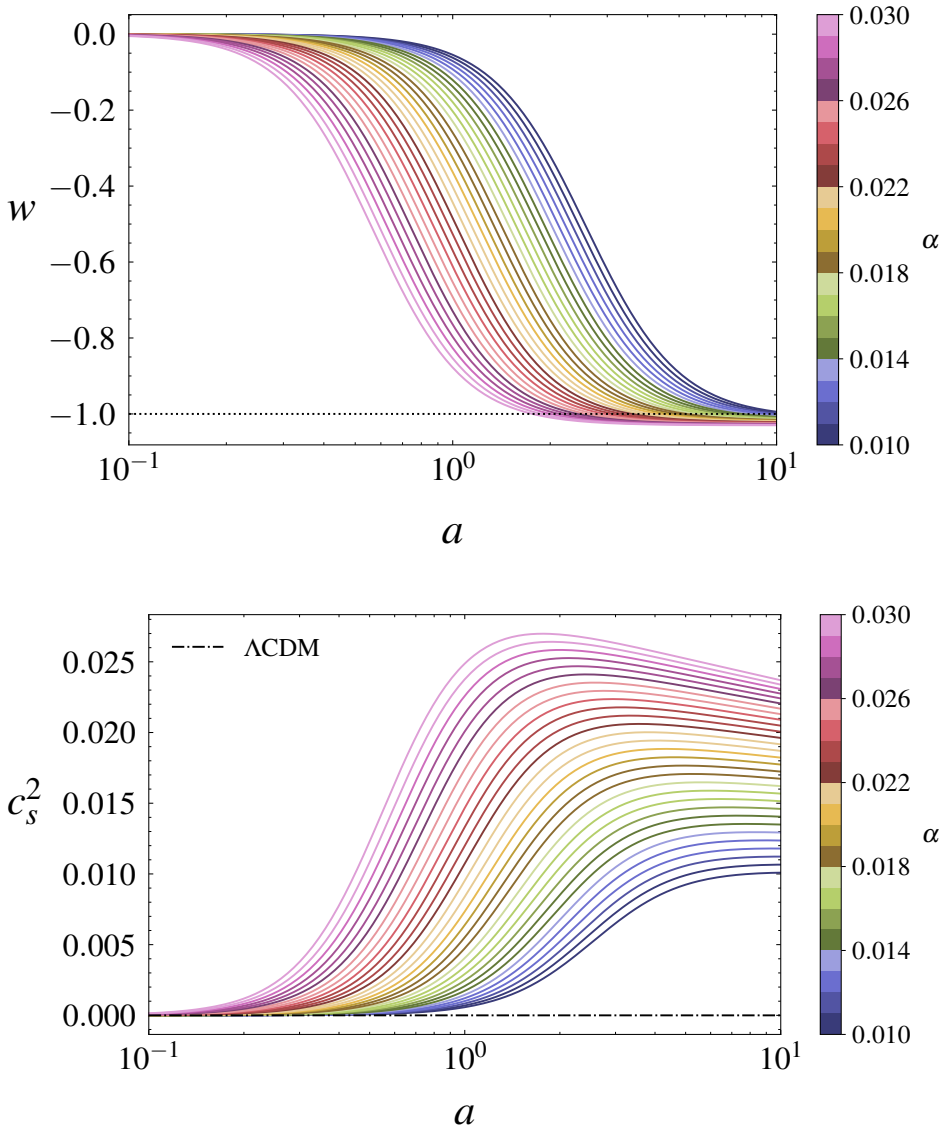

FIGURE 4.1: Numerical solutions for the background EoS and sound speed for free parameters $0.01 \leq \alpha \leq 0.03$, $A_\star = 1.07 \times 10^{-5}\rho_{cr}$ and $\rho_\star = \rho_{Pl}$ for the Murnaghan UDE model.

4.2 Evolution of perturbations

Building upon our prior discussions, it is established that matter perturbations are markedly influenced by the presence of dark matter—a form of matter devoid of light emission, absorption, or reflection and primarily interacting through gravity. In the context of an initial examination, we can scrutinize the growth of matter perturbations, specifically in the linear case. By utilizing Equation (3.65) and presuming the clustering component to be dark matter, we assign $w_{de} = 0$. Consequently, (3.65) simplifies to Equation (3.67). Therefore, the key requirement lies in obtaining the expression for the sound speed corresponding to the Murnaghan EoS. We can achieve this by employing a single-fluid solution, where clustering is attributed to baryonic matter. Consequently, our total density is

described by,

$$\ddot{\delta} + 2H\dot{\delta} - 4\pi G\delta\rho_m = 0. \tag{4.40}$$

The radiation-dominated period, occurring at high redshifts (i.e., early times), is negligible for our current analysis. This equation is frequently employed to evaluate small scales for linear perturbations. In this context, the variable ρ_m signifies the total matter density, implying that matter plays a pivotal role in structure formation. The term $2H\dot{\delta}$ functions as a drag term, reflecting the expansion of the Universe and resisting the collapse of structures.

The continuity and Euler equations are expressed as,

$$\frac{\partial\rho}{\partial t} + 3(c_s^2 - w)\rho + \vec{\nabla}\cdot\left[(1+w)\,\rho\vec{u}\right] = 0. \tag{4.41}$$

If we let $\delta = \delta\rho/\rho$, $\theta = \vec{\nabla}\cdot u$ and $c_s^2 = s$ then the continuity equation becomes,

$$\delta' + 3(s-w)\delta + (1+w)\tilde{\theta} = 0, \tag{4.42}$$

where we have let $\delta' = \partial\delta/\partial N$. To derive the Euler equation we define the variable for the effective matter density, similarly to [105],

$$\Omega_m(a) = \frac{\rho_m}{\rho_m + \rho_{de}}. \tag{4.43}$$

$$\tilde{\theta}'\left(2 + \frac{H'}{H}\right)\tilde{\theta} + \frac{3}{2}(1+3s)\Omega_m(a)\delta = 0. \tag{4.44}$$

We can use the same methodology performed in [73] by defining function A, B and f,

$$A = 3(s-w), \tag{4.45a}$$

$$B = 1 + w, \tag{4.45b}$$

$$f = \frac{3}{2}(1+3s)\Omega(a), \tag{4.45c}$$

with derivatives,

$$A' = 3(s'-w'), \tag{4.46a}$$

$$B' = w'. \tag{4.46b}$$

Inserting this into the continuity equation yields an expression similar to the one obtained in Ref. [48], and given by,

$$\delta'' + (A\delta)' + (\delta' + A\delta)\left[\left(2 + \frac{H'}{H}\right) - \frac{B'}{B}\right] - Bf\delta = 0, \tag{4.47}$$

where $(A\delta)' = A'\delta + A\delta'$. The partial derivative with respect to time results in the general expression given below, where $c_s^2 \neq 0$, and leads to clustering similar to dark matter [73]. Since we assume $w_{de} = 0$, we can simplify the above perturbation by setting $w = 0$ (since we are only dealing with the matter perturbations i.e. the linear case.)

To streamline the number of varying inputs, we invoke the barotropic nature of our UDE model. Consequently, we can express the term H'/H in terms of the barotropic index,

$$\frac{H'}{H} = -\frac{3}{2}(w+1), \tag{4.48}$$

Incorporating the total background, which encompasses the contributions from dark energy and dark matter, we find that for $w = 0$, the expression aligns with that employed for the Logotropic and Generalized Chaplygin Gas (GCG) models as presented earlier in Equation (3.67),

$$\delta'' + 3(s\delta)' + (\delta' + 3s\delta)\left(2 + \frac{H'}{H}\right) - \frac{3}{2}(1+3s)\Omega(a)\delta = 0. \tag{4.49}$$

We can calculate s and s', necessitating the time derivative of the matter density as provided in Equation (4.12). In the context of e-foldings denoted by $N = \ln a$, this simplification results in,

$$\rho'_M(N) = \frac{\partial}{\partial N}\left(\rho_{m,0}e^{-3N} + \frac{A}{\alpha}\left[\frac{1}{1+\alpha}\left(\frac{\rho_{m,0}e^{-3N}}{\rho_\star}\right)^{-\alpha} - 1\right]\right) = -3\rho_m(N) + \frac{3A}{\alpha+1}\left(\frac{\rho_m(N)}{p_{Pl}}\right)^{-\alpha}. \tag{4.50}$$

The expression for the sound speed $c_s^2 = s$ and its time derivative is therefore given by,

$$s_M = \frac{\mathrm{d}p}{\mathrm{d}\rho} = \frac{A}{\rho_M}\left(\frac{\rho_M}{\rho_{Pl}}\right)^{-\alpha}, \tag{4.51a}$$

$$s'_M = \frac{\partial}{\partial N}s_M = -\frac{A(\alpha+1)\rho'_M}{\rho_M^2}\left(\frac{\rho_M}{\rho_{Pl}}\right)^{-\alpha}. \tag{4.51b}$$

From Figure 4.2, it is evident that at very early times, for all values of α, the growth factor f flattens out and approaches unity as required. Fine-tuning the free parameters leads to a variation in the rate of growth. Specifically, the Murnaghan model evolves either faster or slower than ΛCDM, contingent on the values of α and $A_\star$. Consequently, we infer that within a particular range or for a specific value of α, a substantial deviation from the ΛCDM paradigm occurs, resulting in a more efficient growth of perturbations. Examining the definition in Equation (4.43), the contributions of dark matter density and dark fluid are intricately intertwined. Consequently, $\Omega_m(a)$ encapsulates the total dark fluid density, potentially amplifying the growth of perturbations. This phenomenon could be attributed to the non-zero sound speed during late times. A more comprehensive and

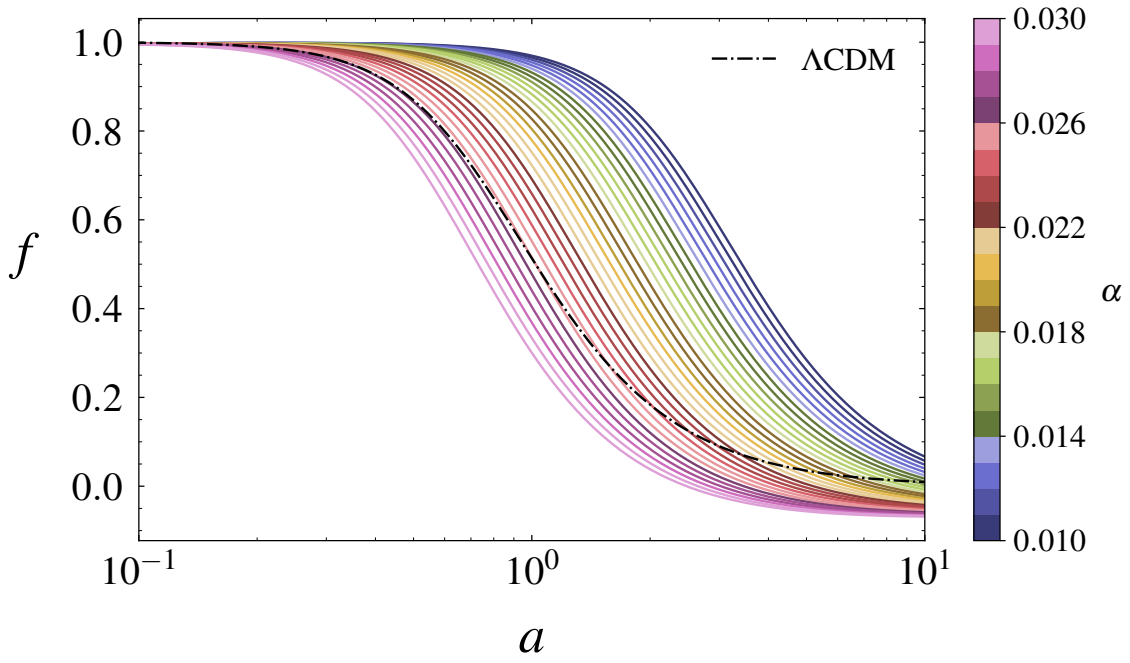

FIGURE 4.2: ΛCDM case where $s = 0 = w$ and Murnaghan model with parameters $0.01 \leq \alpha \leq 0.03$, $A_\star = 1.07 \times 10^{-5}\rho_{cr}$ and $\rho_\star = \rho_{Pl}$

rigorous comparison involves combining the results for the Generalized Chaplygin Gas (GCG) and Logotropic models to ascertain which model more effectively fosters the growth of perturbations.

Given that the numerical values are defined in terms of e-foldings, we redefine the primes to denote derivatives with respect to N. This adjustment allows us to equate and plot the growth factor using the relation,

$$f = \frac{\mathrm{d}\ln\delta}{\mathrm{d}\ln a} = \frac{\delta'}{\delta}. \tag{4.52}$$

Using the definition in Equation (3.23), γ can be derived by taking the natural logarithm of the growth factor f and total energy energy,

$$\gamma = \frac{\ln f}{\ln \Omega_m(a)} \tag{4.53}$$

where $\Omega_m(a)$ is defined in Equation (4.43). The plot for γ depicted in Figure 4.3 signifies a notably greater growth factor when compared with the ΛCDM scenario. The variances in the values of γ may be ascribed to the non-constant values of the adiabatic sound speed and background EoS. This is due to the fact that the rate of growth for matter perturbations incorporates contributions from both matter and dark energy, manifesting in the barotropic index. The MDE favours smaller values for α for the chosen range, as shown in Figure 4.3, where the blue range tends toward the ΛCDM scenario. The subsequent phase of our analysis involves comparing GCG and Logotropic cosmologies with the Murnaghan Dark Energy (MDE) model at a background level. To enhance our

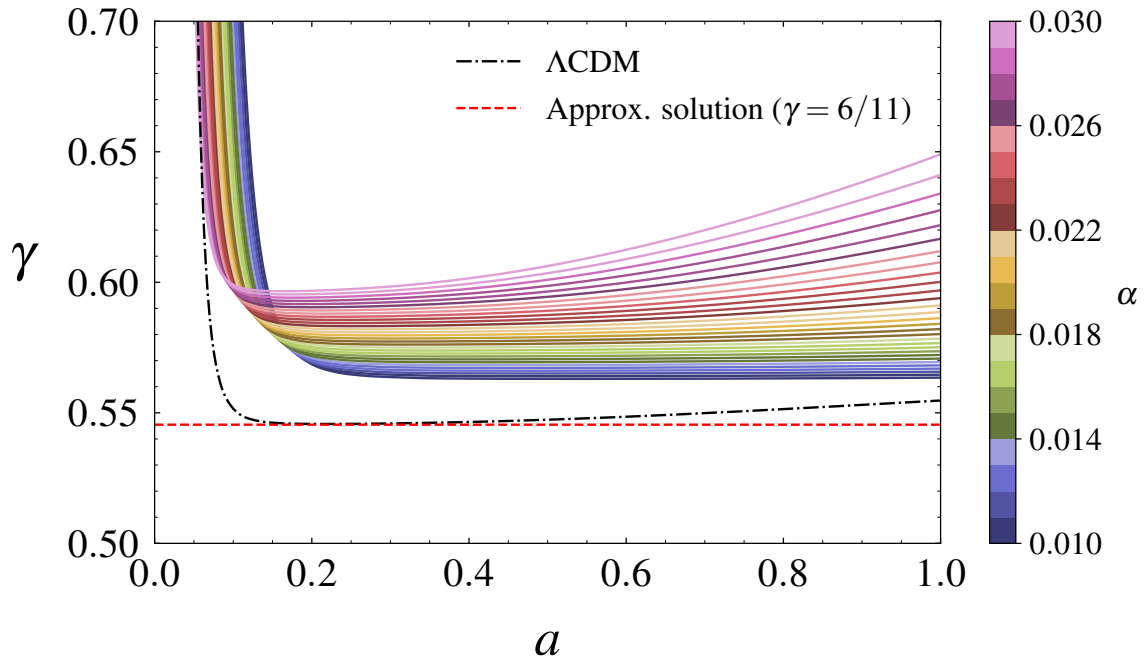

FIGURE 4.3: ΛCDM case where $s = 0 = w$ and Murnaghan model with parameters $0.01 \leq \alpha \leq 0.03$, $A_\star = 1.07 \times 10^{-5}\rho_{cr}$ and $\rho_\star = \rho_{Pl}$

progress, we must confront these models with cosmological datasets. A comprehensive comparison is currently hindered by the less tightly constrained parameters of the MDE model, in contrast to the more extensively reviewed GCG and Logotropic models. However, initial background tests indicate a favorable trend for the MDE model, as it demonstrates consistent performance against the ΛCDM model compared to its predecessors. As demonstrated in the works by Ref. [104] in §4.1.2, the free parameter α is not well-constrained. Therefore, additional efforts are necessary to refine the parameter values. Chapter 5 outlines the methodology required for this purpose which involves the usage of MCMC numerical methods, following this we conclude the dissertation with a discussion of future work in Chapter 6.

Chapter 5

Review of statistical approaches

In this dissertation, the computation of MCMC parameter estimates will not be undertaken, as this aspect is reserved for future work. This would involve the marginalization of the likelihood function over the free parameters; α, $A_\star$, and $\rho_\star$. The Equation of State (EoS) for the Murnaghan Dark Energy (MDE) model was adopted, and the parameters specified in [104] were utilized to determine various background quantities. These quantities include the background EoS (w), sound speed (c_s^2), growth function (f), and growth factor (γ). To achieve this, extreme cases of the MDE were considered, representing late and early times regimes, thereby approximating a simplified EoS. We shall now examine various statistical methods employed in cosmological modeling to delineate the approach for acquiring precise parameter estimates in subsequent research work.

Statistical methods play a pivotal role in validating UDE models through the comparison with observational data. To achieve this, rigorous statistical techniques are employed. These techniques entail determining the best-fit parameters and confidence intervals for either a single test model or multiple models. By varying the parameters, we search for the optimal values that yield the closest match to the data, commonly referred to as the "true" value. However, model selection presents a challenge due to varying numbers of parameters across different models, necessitating the utilization of information criteria.

Various statistical methods are employed to assess the validity of UDE models, with likelihood analysis and Bayesian analysis being prominent among them. Likelihood analysis involves comparing the predicted outcomes of a model with observed data and assessing the goodness-of-fit using statistical measures like the χ^2 test. This approach is commonly utilized to constrain the model parameters and gauge the likelihood of its accuracy [106].

In contrast, Bayesian analysis calculates the posterior probability distribution of model parameters based on observed data. This approach integrates prior knowledge about the parameters and enables the estimation of parameter uncertainties. Additionally, it facilitates model comparison and

the identification of the most probable model given the data. It's crucial to recognize that adding extra parameters will enhance the fit to the dataset. Consequently, a straightforward comparison based solely on the maximum likelihood value will consistently favour the model with more parameters, regardless of the relevance of these additional parameters. Thus, selecting relevant parameters are key in assessing the statistical validity for particular UDE models.

5.1 Likelihood analysis

Likelihood analysis is a statistical method employed to gauge the compatibility of a model with observed data by quantifying the probability of obtaining the observed data given the model and its parameters. Constructed based on the assumed statistical distribution of the data, the likelihood function represents how well the model aligns with observed values. In the context of UDE models, likelihood analysis helps constrain model parameters, and the values maximizing the likelihood function are considered the best-fitting ones.

In the evaluation of UDE models, the likelihood function plays a pivotal role, indicating the probability of observed data given certain model parameters. This likelihood is central to Bayesian inference, updating prior beliefs about model parameters based on observed data to yield a posterior distribution, as per Bayes' theorem. The maximum likelihood for a model can be assessed by determining the Akaike Information Criterion (AIC) [107] and Bayesian Information Criterion (BIC) [108]. In the paper by [73], the AIC and BIC are employed as indicators to determine which model performs better.

- The AIC is defined as,

$$\mathrm{AIC} = -2\ln\mathcal{L} + 2k \tag{5.1}$$

  where $\mathcal{L}$ is the maximum likelihood for the model and k is the number of parameters of the model. We aim to find the model that minimizes the AIC, without the constraint that the models need to be nested.

- The BIC is defined as,

$$\mathrm{BIC} = -2\ln\mathcal{L} + k\ln N \tag{5.2}$$

  where N is the number of data points used for the fit. The BIC operates under the assumption that the data points are independent and identically distributed, a condition that may or may not hold depending on the datasets utilized.

In testing UDE models, AIC and BIC serve as valuable tools for model selection. By calculating the AIC and BIC values for different UDE models, one can assess the trade-off between model goodness of fit and complexity [109]. Models with lower AIC or BIC values are considered more favourable, with substantial differences suggesting stronger evidence in favour of the model with the lower value. The choice between AIC and BIC depends on preferences regarding model simplicity, as the latter penalizes additional parameters more rigorously [110]. Ultimately, these criteria aid in objectively comparing and selecting UDE models, offering a balance between fit to data and model parsimony. Consideration of other factors, such as physical interpretability and prior knowledge, complements the use of AIC and BIC in the model selection process.

Markov Chain Monte Carlo (MCMC) methods, like Metropolis-Hastings or Gibbs sampler, are crucial in exploring the parameter space and generating samples that approximate the posterior distribution. These samples are leveraged for parameter estimation, uncertainty quantification, and model comparison. The latter involves evaluating likelihood functions for different UDE models, with Bayesian model comparison employing the Bayes factor to select the most suitable model [93]. Essentially, the likelihood function, Bayesian inference, and MCMC methods cohesively contribute to the robust evaluation and refinement of UDE models.

The likelihood function is pivotal in UDE modelling, encapsulating the probability of observing specific data given model parameters. Various cosmological data sets, including the Cosmic Microwave Background, large-scale structure surveys, supernovae, Baryon Acoustic Oscillations, Hubble parameter measurements, and redshift-space distortions, contribute to this likelihood. Constructed based on the statistical distribution of these data, the likelihood function quantifies compatibility between the UDE model and observational realities. Bayesian inference utilizes the likelihood function to update prior beliefs, resulting in a posterior distribution. Model comparison, facilitated by the likelihood function, aids in selecting the UDE model aligning best with observed data. This integrated approach, involving diverse observational data, the likelihood function, and MCMC methods, provides a rigorous framework for UDE model assessment.

5.1.1 MCMC methods

In the domain of cosmological modeling, a variety of MCMC methods are applied to navigate the complex parameter spaces inherent in these models. The MCMC technique [93] is widely employed for its capacity in parameter estimation and uncertainty quantification. The Gibbs Sampler, another prominent method, iteratively samples from conditional distributions, offering utility in scenarios where joint distributions are intricate. Hamiltonian Monte Carlo (HMC) integrates principles from Hamiltonian dynamics, enhancing efficiency in high-dimensional spaces and facilitating faster convergence. Parallel Tempering involves running chains at different "temperatures", aiding exploration

of rugged posterior distributions. Nested Sampling transforms the posterior sampling problem into an exploration of the likelihood space, especially beneficial for models with numerous parameters. Collectively, these MCMC methods play a vital role in efficiently exploring parameter spaces, estimating uncertainties, and comparing diverse UDE models, catering to the distinctive characteristics of each model.

In the paper by Ref. [104], the numerical method employed is the MCMC technique, which picks a "proposal" distribution, lets call this $M(p)$ that is able to predict an observable quantity μ_M given the set of v free parameters $p = \{p_1, p_2, ...p_v\}$ of the theory. For a set of observations n, we want the probability p using model $M(p)$ to deliver the **right** results given a set of $k = \{\mu_1, \mu_2, ...\mu_n\}$ i.e. $P(p|k)$. We can rewrite this in the form known as Bayes' Theorem,[1]

$$P(p|k) = \frac{P(p)}{P(k)} P(k|p). \tag{5.3}$$

The probability, denoted as $P(k)$, is referred to as the evidence, serving as a constant normalization factor for the posterior probability. $P(p)$ represents the prior probability of parameter p. For each parameter p_i, it is assumed to be uniform within a given interval. If the parameter is inferred from another cosmological observation, a normal distribution can also be assumed, where the parameter is expected to have a certain mean value and standard deviation. The term $P(k|p)$ represents the probability of obtaining the data k given the model parameters, which constitutes the actual likelihood. In accordance with Ref. [106] Chapter 15, the likelihood for a single data point can be expressed as (with N denoting the number of data points),

$$P(k|p) \propto \exp\left[-\sum_i \frac{(\mu_i - \mu\,(p))^2}{2\sigma_i^2}\right]. \tag{5.4}$$

This holds true only when all data points are independent. However, in cosmological observations, this assumption may not always be valid, as errors from various measurements can be correlated. Therefore, in general, we can represent the likelihood function using a multivariate Gaussian distribution [27],

$$L \approx N \exp\left[-\frac{1}{2}(\theta_i - \hat{\theta}_i) F_{ij} (\theta_j - \hat{\theta}_j)\right], \tag{5.5}$$

where $\hat{\theta}_i$ represents the maximum likelihood estimators, which are functions derived from the data, while F_{ij} denotes the Fisher matrix, the inverse of the correlation matrix [111]. It is crucial to note that the likelihood is a Gaussian function of the parameters, not of the data. The expression in (5.5) is a generic approximation but serves as a method to compute parameter estimates using less computational power. Relating the likelihood function with our probabilities, and letting C be the covariance

[1] Using the rule for conditional probabilities $P(p \cap k) = P(p|k)P(k) = P(k|p)P(p)$,

matrix, we can say,

$$\chi^2 = [k - \mu(p)]C^{-1}[k - \mu(p)]^T, \tag{5.6}$$

where T is the transpose. To elaborate, we can use the Pantheon dataset as an example of this implementation in assessing the background. This is left for future work.

5.2 Data sets

A departure from the approach followed in Ref. [104] involves employing the first law of thermodynamics, facilitating the construction of the total energy density. This total energy density incorporates a term associated with a dark fluid denoted as $u(\rho)$, as outlined in Equation (4.9). By leveraging the Pantheon data set [112], we can visualize the bounds on our free parameters using a 2-dimensional contour plot. Future efforts will be directed towards this particular aspect.

5.2.1 Pantheon sample (SNIa)

The Pantheon dataset consists of 1048 supernova type Ia (SNIa) redshifts [112, 113]. This dataset holds significance because Type Ia supernovae (SNIa) are recognized for their nearly constant absolute magnitude, typically represented as M, at the peak of their luminosity. Consequently, one can infer the distance of a given SNIa for a measured redshift, making them a useful probe for assessing late-time cosmic expansion. For a spatially flat geometry, the luminosity distance is defined as,

$$\mathrm{d}_L(z) = (1+z)\int_0^z \frac{\mathrm{d}z'}{H(z')}, \tag{5.7}$$

where the distance modulus is typically written as,

$$\mu_{th} = m(z) - M = 5\log\left(\frac{\mathrm{d}_L(z)}{Mpc}\right) + 25 = 5\log\left(H_0\,\mathrm{d}_L(z)\right) + \tilde{M}, \tag{5.8}$$

where $\tilde{M}$ is designated as a nuisance parameter. We can write this in terms of our data set as [114],

$$\mu = m_B - M - \alpha x_1 + \beta c + \Delta_M + \Delta_B, \tag{5.9}$$

where m_B represents the natural logarithm of the overall flux normalization, x_1 denotes the light-curve shape parameter (where α signifies the luminosity-stretch coefficient), c represents the supernova colour at maximum brightness, with its coefficient indicated by β, and the terms Δ_M and Δ_B represent distance corrections [114]. Subsequently, we can formulate the log-likelihood function by

simplifying our notation by letting $\theta = (\Omega_m, \Omega_{de}, w)$, resulting in,

$$\chi^2(\theta) = \sum_{i=1}^{N} \frac{\left[m^i_{obs} - m_{th}(\theta)\right]^2}{\sigma_i^2}, \tag{5.10}$$

where m_{obs} is the rest-frame peak B band magnitude and m_{th} is the predicted magnitude, given a cosmological model. Defining the chosen likelihood as,

$$\mathcal{L} = \exp\left(\frac{-\chi^2}{2}\right), \tag{5.11}$$

with some prior $\pi(\theta)$, the integration can be written as,

$$\chi^2_\theta = -2\ln\left[\int_{-\infty}^{\infty} \mathrm{d}\theta \exp\left(-\frac{1}{2}\chi^2\right)\pi(\theta)\right]. \tag{5.12}$$

Defining the vector of the residuals between the model magnitudes and observed magnitudes as $\Delta\mu \equiv \mu - \mu_{th}$, results in the expression,

$$\chi^2 = (\Delta\vec{\mu} - \theta\vec{\mathbf{1}})^T \mathbf{C}^{-1} (\Delta\vec{\mu} - \theta\vec{\mathbf{1}}). \tag{5.13}$$

To determine the distance modulus required by a model, we calculate the luminosity distance corresponding to the observed redshift of Type Ia supernovae, denoted as $\mathrm{d}L(z_{obs})$. Using the relation given in (5.8) one can obtain the theoretical value for the distance modulus $\Delta\mu$. Denoting our variables similarly to [114],

$$a \equiv \Delta\vec{\mu}^T \mathbf{C^{-1}} \Delta\vec{\mu}, \tag{5.14a}$$

$$b \equiv \Delta\vec{\mu}^T \mathbf{C^{-1}} \vec{\mathbf{1}}, \tag{5.14b}$$

$$e \equiv \vec{\mathbf{1}}^T \mathbf{C^{-1}} \vec{\mathbf{1}}. \tag{5.14c}$$

The resulting solution to the integral is therefore,

$$\chi^2_\theta = a + \ln\left(\frac{e}{2\pi}\right) - \frac{b^2}{e}. \tag{5.15}$$

Thus the log-likelihood can be written as,

$$\ln\mathcal{L}_{\mathrm{SN}} = -\frac{1}{2}\left[a + \ln\left(\frac{e}{2\pi}\right) - \frac{b^2}{e}\right]. \tag{5.16}$$

5.2.2 Hubble rate data (OHD)

The differential age method, introduced by [115], offers a valuable approach to evaluate measurements of $H(z)$. It suggests that the derivative of cosmic time concerning redshift can effectively measure the EoS of dark energy over a range of redshifts. We can write the luminosity distance as,

$$\mathrm{d_L} = (1+z)\int_z^0 \left(1+z'\right)\frac{\mathrm{d}t}{\mathrm{d}z'}\,\mathrm{d}z'. \tag{5.17}$$

The approach enhances the sensitivity of $w(z)$ by directly measuring the integrand of Equation (5.7). The technique employs a clock based on spectroscopic dating of galaxy ages to record variations in the Universe's age with respect to redshift. By assessing the age difference (Δt) between two passively evolving galaxies that originated simultaneously but are separated by a small redshift interval (Δz), one can deduce the derivative ($\mathrm{d}z/\,\mathrm{d}t$) from the ratio ($\Delta z/\Delta t$). Improving the statistical robustness of the measurement entails selecting unbiased samples of passively evolving galaxies at two distinct redshifts and examining the upper limit in their age distributions. It is imperative to choose galaxies with similar metallicities and low star formation rates (manifested by a red color) to ensure that the average age of their stars notably surpasses the age difference (Δt) between the two galaxy sets. The dataset can be found in Ref.[116, 117] and consists of $N = 32$ points. The log-likelihood can be determined by following a similar procedure in 5.1.1,

$$\ln \mathcal{L}_{\mathrm{OHD}} = -\frac{1}{2}\sum_{i=1}^{N}\ln\left(2\pi\sigma_{\mathrm{H_i}}^2\right) - \frac{1}{2}\sum_{i=1}^{N}\left[\frac{H_{\mathrm{i}} - H\left(\mathbf{x}, z_i\right)}{\sigma_{\mathrm{H_i}}}\right]^2. \tag{5.18}$$

5.2.3 Cosmic Microwave Background (CMB)

The Cosmic Microwave Background (CMB) data set from the Planck satellite mission [3, 5] provides an incredibly detailed snapshot of the universe's early moments, capturing the last scattering horizon. Planck's precision instruments meticulously measured the temperature and polarization of the CMB radiation, offering profound insights into the composition, evolution, and geometry of the cosmos. The CMB is classified as a standard ruler since we can measure the angular diameter distance through a known comoving size (this is only applicable for a flat universe), where the expression for the angular diameter distance is,

$$\mathrm{d}(z) = \frac{1}{1+z}\int_0^z \mathrm{d}z'\frac{1}{H\left(z'\right)}. \tag{5.19}$$

We can construct the scaled distance to recombination by setting,

$$R = \sqrt{\Omega_{m,0}H_0^2}\,r(z_{\mathrm{CMB}}), \tag{5.20}$$

where $r(z_{\mathrm{CMB}})$ represents the comoving distance from the observer to a redshift z. The (CMB) spectrum can be derived for various cosmological models using numerical solvers for the Einstein and Boltzmann equations, such as `CLASS` [118]. More information on numerical solvers will follow.

5.2.4 Baryonic Acoustic Oscillations (BAO)

Baryonic acoustic oscillations (BAO) are observable phenomena formed due to the propagation of sound waves during the development of large-scale structures in the early universe [21]. They provide an additional dataset for comparisons and for conducting cosmological fits. We can measure the position of the BAO peak by measuring a combination of the angular and luminosity distance; the dilation scale [119, 120],

$$D_V\left(z_{\mathrm{BAO}}\right) = \left[\left(\int_0^{z_{\mathrm{BAO}}} \frac{\mathrm{d}z}{H(z)}\right)^2 \frac{z_{\mathrm{BAO}}}{H\left(z_{\mathrm{BAO}}\right)}\right]^{1/3}, \tag{5.21}$$

which tracks the comoving volume and encodes the visual distortion of a spherical object due to the non-Euclideanity of an FRLW spacetime [120, 121]. Note this is only applicable for the CMB case i.e. the uncorrelated data. Similarly to the above, we construct the χ^2 distribution by using the inverse covariance matrix given by the data set [119]. Thus the uncorrelated BAO log-likelihood function can be written as,

$$\ln \mathcal{L}_{\mathrm{BAO}} = -\frac{1}{2}\sum_{i=1}^{N} \ln\left(2\pi\sigma_{\mathrm{B_i}}^2\right) - \frac{1}{2}\sum_{i=1}^{N}\left[\frac{\mathrm{B_i} - \mathrm{B}\left(\mathbf{x}, z_i\right)}{\sigma_{\mathrm{B_i}}}\right]^2. \tag{5.22}$$

5.3 Parameter estimation using MCMC solvers

Depending on the method of parameter estimation we use, we may be able to simplify our analysis. The available tools aid in maintaining numerical consistency among studies, as some numerical methods may deviate, leading to biased results. Some tools that we may employ include `CosmoMC` [122], `emcee` [123], and `MontePython` [124]. To solve the full Einstein and Boltzmann equations, we can estimate parameters using `CLASS` (the Cosmic Linear Anisotropy Solving System [125]) or `CAMB` (Code for Anisotropies in the Microwave Background [126]).

`CLASS` is a versatile numerical code designed for computing the linear evolution of cosmological perturbations by solving the Einstein and Boltzmann equations. The solver is coded in the `C` language to ensure faster and more accurate results. `CAMB`, which predates `CLASS`, functions as a cosmological code designed to compute various parameters including the CMB, lensing, galaxy count, dark-age 21cm power spectra, matter power spectra, and transfer functions. It also incorporates general utility functions for cosmological computations such as background expansion and distances. The main

code is written in Python, with numerical calculations efficiently implemented in Fortran. For a comprehensive comparison, refer to [118]; however, the main conclusion is that `CLASS` outperforms `CAMB` by being 2.5 times faster (when using the same cosmological model), with both solvers in agreement with high precision regarding numerics. Future work will involve utilizing either `CLASS` or `CAMB` to analyze the evolution of the Murnaghan EoS in comparison to existing models and other UDE models. Since priors for the model parameters have already been determined by Ref. [104], this provides a solid foundation for precise statistical assessment.

We have explored the different statistical tools used in cosmological parameter estimation. Following this dissertation, the statistical methods outlined in this Chapter will be explored numerically. The following Chapter 6 concludes this dissertation, with key points raised regarding our initial postulate.

Chapter 6

Final remarks

The primary objectives of this dissertation involve investigating the feasibility of replicating observed phenomena by postulating the presence of a dark sector, comprising both dark matter and dark energy (CDM and a cosmological constant). We model the dark sector as a unified perfect fluid, allowing us to utilize thermodynamic relations and typical fluid mechanics principles. We examined the currently accepted cosmological model, which comprises of two unknown components stated previously. Following this exploration, we investigated three unified dark energy models falling under the category of Quartessence, to be distinguished from Quintessence. Chapter 2 introduced the Chaplygin gas model and the Logotropic EoS. These models were modified from their original forms to address physical inconsistencies observed during initial background tests.

The Generalized Chaplygin gas model (GCG) introduces an unknown parameter α to add more variability to the model's behaviour. However, constraints on α were established because values of $\alpha < 0$ introduced late-time oscillations (exponential growth) of the matter power spectrum, as demonstrated by Ref. [64]. These oscillations do not contribute to structure formation, which is the ultimate goal in numerically reproducing observed formations. However, the GCG successfully aligns with the ΛCDM model at the background level, as demonstrated in §2.1.2. A similar result was found for the pure logotropic case in §2.1.5; however, the behaviour of the sound speed results in non-physical characteristics, i.e. imaginary sound speeds and thus no structure formation at the perturbative level. This result underscores the significance of introducing variability in the EoS, where the generalization of the Anton-Schmidt equation takes the stage. §3.3.2 provides motivation for another degree of freedom by linking the free parameter B to the Planck density[1], a crucial experimental quantity in atomic physics. To evaluate the evolution of growth, we employ the spherical collapse model, as linearity at late and early times is not guaranteed. This approach helps us determine the behaviour of the density contrast and growth function over our chosen timescale. The GCG EoS exhibits promising characteristics, however, the desirable growth factor was not in agreement

[1] shown in §3.3.3

with the approximate solution of $\gamma \sim 6/11$. Since the sound speed is embedded in determining the evolution of growth, the Logotropic EoS yields a decayed growth rate.

Chapter 4 introduces a new UDE model capable of reproducing the behaviour of both the GCG and Logotropic EoS, and similarly shown by [104]. To demonstrate consistency among UDE models, the same procedure was performed to assess the background. The Murnaghan EoS is promising since it is capable of reproducing late-time behaviour typically seen with the ΛCDM model. It transitions from a matter-like behaviour and approaches a cosmological constant. The growth function in §4.2 indicates results in agreement with the behaviour of the ΛCDM model. However, since α is not well constrained, more work is required in determining the physical implications of varying this parameter to either a narrower or wider range. The advantage of this model over the GCG and Logotropic models is that the Murnaghan model introduces **pressure and matter** at late times. This implies that during late times, we may experience a faster growth regime compared to the ΛCDM model. Upon comparing the background and perturbations of the GCG and Logotropic models with the Murnaghan model, favorable outcomes emerge for our novel Unified Dark Energy (UDE) model. It demonstrates consistency across both the background and perturbative levels in comparison with the ΛCDM model. This observation serves as significant indication to further scrutinize the model parameters and conduct rigorous statistical fits.

This leads on to Chapter 5 which outlines the statistical methods used in parameter estimation within cosmology. Boltzmann solvers provide a systematic and ubiquitous tool in computing numerical cosmological calculations and functions used to describe the evolution of different cosmological models.

6.1 Future work

In the realm of cosmological investigations, the Murnaghan EoS stands out for its promising features, notably its capability to replicate late-time behavior reminiscent of the well-established ΛCDM model. Looking ahead, a pivotal avenue for advancing our comprehension and fine tuning the Murnaghan EoS involves the use of rigorous numerical analysis methodologies, particularly through the implementation of Markov Chain Monte Carlo (MCMC) methods and established solvers such as `CAMB` and `CLASS`.

One key future endeavor centers around employing MCMC techniques for robust parameter estimation of the Murnaghan EoS. Through the flexibility offered by MCMC, we can systematically navigate the parameter space, yielding probability distributions for the model parameters. Furthermore, the versatility of MCMC methods allows for the integration of multi-dataset analysis. This integration, encompassing data from diverse cosmological probes and experiments such as Type Ia

supernovae, baryon acoustic oscillations, and weak gravitational lensing, enables a holistic evaluation of the Murnaghan EoS across various cosmic epochs.

Throughout this dissertation we have investigated the potential of explaining the observed phenomena related to the cosmological dark sector—commonly assumed to consist of Cold Dark Matter (CDM) and a cosmological constant—by using the single fluid approach. Specifically, our focus has been on a category of Unified Dark Energy (UDE) models described by adiabatic perfect fluids. Our findings reveal that, under the conventional perturbation theory approach, observations impose significant constraints on the behaviour of UDE models, aligning them closely with ΛCDM [127]. This outcome is primarily influenced by the inherent connection between the adiabatic sound speed and the background evolution. In Adiabatic Unified Dark Energy (UDE) models, there is typically a nonzero sound speed as the system transitions from a dark matter phase to a dark energy phase. This results in the appearance of a distinct length scale, which plays a critical role in assessing the stability of linear perturbations. When this length scale is not sufficiently small, it significantly affects the conventional growth of cosmic structures on linear scales. Consequently, to reconcile with observations of large-scale structures, the sound speed in these models must approach zero extremely closely, mandating a background evolution akin to ΛCDM.

It is essential to recognize that this discovery, by itself, does not undermine the overall concept of a single dark fluid or discredit Unified Dark Energy (UDE) models in particular. As discussed in earlier Chapters, the ΛCDM model can be viewed as a single fluid model, represented by a perfect fluid with a sound speed of zero. Furthermore, ΛCDM, characterized solely by negative and constant pressure, can be perceived as the most straightforward UDE model conceivable. However, the stringent limitations imposed on UDE models through linear analysis might discourage the exploration of additional models or parameterizations. A common approach in literature is to tackle the issue of large sound speeds in Unified Dark Energy (UDE) models is to disregard adiabatic perfect fluids and explore alternative factors like non-adiabatic additions to the sound speed, as illustrated in Reference [128].

In conclusion, the future outlook for the Murnaghan EoS hinges on the rigorous application of MCMC methods. Embracing these advanced statistical techniques is essential not only for refining the model's parameters but also for validating its predictions against observational data.

Appendix A

A.1 FLRW metric in terms of the spatial curvature k

The original FLRW metric is given in terms of comoving coordinates (χ, θ, φ),

$$\mathrm{d}s^2 = \mathrm{d}t^2 - a^2(t)\left\{\mathrm{d}\chi^2 + \Sigma^2(\chi)\left(\mathrm{d}\theta^2 + \sin^2\theta \mathrm{d}\varphi^2\right)\right\},$$
$$\text{where} \quad \Sigma^2(\chi) = \begin{cases} \sin^2\chi \\ \chi^2 \\ \sinh^2\chi \end{cases} \tag{A.1}$$

In each of the three cases we introduce a new variable r where we can make the connection,

$$r \equiv \Sigma(\chi) = \begin{cases} \sin\chi \\ \chi \\ \sinh\chi \end{cases}, \qquad \mathrm{d}r = \begin{cases} \cos\chi \mathrm{d}\chi \\ \mathrm{d}\chi \\ \cosh\chi \mathrm{d}\chi \end{cases}, \tag{A.2}$$

where the derivative is given by dr, such that we can we can write the reduced-circumference polar coordinates as,

$$\mathrm{d}\chi^2 = \frac{\mathrm{d}r^2}{1-kr^2}, \quad \text{where} \quad k = \begin{cases} +1 & \text{if} \quad r = \sin\chi \\ 0 & \text{if} \quad r = \chi \\ -1 & \text{if} \quad r = \sinh\chi \end{cases} \tag{A.3}$$

with,

$$\mathrm{d}\Sigma^2 = \frac{\mathrm{d}r^2}{1-kr^2} + r^2\mathrm{d}\Omega^2, \quad \text{where } \mathrm{d}\Omega^2 = \mathrm{d}\theta^2 + \sin^2\theta\,\mathrm{d}\phi^2. \tag{A.4}$$

to obtain the form presented in Chapter 1,

$$\mathrm{d}s^2 = \mathrm{d}t^2 - a^2(t)\left\{\frac{\mathrm{d}r^2}{1-kr^2} + r^2(\mathrm{d}\theta^2 + \sin^2\theta\mathrm{d}\varphi^2)\right\}. \tag{A.5}$$

A.2 Types of fluids

In the context of cosmology, there are differences between adiabatic, barotropic and effective sound speed:

1. Adiabatic Sound Speed: The adiabatic sound speed, denoted by c_s, represents the speed at which small adiabatic density perturbations or sound waves propagate through a cosmological fluid. It characterises the compressibility and stiffness of the fluid and depends on its thermodynamic properties, such as density and pressure. The adiabatic sound speed is relevant for understanding the propagation of sound waves in cosmological fluids, including the early Universe and large-scale structure formation.

$$c_s^2 = \frac{\partial p}{\partial \rho} = \frac{\partial p}{\partial a}\frac{\partial a}{\partial \rho} \tag{A.6}$$

2. Barotropic Sound Speed: The barotropic sound speed, denoted by c_b, is specific to barotropic fluids in cosmology. A barotropic fluid is one in which the pressure is solely determined by the density, following a barotropic EoS. The barotropic sound speed represents the speed at which density perturbations propagate through such a fluid, taking into account the specific EoS. It is defined as the derivative of pressure with respect to density,

$$c_s^2 = \frac{\mathrm{d}p(\rho)}{\mathrm{d}\rho} \tag{A.7}$$

3. Effective Sound Speed: The effective sound speed, denoted by c_{eff}, is a concept used in cosmology to describe the behaviour of density perturbations in a system with both background and collapsed regions. It accounts for the combined effects of the background and perturbed regions on the propagation of sound waves. The effective sound speed can depend on various factors, including the properties of the cosmic fluid, background density, collapsed region density, and perturbation amplitude. It provides insight into the dynamical behaviour of perturbed regions and their evolution within the cosmological context.

$$c_{eff}^2 = \frac{\delta p}{\delta \rho} \tag{A.8}$$

In summary, the adiabatic sound speed represents the speed of sound waves in a cosmological fluid, while the barotropic sound speed is specific to barotropic fluids and accounts for their EoS. The effective sound speed, on the other hand, considers the combined effects of both background and collapsed regions on the propagation of sound waves in cosmology.

A.3 Analytical solutions for ρ

A.3.1 Chaplygin gas model

The expression for energy conservation within the thermodynamical context for an adiabatic fluid (constant pressure) is written as,

$$\mathrm{d}E = -p\mathrm{d}V, \tag{A.9}$$

which can be rewritten in terms of the scale factor a, by letting $V = a^3$ and $E = \rho a^3$,

$$\mathrm{d}\left(\rho a^3\right) + p\,\mathrm{d}\left(a^3\right) = 0. \tag{A.10}$$

Combining this expression with the EoS for the Chaplygin gas model results in,

$$\begin{aligned} \mathrm{d}\left(\rho a^3\right) + p\,\mathrm{d}\left(a^3\right) &= 0, \\ \rho\,\mathrm{d}\left(a^3\right) + a^3\mathrm{d}\rho &= -p\,\mathrm{d}\left(a^3\right), \\ \rho\,\mathrm{d}\left(a^3\right) + p\,\mathrm{d}\left(a^3\right) &= -a^3\mathrm{d}\rho, \quad \rho + p = -\frac{a^3\mathrm{d}\rho}{\mathrm{d}\left(a^3\right)}. \end{aligned} \tag{A.11}$$

The EoS for the Chaplygin gas model,

$$p_C = -\frac{A}{\rho_C}, \tag{A.12}$$

substituting in the expression for pressure,

$$\begin{aligned} \rho_C - \frac{A}{\rho_C} = -a^3\frac{\mathrm{d}\rho_C}{\mathrm{d}\left(a^3\right)}, \quad \frac{\rho_C^2 - A}{\rho_C} &= -a^3\frac{\mathrm{d}\rho_C}{\mathrm{d}a^3} \\ \frac{\rho_C^2}{\rho_C - A}\mathrm{d}\rho_C &= -\frac{1}{a^3}\,\mathrm{d}\left(a^3\right) \\ \frac{1}{2}\ln\left(\rho_C^2 - A\right) &= -\ln\left(a^3\right) + \ln(B). \end{aligned} \tag{A.13}$$

Simplifying this even further,

$$\rho_C = \sqrt{A + \frac{B}{a^6}} \tag{A.14}$$

The energy density for the Chaplygin gas model where B is an integration constant. The scale factor a in terms of the redshift,

$$a = \frac{1}{1+z}, \tag{A.15}$$

therefore we can write the density as,

$$\rho_C = \sqrt{A + B(1+z)^6} \tag{A.16}$$

The same follows for the Generalized Chaplygin gas (GCG) model, where $\alpha \neq 1$

$$\begin{aligned} p &= -A\rho_{GCG}^{-\alpha} \quad \text{and} \quad \rho_{GCG} + p = -a^3 \frac{\mathrm{d}\rho_{GCG}}{\mathrm{d}\left(a^3\right)} \\ \Rightarrow \rho_{GCG} - A\rho_{GCG}^{-\alpha} &= -a^3 \frac{\mathrm{d}\rho_{GCG}}{\mathrm{d}\left(a^3\right)}, \quad \int \frac{\rho_{GCG}^{\alpha}}{\rho_{GCG}^{\alpha+1} - A} \mathrm{d}\rho_{GCG} = \int \frac{1}{a^3}\, \mathrm{d}\left(a^3\right) \\ \frac{\ln\left(A - \rho_{GCG}^{\alpha+1}\right)}{\alpha+1} &= -\ln\left(a^3\right) + \ln B, \quad (\alpha+1)^{-1} \ln\left(A - \rho_{GCG}^{\alpha+1}\right) = -\ln\left(a^3\right) + \ln B \\ (A - \rho_{GCG}^{\alpha+1})^{(\alpha+1)^{-1}} &= -a^3 + B \end{aligned} \tag{A.17}$$

$$\rho_{GCG} = \left[A + \frac{B}{a^{3(1+\alpha)}}\right]^{\frac{1}{1+\alpha}} \tag{A.18}$$

The energy density for the generalized Chaplygin gas model where B is an integration constant.

A.3.2 Thermodynamic derivation of the continuity equation

We can express the conservation equation for the expanding universe in terms of thermodynamics. The First Law of Thermodynamics (conservation of energy) is given by,

$$\Delta U = Q + W, \tag{A.19}$$

where ΔU is the change in energy, Q is the heat and W is work done on the system. Assuming spherical symmetry and a homogeneous universe,

$$Q = 0. \tag{A.20}$$

For some volume with comoving radius $r_c = 1$, we can write the volume mass as,

$$M = \rho V = \frac{4}{3}\pi a^3 r_c^3 \rho. \tag{A.21}$$

The internal energy, denoted,

$$U = \frac{4}{3}\pi a^3 \rho c^2 \tag{A.22}$$

and assuming a small volume segment of the universe, the first law of thermodynamics becomes,

$$\mathrm{d}U = \mathrm{d}Q + \mathrm{d}W. \tag{A.23}$$

For an adiabatic system, $\mathrm{d}Q = 0$ and $\mathrm{d}W = -p\mathrm{d}V$. Taking the time derivative of U,

$$\frac{\mathrm{d}U}{\mathrm{d}t} = \frac{\mathrm{d}}{\mathrm{d}t}\left(\frac{4}{3}\pi a^3 \rho c^2\right) = 4\pi a^2 \rho c^2 \dot{a} + \frac{4}{3}\pi a^3 c^2 \dot{\rho}. \tag{A.24}$$

The time derivative of V,

$$\frac{\mathrm{d}V}{\mathrm{d}t} = \frac{\mathrm{d}}{\mathrm{d}t}\left(\frac{4}{3}\pi a^3 r_c^3\right) = 4\pi a^2 \dot{a}, \tag{A.25}$$

thus,

$$\begin{aligned} \mathrm{d}U + p\mathrm{d}V &= 0 \\ 4\pi a^2\left[\left(\rho c^2 + p\right)\dot{a} + \frac{1}{3}ac^2\dot{\rho}\right] &= 0 \\ \dot{\rho} + 3\frac{\dot{a}}{a}\left(\rho + \frac{p}{c^2}\right) &= 0. \end{aligned} \tag{A.26}$$

Where $H = \dot{a}/a$, which is equivalent to (where $c = 1$),

$$\dot{\rho} + 3H\left(\rho + p\right) = \dot{\rho} + 3H\left(1 + w\right)\rho = 0 \tag{A.27}$$

A.3.3 Anton Schmidt's equation of state: n and γ_G as free coefficients

The Logotropic equation of state (EoS) stems from principles in solid-state physics and belongs to the broader Anton-Schmidt EoS category. It serves to characterize the pressure exerted by crystalline solids experiencing isotropic stress [26].

To determine a barotropic Anton-Schmidt EoS[1] we begin with the equation in terms of the pressure in the Debye approximation, which is typically given by,

$$p(V) = -\beta\left(\frac{V}{V_0}\right)^{-\frac{1}{6}-\gamma_G} \ln\left(\frac{V}{V_0}\right). \tag{A.28}$$

Where β is the bulk modulus at V_0, $p(V)$ is the pressure, V is the volume and γ_G is the Güneisen parameter. To derive Equation (A.28) we express the volume in terms of mass density, since $V \propto \rho^{-1}$. We can also let $n = -\frac{1}{6} - \gamma_G$ and $\rho_\star$ correspond to the equilibrium volume V_0 which indicates the limit when the pressure vanishes as shown in Ref. [73]. Assuming the universe is filled with a single dark fluid this will yield a barotropic EoS,

$$p(\rho) = A\left(\frac{\rho^{-n}}{\rho_\star^{-n}}\right) \ln\left(\frac{\rho}{\rho_\star}\right), \tag{A.29}$$

[1] The Anton-Schmidt EoS typically refers to crystalline solids which when integrated can give us the total energy.

where n is the number density which is constrained by the conservation of the number of particles and scales as $n \propto a^{-3}$. The background EoS where $n \neq 0$, using the relation $w = p/\rho$, results in,

$$w(\rho) = A\left(\frac{\rho^{-n(T)-1}}{\rho_\star^{-n(T)}}\right)\ln\left(\frac{\rho}{\rho_\star}\right). \tag{A.30}$$

From previous explanation, we know that the continuity equation governs the dynamics of the FLRW universe where the total matter content is given by ρ and p,

$$\frac{\mathrm{d}\rho}{\mathrm{d}t} + 3H(\rho + p) = 0. \tag{A.31}$$

Confirming the consistency with the first law of thermodynamics as seen in §A.3.2. Substituting the EoS in terms of pressure into the first law of thermodynamics yields the expression,

$$\begin{aligned}\epsilon = \rho + \rho\int^\rho \frac{p(\rho')}{\rho^{2'}}\mathrm{d}\rho' &= \rho + \rho\int^\rho A\left(\frac{\rho^{-n}}{\rho_*^{-n}}\right)\ln\left(\frac{\rho}{\rho_*}\right)\frac{1}{\rho^{2'}}\mathrm{d}\rho' \\ &= \rho + \frac{\rho}{\rho_*^2}\int^\rho A\left(\frac{\rho'}{\rho_*}\right)^{-n-2}\ln\left(\frac{\rho}{\rho_*}\right)\mathrm{d}\rho',\end{aligned} \tag{A.32}$$

Allowing $x = \rho/\rho_\star$ and $\mathrm{d}\rho' = \rho_*\mathrm{d}x$, results in,

$$\epsilon = \rho + \frac{\rho}{\rho_*^2}\int^\rho Ax^{-n-2}\ln(x)\rho_*\mathrm{d}x = \rho + x\int^\rho Ax^{-n-2}\ln(x)\mathrm{d}x, \tag{A.33}$$

where the resulting integral is given by,

$$\int^\rho Ax^{-n-2}\ln(x)\mathrm{d}x = -\frac{x^{-n-1}\left((n+1)\ln(x)+1\right)}{(n+1)^2} = -\left(\frac{x^{-n-1}(n+1)\ln(x)}{(n+1)^2} + \frac{x^{-n-1}+1}{(n+1)^2}\right). \tag{A.34}$$

Therefore the expression for the total energy density can be expressed as,

$$\epsilon = \rho + xA\left(-\frac{\ln(x)}{(n+1)}x^{-n-1} - \frac{1}{(n+1)^2}x^{-n-1}\right) = \rho - A\frac{x^{-n}}{(n+1)}\left(\ln(x) + \frac{1}{(n+1)}\right). \tag{A.35}$$

Recall $x = \rho/\rho_*$ which contains both the de and dm components. Setting the de component as,

$$\rho_{de} = \frac{\rho_{de,0}}{\rho_*}a^{-3} = a^{-3} \tag{A.36}$$

indicating a matter-like behaviour, results in

$$x = \frac{\rho}{\rho_*} = \frac{\rho_{m,0}}{\rho_*} + a^{-3}, \quad \ln(x) = \ln\left(\frac{\rho_{m,0}}{\rho_*}\right) - 3\ln a. \tag{A.37}$$

Substituting this into the above expression for ϵ results in,

$$\epsilon = \rho - \frac{A}{(n+1)}\left(\frac{\rho}{\rho_*}\right)^{-n}\left(\ln\left(\frac{\rho_{m,0}}{\rho_*}\right) - 3\ln a + \frac{1}{(n+1)}\right). \tag{A.38}$$

We note however that,

$$\left(\frac{\rho}{\rho_*}\right)^{-n} = \left(\frac{\rho_{m,0}}{\rho_*} + a^{-3}\right)^{-n} = \left(\frac{\rho_{m,0}}{\rho_*}\right)^{-n} + a^{3n}. \tag{A.39}$$

Substituting this back in yields,

$$\begin{aligned}\epsilon &= \rho - \frac{A}{(n+1)}\left(\frac{\rho_{m,0}}{\rho_*}\right)^{-n} a^{3n}\left(\ln\left(\frac{\rho_{m,0}}{\rho_*}\right) - 3\ln a + \frac{1}{(n+1)}\right) \\ &= \rho + \frac{3A}{(n+1)}\left(\frac{\rho_{m,0}}{\rho_*}\right)^{-n} a^{3n}\ln a - \frac{A}{(n+1)}\left(\frac{\rho_{m,0}}{\rho_*}\right)^{-n} a^{3n}\left(\ln\left(\frac{\rho_{m,0}}{\rho_*}\right) + \frac{1}{(n+1)}\right),\end{aligned} \tag{A.40}$$

where last term is the dark matter component at current time. The total energy is written as,

$$\epsilon = \rho + \frac{3A}{(n+1)}\left(\frac{\rho_{m,0}}{\rho_*}\right)^{-n} a^{3n}\ln a + \epsilon_{de,0}a^{3n} \tag{A.41}$$

where the expression for the de density at current time is expressed as,

$$\epsilon_{de,0} = -\frac{A}{(n+1)}\left(\frac{\rho_{m,0}}{\rho_*}\right)^{-n}\left(\ln\left(\frac{\rho_{m,0}}{\rho_*}\right) + \frac{1}{(n+1)}\right). \tag{A.42}$$

The full de component is thus written as,

$$\epsilon_{de} = \frac{3A}{(n+1)}\left(\frac{\rho_{m,0}}{\rho_*}\right)^{-n} a^{3n}\ln a + \epsilon_{de,0}a^{3n}. \tag{A.43}$$

The energy density for the matter component is given below by substituting the expressions for $\epsilon_{de,0}$ and $\epsilon_{m,0}$ into the Hubble parameter (since $\epsilon = \epsilon_m + \epsilon_{de}$),

$$\epsilon_m = \rho_m c^2 \rightarrow \rho_m. \quad c = 1 \tag{A.44}$$

The evolution of the mass density as derived in [129] and given by,

$$\rho = \frac{\rho_{m,0}}{a^3}, \tag{A.45}$$

and shown to be,

$$\epsilon_m = \frac{\rho_{m,0}}{a^3} = \epsilon_{m,0} a^{-3}. \tag{A.46}$$

The Hubble parameter can be rewritten in terms of matter and dark fluid components,

$$H^2 = H_0^2 \left(\frac{\epsilon_m}{\epsilon_c} + \frac{\epsilon_{de}}{\epsilon_c} \right), \tag{A.47}$$

where $\epsilon_c = 3H_0^2/(8\pi G)$. Substituting in the expressions for the dark components and matter (A.43), (A.46),

$$H^2 = H_0^2 \left(\frac{\epsilon_{m,0} a^{-3}}{\epsilon_c} + \frac{\epsilon_{de,0} a^{3n}}{\epsilon_c} + \frac{3A}{(n+1)} \left(\frac{\rho_{m,0}}{\rho_\star} \right)^{-n} a^{3n} \ln a \left(\frac{1}{\epsilon_c} \right) \right). \tag{A.48}$$

Inserting the convenient term (derived from B),

$$\left(\ln \left(\frac{\rho_*}{\rho_{m,0}} \right) + \frac{1}{n+1} \right)^{-1}, \tag{A.49}$$

the Hubble parameter becomes,

$$\begin{aligned} H^2 =& H_0^2 \left(\frac{\epsilon_{m,0} a^{-3}}{\epsilon_c} + \frac{\epsilon_{de,0} a^{3n}}{\epsilon_c} + 3 \left(\frac{\epsilon_{de,0}}{\epsilon_c} \right) \left(\ln \left(\frac{\rho_\star}{\rho_{m,0}} \right) + \frac{1}{n+1} \right)^{-1} a^{3n} \ln a \right) \\ =& H_0^2 \left(\frac{\epsilon_{m,0} a^{-3}}{\epsilon_c} + \frac{\epsilon_{de,0} a^{3n}}{\epsilon_c} + 3 \left(\frac{\epsilon_{de,0}}{\epsilon_c} \right) B a^{3n} \ln a \right) \end{aligned} \tag{A.50}$$

We define the normalized matter and dark matter energy densities as,

$$\Omega_{m,0} = \frac{\epsilon_{m,0}}{\epsilon_c}, \tag{A.51a}$$

$$\Omega_{de,0} = \frac{\epsilon_{de,0}}{\epsilon_c}, \tag{A.51b}$$

Substituting this into the above equation results in the Hubble parameter expressed in terms of dimensionless parameters,

$$\begin{aligned} H^2 &= H_0^2 \left(\Omega_{m,0} a^{-3} + \Omega_{de,0} a^{3n} + 3 \left(\Omega_{de,0} \right) B a^{3n} \ln a \right) \\ &= H_0^2 \left(\Omega_{m,0} a^{-3} + \Omega_{de,0} \left(1 + 3B \ln a \right) a^{3n} \right). \end{aligned} \tag{A.52}$$

Resulting in an expression for the Hubble rate given by,

$$H = H_0 \left(\Omega_{m,0} a^{-3} + \Omega_{de,0} \left(1 + 3B \ln a \right) a^{3n} \right)^{1/2}. \tag{A.53}$$

To calculate the EoS parameters we note that, $w = p/\epsilon$ where

$$p(\rho) = A\left(\frac{\rho}{\rho_\star}\right)^{-n} \ln\left(\frac{\rho}{\rho_*}\right), \tag{A.54}$$

where the sum of the rest-mass energy density and dark fluid components is given by,

$$\epsilon = \epsilon_m + \epsilon_{de} = \epsilon_{de}, \tag{A.55}$$

where the dominating term is the dark energy. Thus we can say,

$$\begin{aligned} p &= A\left(\frac{\rho}{\rho_\star}\right)^{-n} \ln\left(\frac{\rho}{\rho_*}\right) = w(\epsilon_{de}) \\ &= A\left(\frac{\rho_{m,0}^{-n-1}}{\rho_*^{-n}}\right) \ln\left(\frac{\rho_{m,0}}{\rho_*}\right) \left(\left[\frac{3A}{(n+1)}\left(\frac{\rho_{m,0}}{\rho_*}\right)^{-n} a^{3n}\ln a + \epsilon_{de,0}a^{3n}\right]\frac{1}{\epsilon_c}\right), \end{aligned} \tag{A.56}$$

introducing the parameter B, we insert the de components,

$$B = \frac{A}{n+1}\left(\frac{\rho_{m,0}}{\rho_*}\right)^{-n}\frac{1}{\epsilon_c\Omega_{dc,0}} \tag{A.57}$$

therefore the pressure becomes,

$$\begin{aligned} p &= A\left(\frac{\rho_{m,0}^{-n-1}}{\rho_*^{-n}}\right) \ln\left(\frac{\rho_{m,0}}{\rho_*}\right) \left(\left[\frac{3A}{(n+1)}\left(\frac{\rho_{m,0}}{\rho_*}\right)^{-n} a^{3n}\ln a + \epsilon_{de,0}a^{3n}\right]\frac{1}{\epsilon_c}\right) \\ &= A\left(\frac{\rho_{m,0}^{-n-1}}{\rho_*^{-n}}\right) \ln(a) \left(\left[\frac{3A}{(n+1)}\left(\frac{\rho_{m,0}}{\rho_*}\right)^{-n} a^{3n}\ln a + \epsilon_{de,0}a^{3n}\right]\frac{1}{\epsilon_c}\right) \\ &= -\Omega_{de,0}\left[B + n + 3Bn\ln a + 1 + 3B\ln a\right]a^{3n} \\ &= -\epsilon_c\left(\Omega_{de,0}\right)\left[B + (n+1)(1+3B\ln a)\right]a^{3n}. \end{aligned} \tag{A.58}$$

To derive the full energy density we include the matter term,

$$\epsilon = \epsilon_m + \epsilon_{de} = \epsilon_{m,0}a^{-3} + \frac{3A}{(n+1)}\left(\frac{\rho_{m,0}}{\rho_*}\right)^{-n} a^{3n}\ln a + \epsilon_{de,0}a^{3n}. \tag{A.59}$$

The dimensionless energy density can be written in terms of the critical density as,

$$\epsilon = \Omega_{m,0}a^{-3}\epsilon_c + \Omega_{de,0}\left(1 + 3B\ln a\right)a^{3n}\epsilon_c, \tag{A.60}$$

where the expression for the background can be expressed as,

$$\begin{aligned} w = \frac{p}{\epsilon} &= \frac{-\epsilon_c \left(\Omega_{de,0}\right) \left[B + (n+1)(1+3B\ln a)\right] a^{3n}}{\Omega_{m,0} a^{-3} \epsilon_c + \Omega_{de,0} \left(1 + 3B \ln a\right) a^{3n} \epsilon_c} \\ &= -\frac{\left(\Omega_{de,0}\right) \left[B + (n+1)(1+3B\ln a)\right] a^{3n}}{\Omega_{m,0} a^{-3} + \left(1 - \Omega_{m0}\right) \left(1 + 3B \ln a\right) a^{3n}}. \end{aligned} \tag{A.61}$$

To derive the dark energy EoS parameter, we instead use the de components of pressure and energy density, $w_{de} = p_{de}/\epsilon_{de}$, where we assume the matter contributions are negligible at early time,

$$p_{de} = -\epsilon_c \left(1 - \Omega_{m,0}\right) \left[B + (n+1)(1+3B\ln a)\right] a^{3n} \tag{A.62}$$

and,

$$\epsilon_{de} = \Omega_{m,0} a^{-3} \epsilon_c + \Omega_{de,0} \left(1 + 3B \ln a\right) a^{3n} \epsilon_c = \epsilon_c \left(\Omega_{de,0}\right) \left(1 + 3B \ln a\right) a^{3n}, \tag{A.63}$$

thus the expression for the de component is expressed as,

$$\begin{aligned} w_{de} = \frac{p_{de}}{\epsilon_{de}} &= \frac{-\epsilon_c \left(\Omega_{de,0}\right) \left[B + (n+1)(1+3B\ln a)\right] a^{3n}}{\epsilon_c \left(\Omega_{de,0}\right) \left(1 + 3B \ln a\right) a^{3n}} \\ &= -\frac{B}{(1+3B\ln a)} - \frac{(n+1)(1+3B\ln a)}{(1+3B\ln a)} = -\frac{B}{(1+3B\ln a)} - (n+1). \end{aligned} \tag{A.64}$$

To derive the adiabatic speed of sound we use the relationship shown in §A.2,

$$c_s^2 = \frac{\partial p}{\partial a} \left(\frac{\partial \rho}{\partial a}\right)^{-1}. \tag{A.65}$$

The first partial differential reads,

$$\begin{aligned} \frac{\partial p}{\partial a} &= \frac{\partial}{\partial a} \left(-\epsilon_c \left(\Omega_{de,0}\right) \left[B + (n+1)(1+3B\ln a)\right] a^{3n}\right) \\ &= -\epsilon_c \left(\Omega_{de,0}\right) 3a^{3n-1} \left[3B(n+1)n \ln a + 2Bn + B + n^2 + n\right] \\ &= -\epsilon_c \left(\Omega_{de,0}\right) 3a^{3n-1} \left[3B(n+1)n \ln a + B(2n+1)n(n+1)\right], \end{aligned} \tag{A.66}$$

the second integral,

$$\frac{\partial \rho}{\partial a} = \frac{\partial}{\partial a} \epsilon_{m,0} a^{-3} = \frac{\partial}{\partial a} \frac{\epsilon_{m,0} \epsilon_c}{\epsilon_c} a^{-3} = -\frac{3\epsilon_c \Omega_{m,0}}{a^4}. \tag{A.67}$$

The sound speed is therefore,

$$\begin{aligned} c_s^2 &= -\epsilon_c \left(\Omega_{de,0}\right) \left(3a^{3n-1} \left[3B(n+1)n \ln a + B(2n+1)n(n+1)\right]\right) \left(-\frac{3\epsilon_c \Omega_{m,0}}{a^4}\right)^{-1} \\ &= \frac{\Omega_{de,0}}{\Omega_{m,0}} a^{3n-1+4} \left[3B(n+1)n \ln a + B(2n+1)n(n+1)\right] \\ &= \frac{\Omega_{de,0}}{\Omega_{m,0}} a^{3(n+1)} \left[B(1+2n) + n(n+1)(1+3B\ln a)\right] \end{aligned} \tag{A.68}$$

For the most general case in the A-S model regime as shown by [73].

A.3.4 Solution for ϵ using the first law of thermodynamics

The first law of thermodynamics can be written as,

$$\begin{aligned}\epsilon &= \rho + \rho \int^{\rho} \frac{p(\rho')}{\rho^{2'}} \mathrm{d}\rho' = \rho + \rho \int^{\rho} -\frac{A}{-\alpha} \left[\left(\frac{\rho}{\rho_\star} \right)^{\alpha} - 1 \right] \frac{1}{\rho^{2'}} \mathrm{d}\rho' \\ &= \rho - \frac{A\rho}{\alpha} \int^{\rho} \left(\frac{\rho}{\rho_\star} \right)^{-\alpha} \frac{1}{\rho'^2} - \frac{1}{\rho^{2'}} \mathrm{d}\rho' = \rho - \frac{A\rho}{\alpha} \left[\left(\frac{\rho}{\rho_\star} \right)^{-\alpha} \frac{1}{\alpha\rho + \rho} - \frac{1}{\rho} \right].\end{aligned} \tag{A.69}$$

Resulting in the solution for density given by,

$$\epsilon = \rho + \frac{A}{\alpha} \left[\left(\frac{\rho}{\rho_\star} \right)^{-\alpha} \frac{1}{\alpha + 1} + 1 \right] \tag{A.70}$$

A.4 Derivation of the Murnaghan equation of state

A solid possesses a specific equilibrium volume, denoted as V_0, and its energy increases quadratically when the volume is either increased or decreased slightly from this value. Building upon the previous argument establishing the consistency between the first law of thermodynamics and the continuity equation, both approaches aim to derive density through conservative methods. Consequently, we can express the first and second principles as,

$$T\mathrm{d}S = \mathrm{d}\big(\rho V\big) + p\mathrm{d}V = \mathrm{d}\big(\rho + p\big)\, V - V\mathrm{d}p, \tag{A.71}$$

and since,

$$\frac{\partial^2 S}{\partial T \partial V} = \frac{\partial^2 S}{\partial V \partial T}, \tag{A.72}$$

resulting in,

$$\mathrm{d}p = (\rho + p)\frac{\mathrm{d}T}{T}. \tag{A.73}$$

Remaining consistent with thermodynamic theory, recasting the continuity equation we get,

$$\mathrm{d}\left[\frac{(\rho + p)V}{T} \right] = 0, \tag{A.74}$$

resulting in the fact that $S =$ constant. This is equivalent to the case if the system is adiabatic. The simplest plausible dependence of energy on volume would be a harmonic solid, with energy given

by,

$$E = E_0 + \frac{1}{2} K_0 \frac{(V - V_0)^2}{V_0}. \tag{A.75}$$

The next simplest reasonable model would be with a constant bulk modulus

$$K_0 = -V \left(\frac{\partial p}{\partial V} \right)_T. \tag{A.76}$$

Integrating results in an expression for pressure in terms of constants,

$$\begin{aligned} p &= K_0 \ln\left(\frac{V_0}{V}\right) = V_0 \exp\left(\frac{-p}{K_0}\right) \\ &= E_0 + K_0 \left[V_0 - V + V \ln\left(\frac{V_0}{V}\right) \right]. \end{aligned} \tag{A.77}$$

We consider the pressure,

$$p = -\left(\frac{\partial E}{\partial V} \right)_S, \tag{A.78}$$

with bulk modulus,

$$K = -V \left(\frac{\partial p}{\partial V} \right)_T. \tag{A.79}$$

Experimentally, the bulk modulus pressure derivative is expressed as,

$$K' = \left(\frac{\partial K}{\partial p} \right)_T, \tag{A.80}$$

and found to change little with pressure. Setting $K' = K_0'$ to be a constant, then,

$$K = K_0 + K_0' p, \tag{A.81}$$

where K_0 is the value of K when $p = 0$. We may equate this with (A.79) and rearrange as,

$$\frac{\mathrm{d}V}{V} = -\frac{\mathrm{d}p}{K_0 + K_0' p}. \tag{A.82}$$

Integrating this results in an expression for pressure in terms of volume,

$$p(V) = \frac{K_0}{K_0'} \left[\left(\frac{V_0}{V} \right)^{K_0'} - 1 \right], \tag{A.83}$$

or equivalently

$$V(p) = V_0 \left(1 + K_0' \frac{p}{K_0} \right)^{-1/K_0'}. \tag{A.84}$$

Substituting (A.83) into $E = E_0 - \int p \, \mathrm{d}V$ when $T = 0$ then energy can be expressed as,

$$E(V) = E_0 + \frac{K_0 V}{K_0'} \left(\frac{(V_0/V)^{K_0'}}{K_0' - 1} + 1 \right) - \frac{K_0 V_0}{K_0' - 1}. \tag{A.85}$$

Appendix B

Appendices

B.1 Spherical collapse model

The expression for the Newtonian evolution of the density contrast is given by,

$$\ddot{\delta} + 2H\dot{\delta} - 4\pi G\rho_m\delta = 0, \tag{B.1}$$

where the last term arises due to the influence of gravitation. Without gravitation, this equation resembles a wave equation for free sound waves in a fluid, however the gravitational field introduces a forcing term. The perturbations are decomposed into two components, representing matter and smooth dark energy. Consequently, the standard growth factor equation is associated with the dark matter component. To determine the continuity and Euler equations we express the time derivative of density as,

$$\frac{\partial\rho}{\partial t} + 3(c_s^2 - w)\rho + \vec{\nabla}\cdot\left[(1+w)\,\rho\vec{u}\right] = 0. \tag{B.2}$$

Denoting $\delta = \delta\rho/\rho$, $\theta = \vec{\nabla}\cdot u$ and $c_s^2 = s$, the continuity equation becomes,

$$\delta^{'} + 3(s-w)\delta + (1+w)\tilde{\theta} = 0, \tag{B.3}$$

where $\delta/\delta t = \delta'$. Thus Euler's equation can be written as,

$$\tilde{\theta}' + \left(2 + \frac{H^{'}}{H}\right)\tilde{\theta} + \frac{3}{2}(1+3s)\Omega(a)\delta = 0. \tag{B.4}$$

The dimensionless energy density can expressed as,

$$\Omega_m(a) = \frac{\rho_m}{\rho_m + \rho_{de}}, \tag{B.5}$$

similarly to [105] to express the effective matter density. To arrive at a similar solution to Ref.[73], we define our variables as $A = 3(s-w)$, $B = 1+w$ and $f = 3/2(1+3s)\Omega(a)$. Substituting into the continuity equation (B.3), and taking the partial derivative with respect to time results in,

$$\begin{aligned} \delta' + 3(s-w)\delta + (1+w)\tilde{\theta} = \delta' + A\delta + B\tilde{\theta} = 0, \\ \frac{\partial}{\partial t}\left(\delta' + A\delta + B\tilde{\theta}\right) = \delta'' + (A\delta)' + B\tilde{\theta}' = 0, \\ \tilde{\theta}' = \frac{-\delta'' - (A\delta)'}{B'}. \end{aligned} \tag{B.6}$$

Note the expression for $\tilde{\theta}$ is determined by,

$$\delta' + A\delta + B\tilde{\theta} = 0 \quad \Rightarrow \tilde{\theta} = \frac{-\delta' - A\delta}{B}. \tag{B.7}$$

Substituting (B.7) and the expression for f into (B.4) we can derive the following,

$$\begin{gathered} \tilde{\theta}' + \left(2 + \frac{H'}{H}\right)\tilde{\theta} + \frac{3}{2}(1+3s)\Omega(a)\delta = 0 \\ \frac{-\delta'' - (A\delta)'}{B'} + \left(2 + \frac{H'}{H}\right)\left(\frac{-\delta' - A\delta}{B}\right) + f\delta = \frac{\delta'' + (A\delta)'}{B'} + \left(2 + \frac{H'}{H}\right)\left(\frac{\delta' + A\delta}{B}\right) - f\delta = 0. \end{gathered} \tag{B.8}$$

Multiplying each term by B results in the second derivative of the density contrast,

$$\delta'' + (A\delta)' + (\delta' + A\delta)\left[\left(2 + \frac{H'}{H}\right) - \frac{B'}{B}\right] - Bf\delta = 0. \tag{B.9}$$

We can simplify this result further by switching back to the original expression of f and letting $A = 3s$ and $B = 1$ (making the derivative $B' = 0$) and $w \neq 0$. The density contrast can now be expressed in terms of w and c_s^2 as,

$$\delta'' + 3\left[(s-w)\delta\right]' + \left(2 + \frac{H'}{H} - \frac{w'}{1+w}\right)\left[\delta' + 3(s-w)\delta\right] - \frac{3}{2}(1+3s)(1+w)\Omega(a)\delta = 0\,. \tag{B.10}$$

The growth index derived by Ref. [82] is proportional to the linear density perturbation $\delta_\rho = \delta\rho/\rho$ and normalized to $g_{(a=0)} = 1$[1],

$$f = \frac{\mathrm{d}\ln\delta_\rho}{\mathrm{d}\ln a} \approx \Omega_m^\gamma(a). \tag{B.11}$$

By examining the logarithmic derivative of the growth factor, denoted as f, where the prime indicates differentiation with respect to $\ln a$, we find that for the matter-only scenario, f equals 1. This allows

[1] where $g(a)$ is the growth factor

us to express the following relationship,

$$f = \frac{\mathrm{d}\ln\delta}{\mathrm{d}\ln a} = \frac{\mathrm{d}\ln\delta}{\mathrm{d}\delta}\frac{\mathrm{d}\delta}{\mathrm{d}\ln a} = \frac{1}{\delta}\delta^{'} = \frac{\delta^{'}}{\delta}, \tag{B.12}$$

thus,

$$f^{'} = \frac{\delta^{''}}{\delta} - \frac{\delta^{'2}}{\delta^2} = \frac{\delta^{''}}{\delta} - f^2 \Rightarrow \delta^{''} = \delta(f^{'} + f^2), \tag{B.13}$$

applying this to Equation (B.10) results in,

$$\begin{aligned}
\delta'' + 3(s\delta)' + (\delta' + 3s\delta)\left(2 + \frac{H'}{H}\right) - \frac{3}{2}(1+3s)\Omega(a)\delta = 0,\\
\frac{\mathrm{d}}{\mathrm{d}\ln a}(\ln\delta'') + \frac{\mathrm{d}}{\mathrm{d}\ln a}\left[\ln 3(s\delta)'\right] + \frac{\mathrm{d}}{\mathrm{d}\ln a}(\ln\Big(\delta' + 3s\delta\Big))\left(2 + \frac{H'}{H}\right) - \frac{\mathrm{d}}{\mathrm{d}\ln a}\left[\frac{3}{2}(1+3s)\Omega(a)\ln\delta\right] = 0,\\
f' + f^2 + 3\left[s\frac{\mathrm{d}\ln\delta'}{\mathrm{d}\ln a} + s'\frac{\mathrm{d}\ln\delta}{\mathrm{d}\ln a}\right] + \left(\frac{\mathrm{d}\ln\delta'}{\mathrm{d}\ln a} + 3s\frac{\mathrm{d}\ln\delta}{\mathrm{d}\ln a}\right)\left(2 + \frac{H'}{H}\right) - \frac{3}{2}(1+3s)\frac{\mathrm{d}\delta}{\mathrm{d}\ln a}\Omega(a) = 0,\\
f' + f^2 + 3(s' + sf) + (f + 3s)\left(2 + \frac{H'}{H}\right) - \frac{3}{2}(1+3s)\Omega_m = 0.
\end{aligned} \tag{B.14}$$

B.1.1 ΛCDM case

The Friedmann equation is written in terms of the sum of mass components, where Λ is defined as an unknown described by,

$$H^2 = \frac{\kappa^2}{3}\left(\rho_m + \rho_r + \rho_\Lambda\right), \tag{B.15}$$

where $\kappa = \sqrt{8\pi G}$ for simplicity. We can express the time derivative as follows, (where the dot is refers to the derivative in cosmic time),

$$\begin{aligned}
2H\dot{H} &= \frac{\kappa^2}{3}\left(-3H\rho_m - 4H\rho_r\right)\\
\dot{H} &= -\frac{\kappa^2}{6}\left(3\rho_m + 4\rho_r\right)
\end{aligned} \tag{B.16}$$

Switching to conformal time (η) denoted by primes, we can express the Hubble rate as,

$$\frac{\mathrm{d}H}{\mathrm{d}t} = H^{'}H, \tag{B.17}$$

therefore,

$$\frac{H^{'}}{H} = -\frac{\kappa^2}{6}\left(3\frac{\rho_m}{H^2} + 4\frac{\rho_r}{H^2}\right). \tag{B.18}$$

Expressing ρ in terms of dimensionless density parameters Ω_i allows to express,

$$\Omega_i \equiv \frac{\kappa^2 \rho_i}{3H^2}, \tag{B.19}$$

$$\frac{H^{'}}{H} = -\frac{\kappa^2}{6}\left(3\frac{3}{\kappa^2}\Omega_m + 4\frac{3}{\kappa^2}\Omega_r\right) = -\frac{1}{2}\left(3\Omega_m + 4\Omega_r\right). \tag{B.20}$$

The conservation energy density given by the relationship $\Omega_\Lambda + \Omega_m + \Omega_r = 1$,

$$\frac{H^{'}}{H} = -\frac{1}{2}\left[3(1-\Omega_r-\Omega_\Lambda) + 4\Omega_r\right] = -\frac{1}{2}\left(3 - 3\Omega_\Lambda + \Omega_r\right). \tag{B.21}$$

Using the following relation,

$$\delta^{''} + 3\left[(s-w)\delta\right]^{'} + \left(2 + \frac{H^{'}}{H} - \frac{w^{'}}{1+w}\right)\left[\delta^{'} + 3(s-w)\delta\right] - \frac{3}{2}(1+3s)(1+w)\Omega(a)\delta = 0, \tag{B.22}$$

and setting $s = w = 0$ for the ΛCDM case simplifies to,

$$\delta_m^{''} + \left(2 + \frac{H^{'}}{H}\right)\delta_m^{'} - \frac{3}{2}\Omega(a)_m\delta_m = 0, \tag{B.23}$$

describing the linear differential equation similarly found in [95].

B.2 Newtonian Gauge for a single fluid

Referencing the methodology used in [27], the perturbed Einstein equations in terms of the Fourier mode k is expressed as,

$$k^2\Phi + 3\mathcal{H}\left(\Phi^{'} - \mathcal{H}\Psi\right) = 4\pi G a^2 \rho\delta, \tag{B.24a}$$

$$k^2\left(\Phi^{'} - \mathcal{H}\Psi\right) = -4\pi G a^2(1+w)\rho\theta, \tag{B.24b}$$

$$\Psi = -\Phi, \tag{B.24c}$$

$$\Phi^{''} + 2\mathcal{H}\Phi^{'} - \mathcal{H}\Psi^{'} - \left(\mathcal{H}^2 + 2\mathcal{H}^{'}\right)\Psi = -4\pi G a^2 c_s^2 \rho\delta, \tag{B.24d}$$

where Equations B.24a and B.24b can be combined to obtain an expression for the relativistic Poisson equation,

$$\begin{aligned} k^2\Phi + 3\mathcal{H}\left(-4\pi G a^2(1+w)\rho\theta k^{-2}\right) &= 4\pi G a^2\rho\delta, \\ k^2\Phi &= 4\pi G a^2\rho\left[\delta + 3\mathcal{H}(w+1)\theta k^{-2}\right], \end{aligned} \tag{B.25}$$

where the total-matter variable is denoted as,

$$\delta^* = \delta + 3\mathcal{H}(w+1)\theta/k^2, \tag{B.26}$$

resulting in the relativistic Poisson equation,

$$k^2\Phi = 4\pi G a^2 \rho \delta^*. \tag{B.27}$$

The perturbed continuity equation can be expressed as,

$$\begin{aligned} (\delta\rho)^{'} + 3\mathcal{H}(\delta\rho + \delta p) &= -(\rho + p)\left(\theta + 3\Phi^{'}\right), \\ \delta^{'} + 3\mathcal{H}\left(c_s^2 - w\right)\delta &= -(1+w)\left(\theta + 3\Phi^{'}\right), \end{aligned} \tag{B.28}$$

where the unperturbed continuity equation is used along with the background equation of state $w = p/\rho$ and sound speed $c_s^2 = \delta p/\delta\rho$. Since we are working on small scales we only consider the background,

$$H^2 = \frac{8\pi G}{3}\left(\rho_M + \rho_r\right), \tag{B.29}$$

where ρ_M refers to the Murnaghan density. The equation for the density perturbations for a given mode k, i.e. $k \gg Ha$ can be derived from the perturbed field equations. Thus we can express the evolution of scalar perturbations similarly to [27],

$$\left(\delta^*\right)^{''} + \mathcal{H}\left(1 + 3c_s^2 - 6w\right)\left(\delta^*\right)^{'} - \left[\frac{3}{2}\mathcal{H}^2\left(1 - 6c_s^2 - 3w^2 + 8w\right) - c_s^2k^2\right]\delta^* = 0. \tag{B.30}$$

Since we are working on small scales, and $\mathcal{H} = Ha$, we make the conversion from conformal time to cosmic time,

$$\mathrm{d}t = a\mathrm{d}\eta. \tag{B.31}$$

The density contrast can now be expressed as,

$$a^2(H\delta^{'} + \delta^{''}) + a^2H\left(1 + 3c_s^2 - 6w\right)\delta^{'} - \left[\frac{3}{2}a^2H^2\left(1 - 6c_s^2 - 3w^2 + 8w\right) - c_s^2k^2\right]\delta = 0 \tag{B.32}$$

, resulting in,

$$\left(\delta_k\right)^{''} + \left(2 + 3c_s^2 - 6w\right)H\delta_k^{'} - \left[\frac{3}{2}H^2\left(1 - 6c_s^2 - 3w^2 + 8w\right) - \left(\frac{c_sk}{a}\right)^2\right]\delta_k = 0 \tag{B.33}$$

Translating from cosmic time to the logarithmic scale factor, the density contrast can be expressed in terms of the derivative with respect the the number of e-foldings. To convert we need to make the

substitution for the logarithmic scale factor $x = \ln a$

$$\begin{aligned} \frac{\mathrm{d}}{\mathrm{d}t} &= H\frac{\mathrm{d}}{\mathrm{d}x}, \\ \frac{\mathrm{d}^2}{\mathrm{d}t^2} &= H^2\frac{\mathrm{d}^2}{\mathrm{d}x^2} + \frac{H^2\mathrm{d}H/\mathrm{d}x}{H^2}\frac{\mathrm{d}}{\mathrm{d}x} = H^2\left(\ddot{\delta} + \frac{H^{'}}{H^2}\dot{\delta}\right), \end{aligned} \tag{B.34}$$

making the density contrast expression,

$$\begin{aligned} \ddot{\delta_k} + \left(2 + 3c_s^2 - 6w\right)H\dot{\delta_k} - \left[\frac{3}{2}H^2\left(1 - 6c_s^2 - 3w^2 + 8w\right) - \left(\frac{c_s k}{a}\right)^2\right]\delta_k = 0, \\ H^2\left(\ddot{\delta_k} + \frac{H^{'}}{H^2}\dot{\delta_k}\right) + \left(2 + 3c_s^2 - 6w\right)H\dot{\delta_k} - \left[\frac{3}{2}H^2\left(1 - 6c_s^2 - 3w^2 + 8w\right) - \left(\frac{c_s k}{a}\right)^2\right]\delta_k = 0, \\ \ddot{\delta_k} + \dot{\delta_k}\left(2 + \frac{H^{'}}{H} + 3c_s^2 - 6w\right) - \left[\frac{3}{2}\left(1 - 6c_s^2 - 3w^2 + 8w\right) - \left(\frac{c_s k}{aH}\right)^2\right]\delta_k = 0. \end{aligned} \tag{B.35}$$

Note, the total equation of state satisfies the following relation ([27], Chapter 11),

$$\frac{\mathcal{H}^{'}}{\mathcal{H}} = 1 + \frac{H^{'}}{H} = -\frac{1}{2} - \frac{3}{2}w, \tag{B.36}$$

allowing us to change our variable to solely include the background and sound speed. Define a new variable ξ, similarly to [87], as $\xi = -3/2(1+w)$, we can express the density contrast as,

$$\ddot{\delta_k} + \dot{\delta_k}\left(2 + \xi + 3c_s^2 - 6w\right) - \left[\frac{3}{2}\left(1 - 6c_s^2 - 3w^2 + 8w\right) - \left(\frac{c_s k}{aH}\right)^2\right]\delta_k = 0. \tag{B.37}$$

This allows us to visually describe the behaviour of the density contrast with the correct derivatives. For the ΛCDM case where $w = 0$, $c_s^2 = 0$, the matter density perturbations reduce to,

$$\delta_m^{''} + \left(2 + \frac{H^{'}}{H}\right)\delta_m^{'} - \frac{3}{2}\Omega(a)_m\delta_m = 0\,, \tag{B.38}$$

B.3 Growth index derivation

To derive Equation (3.25), we substitute expression (B.11) into (B.14), but before that we differentiate the first term (f') in (B.11),

$$\begin{aligned} f &= \Omega_m^{\gamma}(a), \\ \ln f = \gamma \ln \Omega_m, \quad \frac{1}{f}f' &= \gamma' \ln \Omega_m + \frac{\gamma}{\Omega_m}\Omega_m', \\ f' &= \gamma'\Omega_m^{\gamma}\ln\Omega_m + \gamma\Omega_m'\Omega_m^{\gamma-1}. \end{aligned} \tag{B.39}$$

Note that the differential is given by,

$$\Omega_m = \frac{\rho_m}{3H^2}, \tag{B.40}$$

and the differential of conservation of energy is given by,

$$\begin{aligned} \frac{\mathrm{d}\rho}{\mathrm{d}t} + 3H(\rho + p) = 0, \\ \dot{\rho_m} = -3H\rho_m. \end{aligned} \tag{B.41}$$

Therefore the dimensionless matter density parameter can be expressed as,

$$\Omega_m' = \frac{\rho_m'}{2H^2} - \frac{2}{3}\frac{\rho_m}{H^2}\frac{H'}{H}, \tag{B.42}$$

$$\rho_m' = -3\rho_m. \tag{B.43}$$

The derivative of Ω_m' will read,

$$\Omega_m' = -3\Omega_m - 2\Omega_m\frac{H'}{H} = -\Omega_m\left(3 + \frac{2H'}{H}\right). \tag{B.44}$$

The final form of f',

$$f' = \gamma'\Omega_m^{\gamma}\ln\Omega_m^{\gamma} - \gamma\Omega_m^{\gamma}\left(3 + \frac{2H'}{H}\right), \tag{B.45}$$

where Equation (3.25) now reads,

$$\gamma'\Omega_m^{\gamma}\ln\Omega_m^{\gamma} - \gamma\Omega_m^{\gamma}\left(3 + \frac{2H'}{H}\right) + \Omega_m^{2\gamma} + 3(s' + sf) + (f + 3s)\left(2 + \frac{H'}{H}\right)\frac{3}{2}(1 + 3s)\Omega_m = 0. \tag{B.46}$$

We need to evaluate the H'/H term by going back to the conservation of energy equation which states,

$$\begin{aligned} 3H^2 = \rho, \quad 6HH' = \rho_m' + \rho_{de}', \\ = -3\rho_m - 3(1 + w_{de})\rho_{de}. \end{aligned} \tag{B.47}$$

The term H'/H is,

$$\begin{aligned} \frac{H'}{H} = -\frac{1}{2}\left[\frac{\rho_m}{H^2} + \frac{\rho_{de}}{H^2}(1 + w_{de})\right] = -\frac{3}{2}\left[\Omega_m + \Omega_{de}(1 + w_{de})\right], \\ = -\frac{3}{2}\left[1 + \Omega_{de}w_{de})\right], \end{aligned} \tag{B.48}$$

therefore,

$$3 + \frac{2H'}{H} = 3 - 3(1 + \Omega_{de}w_{de}) = -3\Omega_{de}w_{de}, \tag{B.49}$$

and,

$$\begin{aligned} 2+\frac{H'}{H} = 2-\frac{3}{2}w_{de}-\frac{3}{2}\Omega_{de} &= \frac{1}{2}-\frac{3}{2}\Omega_{de}w_{de}, \\ &= \frac{1}{2}(1-3\Omega_{de}w_{de}). \end{aligned} \tag{B.50}$$

Substituting this back into our original expression where $f = \Omega_m^\gamma$,

$$\gamma'\Omega_m^\gamma \ln\Omega_m^\gamma - \gamma\Omega_m^\gamma\left(-3\Omega_{de}w_{de}\right) + \Omega_m^{2\gamma} + 3(s' + s\Omega_m^\gamma) + (\Omega_m^\gamma + 3s)(1-3\Omega_{de}w_{de})\frac{3}{4}(1+3s)\Omega_m = 0. \tag{B.51}$$

Dividing throughout by $\Omega_m^\gamma \ln\Omega_m^\gamma$ results in our final solution for (3.25),

$$\gamma^{'} + \frac{3\Omega_{de}w_{de}}{\ln\Omega_m}\gamma + \frac{\Omega_m^\gamma}{\ln\Omega_m} + 3\frac{s+s^{'}\Omega_m^{-\gamma}}{\ln\Omega_m} + \frac{1-3\Omega_{de}w_{de}}{2\ln\Omega_m}\left(1+3s\Omega_m^{-\gamma}\right) - \frac{3(1+3s)}{2\ln\Omega_m}\Omega_m^{1-\gamma} = 0. \tag{B.52}$$

Using the assumption that $\Omega_m \approx O(1)$, $\ln\Omega_m \approx -\Omega_{de}$ and $\Omega_m^\gamma \approx 1-\gamma\Omega_{de}$,

$$\gamma^{'} + \gamma - 3w_{de}\gamma + \frac{3}{2}\gamma + \frac{3}{2}s\left(2+3\Omega_{de}w_{de}\right)\gamma - 3s^{'}\gamma - \frac{3}{2}(1+6s)\left(1-w_{de}\right) - \frac{3s^{'}}{\Omega_{de}} = 0 \tag{B.53}$$

resulting in the derivation for γ,

$$\gamma^{'} + \left[1-3w_{de}+\frac{3}{2}+\frac{3}{2}s\left(2+3\Omega_{de}w_{de}\right)-3s^{'}\right]\gamma = \frac{3}{2}(1+6s)\left(1-w_{de}\right) + \frac{3s^{'}}{\Omega_{de}}. \tag{B.54}$$

Assuming that $s = 0$ and w_{de} is constant results in a first order linear ODE of the form,

$$\begin{aligned} \gamma' + \gamma(1-3w_{de}+\frac{3}{2}+0+0) &= \frac{3}{2}(1)(1-w_{de})+0, \\ \gamma' + \gamma(\frac{5}{2}-3w_{de}) &= \frac{3}{2}(1-w_{de}). \end{aligned} \tag{B.55}$$

Changing the form to a separable ODE and using the variable x instead of γ for simplicity allows us to write,

$$\begin{aligned} \frac{2}{3-3w_{de}-5x+6w_{de}x}x' &= 1 \quad \text{let } x' = \mathrm{d}x/\mathrm{d}t, \\ \int\frac{2\mathrm{d}x}{3-3w_{de}-5x+6w_{de}x} &= \int \mathrm{d}t, \\ \frac{2\ln(3-3w_{de}-5x+6w_{de}x)}{6w_{de}-5} &= t+C. \end{aligned} \tag{B.56}$$

Isolating x results in,

$$x = \frac{e^{\frac{6w_{de}t-5t+6C(w_{de}-5C}{2}}}{-5+6w_{de}} + \frac{3w_{de}}{-5+6w_{de}} - \frac{3}{-5+6w_{de}}. \tag{B.57}$$

Since w_{de} is constant the exponential terms drops off. Changing x back to γ we have the expression for the wCDM case,

$$\gamma = \frac{3w_{de}}{-5+6w_{de}} - \frac{3}{-5+6w_{de}} = \frac{3(1-w_{de})}{6w_{de}-5} \tag{B.58}$$

We will now assume that both w_{de} and s are constant. We consider the whole derivation of γ in Equation (B.54) and that $2+3\Omega_{de}w_{de} \approx 2$. Under these assumptions, Equation(B.54) becomes,

$$\begin{aligned} \gamma^{'} + \left[1 - 3w_{de} + \frac{3}{2} + \frac{3}{2}s\,(2) - 3s^{'}\right]\gamma &= \frac{3}{2}(1+6s)\,(1-w_{de}) + \frac{3s^{'}}{\Omega_{de}}, \\ \gamma^{'} + \left[\frac{5}{2} - 3w_{de} + 3s\right]\gamma &= \frac{3}{2}(1+6s)\,(1-w_{de}) + 3s'(\frac{1}{\Omega_{de}} + \gamma). \end{aligned} \tag{B.59}$$

Since s is constant, $s' = 0$ resulting in,

$$\gamma^{'} + \left[1 - 3w_{de} + \frac{3}{2} + 3s\right]\gamma = \frac{3}{2}(1+6s)\,(1-w_{de})\,. \tag{B.60}$$

To derive the solution for the above case, we use a similar procedure as before,

$$\gamma' + \left(\frac{5}{2} - 3w_{de} + 3s\right)\gamma = \frac{3}{2}(1+6s)(1-w_{de}), \tag{B.61}$$

where the solution is,

$$\gamma = c_1 e^{3w_{de}t - 3st - (5t)/2} + \frac{18w_{de}s}{6w_{de}-6s-5} + \frac{3w_{de}}{6w_{de}-6s-5} - \frac{18s}{6w_{de}-6s-5} - \frac{3}{6w_{de}-6s-5} \tag{B.62}$$

excluding any exponential terms we arrive at,

$$\gamma = \frac{3(1+6s)(1-w_{de})}{5+6(s-w_{de})} \tag{B.63}$$

Bibliography

1. E. Tiesinga, P. J. Mohr, D. B. Newell, B. N. Taylor, *Journal of Physical and Chemical Reference Data* **50**, 033105, ISSN: 0047-2689, (2024; https://doi.org/10.1063/5.0064853) (23rd Sept. 2021).
2. P. S. Wesson, *Space Science Reviews* **27**, ADS Bibcode: 1980SSRv...27..109W, 109–153, ISSN: 0038-6308, (2023; https://ui.adsabs.harvard.edu/abs/1980SSRv...27..109W) (1st Oct. 1980).
3. P. Collaboration *et al.*, *Astronomy & Astrophysics* **641**, A6, ISSN: 0004-6361, 1432-0746, arXiv: 1807.06209[astro-ph], (2023; http://arxiv.org/abs/1807.06209) (Sept. 2020).
4. A. G. Riess *et al.*, *The Astrophysical Journal Letters* **908**, L6, ISSN: 2041-8205, 2041-8213, arXiv: 2012.08534[astro-ph], (2023; http://arxiv.org/abs/2012.08534) (1st Feb. 2021).
5. P. Collaboration *et al.*, *Astronomy & Astrophysics* **641**, A7, ISSN: 0004-6361, 1432-0746, arXiv: 1906.02552[astro-ph], (2023; http://arxiv.org/abs/1906.02552) (Sept. 2020).
6. F. Zwicky, *Helvetica Physica Acta* **6**, in collab. with H. Andernach, Publisher: Birkhaeuser, 110–127, ISSN: 0018-0238, (2023; https://resolver.caltech.edu/CaltechAUTHORS:20190108-092708978) (1933).
7. D. H. Rogstad, G. S. Shostak, *The Astrophysical Journal* **176**, ADS Bibcode: 1972ApJ...176..315R, 315, ISSN: 0004-637X, (2023; https://ui.adsabs.harvard.edu/abs/1972ApJ...176..315R) (1st Sept. 1972).
8. K. C. Freeman, *The Astrophysical Journal* **160**, ADS Bibcode: 1970ApJ...160..811F, 811, ISSN: 0004-637X, (2023; https://ui.adsabs.harvard.edu/abs/1970ApJ...160..811F) (1st June 1970).
9. R. H. Sanders, *Astronomy and Astrophysics* **136**, ADS Bibcode: 1984A&A...136L..21S, L21–L23, ISSN: 0004-6361, (2023; https://ui.adsabs.harvard.edu/abs/1984A&A...136L..21S) (1st July 1984).
10. G. Bertone, T. M. P. Tait, *Nature* **562**, Number: 7725 Publisher: Nature Publishing Group, 51–56, ISSN: 1476-4687, (2023; https://www.nature.com/articles/s41586-018-0542-z) (Oct. 2018).
11. G. Jungman, M. Kamionkowski, A. Kosowsky, D. N. Spergel, *Physical Review Letters* **76**, ADS Bibcode: 1996PhRvL..76.1007J, 1007–1010, ISSN: 0031-9007, (2023; https://ui.adsabs.harvard.edu/abs/1996PhRvL..76.1007J) (1st Feb. 1996).

12. Z. Thomas, D. Tucker-Smith, N. Weiner, *Physical Review D* **77**, Publisher: American Physical Society, 115015, (2023; https://link.aps.org/doi/10.1103/PhysRevD.77.115015) (18th June 2008).

13. T. Rothman, S. Boughn, *Foundations of Physics* **36**, 1801–1825, ISSN: 1572-9516, (2023; https://doi.org/10.1007/s10701-006-9081-9) (1st Dec. 2006).

14. K. Agashe, H. Davoudiasl, G. Perez, A. Soni, *Physical Review D* **76**, 036006, ISSN: 1550-7998, 1550-2368, arXiv: hep-ph/0701186, (2023; http://arxiv.org/abs/hep-ph/0701186) (31st Aug. 2007).

15. M. Davis, F. J. Summers, D. Schlegel, *Nature* **359**, ADS Bibcode: 1992Natur.359..393D, 393–396, ISSN: 0028-0836, (2023; https://ui.adsabs.harvard.edu/abs/1992Natur.359..393D) (1st Oct. 1992).

16. A. R. Liddle, D. H. Lyth, *Physics Reports* **231**, ADS Bibcode: 1993PhR...231....1L, 1–105, ISSN: 0370-1573, (2023; https://ui.adsabs.harvard.edu/abs/1993PhR...231....1L) (1st Aug. 1993).

17. A. Klypin, J. Holtzman, J. Primack, E. Regos, *The Astrophysical Journal* **416**, ADS Bibcode: 1993ApJ...416....1K, 1, ISSN: 0004-637X, (2023; https://ui.adsabs.harvard.edu/abs/1993ApJ...416....1K) (1st Oct. 1993).

18. M. Milgrom, *The Astrophysical Journal* **270**, ADS Bibcode: 1983ApJ...270..365M, 365–370, ISSN: 0004-637X, (2023; https://ui.adsabs.harvard.edu/abs/1983ApJ...270..365M) (1st July 1983).

19. M. Milgrom, *New Astronomy Reviews* **46**, 741–753, ISSN: 13876473, arXiv: astro-ph/0207231, (2023; http://arxiv.org/abs/astro-ph/0207231) (Nov. 2002).

20. S. Dodelson, *International Journal of Modern Physics D* **20**, 2749–2753, ISSN: 0218-2718, 1793-6594, arXiv: 1112.1320[astro-ph,physics:hep-ph], (2023; http://arxiv.org/abs/1112.1320) (31st Dec. 2011).

21. S. Perlmutter *et al.*, *The Astrophysical Journal* **517**, ADS Bibcode: 1999ApJ...517..565P, 565–586, ISSN: 0004-637X, (2023; https://ui.adsabs.harvard.edu/abs/1999ApJ...517..565P) (1st June 1999).

22. B. P. Schmidt *et al.*, *The Astrophysical Journal* **507**, 46–63, ISSN: 0004-637X, 1538-4357, arXiv: astro-ph/9805200, (2023; http://arxiv.org/abs/astro-ph/9805200) (Nov. 1998).

23. A. Einstein, *Cosmological Considerations on the General Theory of Relativity*, Conference Name: Cosmological Constants Pages: 16 ADS Bibcode: 1986coco.conf...16E, (2023; https://ui.adsabs.harvard.edu/abs/1986coco.conf...16E).

24. A. Y. Kamenshchik, U. Moschella, V. Pasquier, *Physics Letters B* **511**, 265–268, ISSN: 03702693, arXiv: gr-qc/0103004, (2023; http://arxiv.org/abs/gr-qc/0103004) (July 2001).

25. V. Gorini, A. Kamenshchik, U. Moschella, *Physical Review D* **67**, 063509, ISSN: 0556-2821, 1089-4918, arXiv: astro-ph/0209395, (2023; http://arxiv.org/abs/astro-ph/0209395) (26th Mar. 2003).

26. H. Anton, P. C. Schmidt, *Intermetallics* **5**, 449–465, ISSN: 0966-9795, (2023; https://www.sciencedirect.com/science/article/pii/S0966979597000174) (1st Jan. 1997).

27. L. Amendola, S. Tsujikawa, *Dark Energy: Theory and Observations*, Google-Books-ID: qKoP-BgAAQBAJ (Cambridge University Press, 10th June 2010), 507 pp., ISBN: 978-0-521-51600-6.

28. P. J. E. Peebles, B. Ratra, *Reviews of Modern Physics* **75**, 559–606, ISSN: 0034-6861, 1539-0756, arXiv: astro-ph/0207347, (2023; http://arxiv.org/abs/astro-ph/0207347) (22nd Apr. 2003).

29. P. Peter, J.-P. Uzan, *Primordial Cosmology*, Google-Books-ID: lI8SDAAAQBAJ (Oxford University Press, 30th July 2009), 857 pp., ISBN: 978-0-19-920991-0.

30. S. Weinberg, *Cosmology*, Google-Books-ID: 2wlREAAAQBAJ (OUP Oxford, 21st Feb. 2008), 612 pp., ISBN: 978-0-19-152360-1.

31. H. C. Rosu, K. V. Khmelnytskaya, *Symmetry, Integrability and Geometry: Methods and Applications*, ISSN: 18150659, arXiv: 1012.1920[gr-qc,physics:math-ph], (2023; http://arxiv.org/abs/1012.1920) (2nd Feb. 2011).

32. F. Beutler *et al.*, *Monthly Notices of the Royal Astronomical Society* **416**, 3017–3032, ISSN: 0035-8711, (2023; https://doi.org/10.1111/j.1365-2966.2011.19250.x) (1st Oct. 2011).

33. A. J. Ross *et al.*, *Monthly Notices of the Royal Astronomical Society* **449**, 835–847, ISSN: 0035-8711, (2023; https://doi.org/10.1093/mnras/stv154) (1st May 2015).

34. S. Alam *et al.*, *Monthly Notices of the Royal Astronomical Society* **470**, 2617–2652, ISSN: 0035-8711, (2023; https://doi.org/10.1093/mnras/stx721) (21st Sept. 2017).

35. I. Debono, G. F. Smoot, *Universe* **2**, 23, ISSN: 2218-1997, arXiv: 1609.09781[astro-ph,physics:gr-qc], (2023; http://arxiv.org/abs/1609.09781) (28th Sept. 2016).

36. N. MacCrann, J. Zuntz, S. Bridle, B. Jain, M. R. Becker, *Cosmic Discordance: Are Planck CMB and CFHTLenS weak lensing measurements out of tune?*, 29th June 2015, arXiv: 1408.4742[astro-ph], (2024; http://arxiv.org/abs/1408.4742).

37. B. Jain, U. Seljak, *The Astrophysical Journal* **484**, 560, ISSN: 0004-637X, (2024; https://dx.doi.org/10.1086/304372) (Aug. 1997).

38. S. Joudaki *et al.*, *Monthly Notices of the Royal Astronomical Society* **471**, 1259–1279, ISSN: 0035-8711, 1365-2966, arXiv: 1610.04606[astro-ph], (2024; http://arxiv.org/abs/1610.04606) (Oct. 2017).

39. A. G. Riess *et al.*, *The Astrophysical Journal Letters* **934**, L7, ISSN: 2041-8205, 2041-8213, arXiv: 2112.04510[astro-ph], (2024; http://arxiv.org/abs/2112.04510) (1st July 2022).

40. E. D. Valentino *et al.*, *Classical and Quantum Gravity* **38**, Publisher: IOP Publishing, 153001, ISSN: 0264-9381, (2024; https://dx.doi.org/10.1088/1361-6382/ac086d) (July 2021).

41. P. Shah, P. Lemos, O. Lahav, *The Astronomy and Astrophysics Review* **29**, 9, ISSN: 1432-0754, (2024; https://doi.org/10.1007/s00159-021-00137-4) (1st Dec. 2021).

42. A. H. Guth, *Physical Review D* **23**, ADS Bibcode: 1981PhRvD..23..347G, 347–356, ISSN: 1550-79980556-2821, (2023; https://ui.adsabs.harvard.edu/abs/1981PhRvD..23..347G) (1st Jan. 1981).

43. M. Hasegawa, *Journal of High Energy Physics* **2020**, 113, ISSN: 1029-8479, arXiv: 1807.04808[hep-ex,physics:hep-lat,physics:hep-ph], (2023; http://arxiv.org/abs/1807.04808) (Sept. 2020).

44. B. Wang, Y. Gong, E. Abdalla, *Physical Review D* **74**, 083520, ISSN: 1550-7998, 1550-2368, arXiv: gr-qc/0511051, (2023; http://arxiv.org/abs/gr-qc/0511051) (27th Oct. 2006).

45. P. Bull *et al.*, *Physics of the Dark Universe* **12**, 56–99, ISSN: 22126864, arXiv: 1512.05356[astro-ph,physics:gr-qc,physics:hep-ph,physics:hep-th], (2023; http://arxiv.org/abs/1512.05356) (June 2016).

46. J. C. Fabris, S. V. B. Goncalves, P. E. de Souza, *General Relativity and Gravitation* **34**, 53–63, ISSN: 0001-7701, 1572-9532, arXiv: gr-qc/0103083, (2023; http://arxiv.org/abs/gr-qc/0103083) (Jan. 2002).

47. R. R. Caldwell, R. Dave, P. J. Steinhardt, *Physical Review Letters* **80**, 1582–1585, ISSN: 0031-9007, 1079-7114, arXiv: astro-ph/9708069, (2023; http://arxiv.org/abs/astro-ph/9708069) (23rd Feb. 1998).

48. L. R. Abramo, R. C. Batista, L. Liberato, R. Rosenfeld, *Journal of Cosmology and Astroparticle Physics* **2007**, 012–012, ISSN: 1475-7516, arXiv: 0707.2882[astro-ph,physics:hep-ph], (2023; http://arxiv.org/abs/0707.2882) (13th Nov. 2007).

49. M. Makler, S. Q. de Oliveira, I. Waga, *Physics Letters B* **555**, 1–6, ISSN: 03702693, arXiv: astro-ph/0209486, (2023; http://arxiv.org/abs/astro-ph/0209486) (Feb. 2003).

50. D. Clowe *et al.*, *The Astrophysical Journal* **648**, L109–L113, ISSN: 0004-637X, 1538-4357, arXiv: astro-ph/0608407, (2023; http://arxiv.org/abs/astro-ph/0608407) (10th Sept. 2006).

51. M. Bradac *et al.*, *The Astrophysical Journal* **652**, 937–947, ISSN: 0004-637X, 1538-4357, arXiv: astro-ph/0608408, (2023; http://arxiv.org/abs/astro-ph/0608408) (Dec. 2006).

52. R. Brandenberger, R. R. Cuzinatto, J. Fröhlich, R. Namba, *Journal of Cosmology and Astroparticle Physics* **2019**, 043–043, ISSN: 1475-7516, arXiv: 1809.07409[astro-ph, physics:gr-qc, physics:hep-ph, physics:hep-th], (2023; http://arxiv.org/abs/1809.07409) (20th Feb. 2019).

53. H. W. Babcock, *Lick Observatory Bulletin* **498**, ADS Bibcode: 1939LicOB..19...41B, 41–51, ISSN: 0075-9317, (2023; https://ui.adsabs.harvard.edu/abs/1939LicOB..19...41B) (1st Jan. 1939).

54. R. von Marttens, D. Barbosa, J. Alcaniz, *Journal of Cosmology and Astroparticle Physics* **2023**, 052, ISSN: 1475-7516, arXiv: 2208.06302[astro-ph, physics:gr-qc], (2023; http://arxiv.org/abs/2208.06302) (1st Apr. 2023).

55. V. Gorini, A. Kamenshchik, U. Moschella, V. Pasquier, presented at the The Tenth Marcel Grossmann Meeting, pp. 840–859, arXiv: gr-qc/0403062, (2023; http://arxiv.org/abs/gr-qc/0403062).

56. R. K. Sachs, A. M. Wolfe, *The Astrophysical Journal* **147**, ADS Bibcode: 1967ApJ...147...73S, 73, ISSN: 0004-637X, (2023; https://ui.adsabs.harvard.edu/abs/1967ApJ...147...73S) (1st Jan. 1967).

57. D. Bertacca, M. Bruni, O. F. Piattella, D. Pietrobon, *Journal of Cosmology and Astroparticle Physics* **2011**, 018–018, ISSN: 1475-7516, arXiv: 1011.6669[astro-ph, physics:gr-qc, physics:hep-ph], (2023; http://arxiv.org/abs/1011.6669) (14th Feb. 2011).

58. P.-H. Chavanis, *Is the Universe logotropic?*, 29th Apr. 2015, arXiv: 1504.08355[astro-ph, physics:gr-qc], (2023; http://arxiv.org/abs/1504.08355).

59. S. A. Chaplygin, *Gas Jets*, Google-Books-ID: 6WYSAAAAIAAJ (National Advisory Committee for Aeronautics, 1944), 236 pp.

60. M. Elmardi, A. Abebe, A. Tekola, *International Journal of Geometric Methods in Modern Physics* **13**, 1650120, ISSN: 0219-8878, 1793-6977, arXiv: 1603.05535[astro-ph, physics:gr-qc], (2024; http://arxiv.org/abs/1603.05535) (Nov. 2016).

61. S. Sahlu, J. Ntahompagaze, M. Elmardi, A. Abebe, *The European Physical Journal C* **79**, 749, ISSN: 1434-6044, 1434-6052, arXiv: 1904.09897[gr-qc], (2024; http://arxiv.org/abs/1904.09897) (Sept. 2019).

62. N. Bilić, G. B. Tupper, R. D. Viollier, *Physics Letters B* **535**, 17–21, ISSN: 0370-2693, (2023; https://www.sciencedirect.com/science/article/pii/S0370269302017161) (23rd May 2002).

63. M. C. Bento, O. Bertolami, A. A. Sen, *Physical Review D* **66**, 043507, ISSN: 0556-2821, 1089-4918, arXiv: gr-qc/0202064, (2023; http://arxiv.org/abs/gr-qc/0202064) (14th Aug. 2002).

64. H. Sandvik, M. Tegmark, M. Zaldarriaga, I. Waga, *Physical Review D* **69**, 123524, ISSN: 1550-7998, 1550-2368, arXiv: astro-ph/0212114, (2023; http://arxiv.org/abs/astro-ph/0212114) (30th June 2004).

65. A. A. Sen, R. J. Scherrer, *Physical Review D* **72**, 063511, ISSN: 1550-7998, 1550-2368, arXiv: astro-ph/0507717, (2023; http://arxiv.org/abs/astro-ph/0507717) (28th Sept. 2005).

66. P. Wu, H. Yu, *Physics Letters B* **644**, 16–19, ISSN: 03702693, arXiv: gr-qc/0612055, (2023; http://arxiv.org/abs/gr-qc/0612055) (Jan. 2007).

67. L. M. G. Beca, P. P. Avelino, *Monthly Notices of the Royal Astronomical Society* **376**, 1169–1172, ISSN: 0035-8711, 1365-2966, arXiv: astro-ph/0507075, (2023; http://arxiv.org/abs/astro-ph/0507075) (11th Apr. 2007).

68. P.-H. Chavanis, *Physics Letters B* **758**, 59–66, ISSN: 03702693, arXiv: 1505.00034[astro-ph,physics:gr-qc], (2023; http://arxiv.org/abs/1505.00034) (July 2016).

69. P.-H. Chavanis, S. Kumar, *Journal of Cosmology and Astroparticle Physics* **2017**, 018–018, ISSN: 1475-7516, arXiv: 1612.01081[astro-ph,physics:gr-qc], (2023; http://arxiv.org/abs/1612.01081) (8th May 2017).

70. S. Chandrasekhar, *An Introduction to the Study of Stellar Structure*, Google-Books-ID: VwPLAgAAQBAJ (Courier Corporation, 1st Jan. 1957), 516 pp., ISBN: 978-0-486-60413-8.

71. D. E. McLaughlin, R. E. Pudritz, *The Astrophysical Journal* **469**, ADS Bibcode: 1996ApJ...469..194M, 194, ISSN: 0004-637X, (2023; https://ui.adsabs.harvard.edu/abs/1996ApJ...469..194M) (1st Sept. 1996).

72. S. Capozziello, R. D'Agostino, O. Luongo, *Cosmic acceleration from a single fluid description*, 12th Dec. 2017, arXiv: 1712.04317[astro-ph,physics:gr-qc,physics:hep-th], (2023; http://arxiv.org/abs/1712.04317).

73. K. Boshkayev, T. Konysbayev, O. Luongo, M. Muccino, F. Pace, *Physical Review D* **104**, 023520, ISSN: 2470-0010, 2470-0029, arXiv: 2103.07252[astro-ph], (2023; http://arxiv.org/abs/2103.07252) (16th July 2021).

74. K. Boshkayev, R. D'Agostino, O. Luongo, *The European Physical Journal C* **79**, 332, ISSN: 1434-6044, 1434-6052, arXiv: 1901.01031[astro-ph,physics:gr-qc], (2023; http://arxiv.org/abs/1901.01031) (Apr. 2019).

75. H. B. Benaoum, P.-H. Chavanis, H. Quevedo, *Generalized Logotropic Models and their Cosmological Constraints*, 16th Feb. 2022, arXiv: 2112.13318[astro-ph,physics:gr-qc,physics:hep-ph], (2023; http://arxiv.org/abs/2112.13318).

76. J. E. Gunn, J. R. Gott III, *The Astrophysical Journal* **176**, ADS Bibcode: 1972ApJ...176....1G, 1, ISSN: 0004-637X, (2023; https://ui.adsabs.harvard.edu/abs/1972ApJ...176....1G) (1st Aug. 1972).

77. L. R. Abramo, R. C. Batista, L. Liberato, R. Rosenfeld, *Physical Review D* **79**, 023516, ISSN: 1550-7998, 1550-2368, arXiv: 0806.3461[astro-ph,physics:gr-qc,physics:hep-ph], (2023; http://arxiv.org/abs/0806.3461) (22nd Jan. 2009).

78. J. Hwang, H. Noh, *Relativistic cosmological hydrodynamics*, 29th Nov. 1997, arXiv: gr-qc/9711085, (2023; http://arxiv.org/abs/gr-qc/9711085).

79. J. A. S. Lima, V. Zanchin, R. Brandenberger, *Monthly Notices of the Royal Astronomical Society* **291**, ADS Bibcode: 1997MNRAS.291L...1L, L1–L4, ISSN: 0035-8711, (2023; https://ui.adsabs.harvard.edu/abs/1997MNRAS.291L...1L) (1st Oct. 1997).

80. R. A. A. Fernandes, J. P. M. de Carvalho, A. Y. Kamenshchik, U. Moschella, A. da Silva, *Physical Review D* **85**, 083501, ISSN: 1550-7998, 1550-2368, arXiv: 1110.6205[astro-ph], (2023; http://arxiv.org/abs/1110.6205) (2nd Apr. 2012).

81. L. R. Abramo, R. C. Batista, L. Liberato, R. Rosenfeld, *Physical Review D* **77**, 067301, ISSN: 1550-7998, 1550-2368, arXiv: 0710.2368[astro-ph,physics:hep-ph], (2023; http://arxiv.org/abs/0710.2368) (6th Mar. 2008).

82. L. Wang, P. J. Steinhardt, *The Astrophysical Journal* **508**, 483–490, ISSN: 0004-637X, 1538-4357, arXiv: astro-ph/9804015, (2023; http://arxiv.org/abs/astro-ph/9804015) (Dec. 1998).

83. E. V. Linder, *Physical Review D* **72**, 043529, ISSN: 1550-7998, 1550-2368, arXiv: astro-ph/0507263, (2023; http://arxiv.org/abs/astro-ph/0507263) (26th Aug. 2005).

84. S. Nesseris, L. Perivolaropoulos, *Physical Review D* **77**, Publisher: American Physical Society, 023504, (2023; https://link.aps.org/doi/10.1103/PhysRevD.77.023504) (7th Jan. 2008).

85. N. Liang, L. Xu, Z.-H. Zhu, *Astronomy & Astrophysics* **527**, A11, ISSN: 0004-6361, 1432-0746, arXiv: 1009.6059[astro-ph], (2023; http://arxiv.org/abs/1009.6059) (Mar. 2011).

86. J. Zheng *et al.*, *The European Physical Journal C* **82**, 582, ISSN: 1434-6052, arXiv: 2208.06167[astro-ph], (2023; http://arxiv.org/abs/2208.06167) (4th July 2022).

87. V. M. Cerdeira Ferreira, Publication Title: Ph.D. Thesis ADS Bibcode: 2021PhDT.....22C, PhD thesis, 1st Dec. 2021, (2023; https://ui.adsabs.harvard.edu/abs/2021PhDT.....22C).

88. T. R. P. Caramês, J. C. Fabris, H. E. S. Velten, *Physical Review D* **89**, 083533, ISSN: 1550-7998, 1550-2368, arXiv: 1401.5608[astro-ph,physics:gr-qc], (2023; http://arxiv.org/abs/1401.5608) (24th Apr. 2014).

89. H. Li, W. Yang, L. Gai, *Astronomy & Astrophysics* **623**, Publisher: EDP Sciences, A28, ISSN: 0004-6361, 1432-0746, (2023; https://www.aanda.org/articles/aa/abs/2019/03/aa33836-18/aa33836-18.html) (1st Mar. 2019).

90. M. Malekjani, A. Khodam-Mohammadi, N. Nazari-Pooya, *Astrophysics and Space Science* **334**, 193–201, ISSN: 0004-640X, 1572-946X, arXiv: 1103.1743[gr-qc], (2023; http://arxiv.org/abs/1103.1743) (July 2011).

91. S. F. Salahedin, M. Malekjani, K. Y. Roobiat, R. Pazhouhesh, *Journal of Astrophysics and Astronomy* **43**, 14, ISSN: 0250-6335, 0973-7758, arXiv: 2111.13845[astro-ph,physics:gr-qc], (2023; http://arxiv.org/abs/2111.13845) (June 2022).

92. P. P. Avelino, L. M. G. Beca, J. P. M. de Carvalho, C. J. A. P. Martins, P. Pinto, *Physical Review D* **67**, 023511, ISSN: 0556-2821, 1089-4918, arXiv: astro-ph/0208528, (2023; http://arxiv.org/abs/astro-ph/0208528) (24th Jan. 2003).

93. L. Verde, in vol. 800, pp. 147–177, arXiv: 0911.3105[astro-ph], (2023; http://arxiv.org/abs/0911.3105).

94. F. Pace, J.-C. Waizmann, M. Bartelmann, *Monthly Notices of the Royal Astronomical Society*, no–no, ISSN: 00358711, 13652966, arXiv: 1005.0233[astro-ph], (2023; http://arxiv.org/abs/1005.0233) (2nd July 2010).

95. F. Pace, S. Meyer, M. Bartelmann, *Journal of Cosmology and Astroparticle Physics* **2017**, 040–040, ISSN: 1475-7516, arXiv: 1708.02477[astro-ph], (2023; http://arxiv.org/abs/1708.02477) (25th Oct. 2017).

96. V. F. Mukhanov, H. A. Feldman, R. H. Brandenberger, *Physics Reports* **215**, 203–333, ISSN: 0370-1573, (2023; https://www.sciencedirect.com/science/article/pii/037015739290044Z) (1st June 1992).

97. H. B. Benaoum, P.-H. Chavanis, O. Luongo, M. Muccino, H. Quevedo, *Astroparticle Physics* **151**, 102852, ISSN: 0927-6505, (2023; https://www.sciencedirect.com/science/article/pii/S0927650523000385) (1st Sept. 2023).

98. V. M. C. Ferreira, P. P. Avelino, *Physics Letters B* **770**, 213–216, ISSN: 0370-2693, (2023; https://www.sciencedirect.com/science/article/pii/S0370269317302770) (10th July 2017).

99. P.-H. Chavanis, *Physical Review D* **106**, 063525, ISSN: 2470-0010, 2470-0029, arXiv: 2201.05908[gr-qc], (2023; http://arxiv.org/abs/2201.05908) (22nd Sept. 2022).

100. L. Amendola, F. Finelli, C. Burigana, D. Carturan, *Journal of Cosmology and Astroparticle Physics* **2003**, 005–005, ISSN: 1475-7516, arXiv: astro-ph/0304325, (2023; http://arxiv.org/abs/astro-ph/0304325) (8th July 2003).

101. F. D. Murnaghan, *Proceedings of the National Academy of Science* **30**, ADS Bibcode: 1944PNAS...30..244M, 244–247, ISSN: 0027-8424, (2023; https://ui.adsabs.harvard.edu/abs/1944PNAS...30..244M) (1st Sept. 1944).

102. P. T. Wedepohl, *Solid State Communications* **10**, ADS Bibcode: 1972SSCom..10..947W, 947–951, ISSN: 0038-1098, (2023; https://ui.adsabs.harvard.edu/abs/1972SSCom..10..947W) (1st May 1972).

103. E. V. Linder, R. J. Scherrer, *Physical Review D* **80**, 023008, ISSN: 1550-7998, 1550-2368, arXiv: 0811.2797[astro-ph,physics:gr-qc,physics:hep-ph], (2023; http://arxiv.org/abs/0811.2797) (22nd July 2009).

104. P. K. S. Dunsby, O. Luongo, M. Muccino, *Unifying the dark sector through a single matter fluid with non-zero pressure*, 30th Aug. 2023, arXiv: 2308.15776[astro-ph,physics:gr-qc], (2023; http://arxiv.org/abs/2308.15776).

105. B. C. Paul, P. Thakur, *Journal of Cosmology and Astroparticle Physics* **2013**, 052–052, ISSN: 1475-7516, arXiv: 1306.4808[astro-ph,physics:gr-qc], (2023; http://arxiv.org/abs/1306.4808) (22nd Nov. 2013).

106. W. H. Press, *Numerical Recipes 3rd Edition: The Art of Scientific Computing*, Google-Books-ID: 1aAOdzK3FegC (Cambridge University Press, 6th Sept. 2007), 1195 pp., ISBN: 978-0-521-88068-8.

107. H. Akaike, *IEEE Transactions on Automatic Control* **19**, Conference Name: IEEE Transactions on Automatic Control, 716–723, ISSN: 1558-2523, (2023; https://ieeexplore.ieee.org/document/1100705) (Dec. 1974).

108. G. Schwarz, *The Annals of Statistics* **6**, Publisher: Institute of Mathematical Statistics, 461–464, ISSN: 0090-5364, (2023; https://www.jstor.org/stable/2958889) (1978).

109. M. Kunz, R. Trotta, D. Parkinson, *Physical Review D* **74**, 023503, ISSN: 1550-7998, 1550-2368, arXiv: astro-ph/0602378, (2023; http://arxiv.org/abs/astro-ph/0602378) (7th July 2006).

110. A. R. Liddle, *Monthly Notices of the Royal Astronomical Society: Letters* **377**, L74–L78, ISSN: 1745-3925, 1745-3933, arXiv: astro-ph/0701113, (2023; http://arxiv.org/abs/astro-ph/0701113) (1st May 2007).

111. M. Goliath, R. Amanullah, P. Astier, A. Goobar, R. Pain, *Astronomy & Astrophysics* **380**, 6–18, ISSN: 0004-6361, 1432-0746, arXiv: astro-ph/0104009, (2023; http://arxiv.org/abs/astro-ph/0104009) (Dec. 2001).

112. D. M. Scolnic *et al.*, *The Astrophysical Journal* **859**, 101, ISSN: 1538-4357, arXiv: 1710.00845[astro-ph], (2023; http://arxiv.org/abs/1710.00845) (29th May 2018).

113. N. Suzuki *et al.*, *The Astrophysical Journal* **746**, ADS Bibcode: 2012ApJ...746...85S, 85, ISSN: 0004-637X, (2023; https://ui.adsabs.harvard.edu/abs/2012ApJ...746...85S) (1st Feb. 2012).

114. A. Conley *et al.*, *The Astrophysical Journal Supplement Series* **192**, 1, ISSN: 0067-0049, 1538-4365, arXiv: 1104.1443[astro-ph], (2023; http://arxiv.org/abs/1104.1443) (1st Jan. 2011).

115. R. Jimenez, A. Loeb, *The Astrophysical Journal* **573**, 37–42, ISSN: 0004-637X, 1538-4357, arXiv: astro-ph/0106145, (2023; http://arxiv.org/abs/astro-ph/0106145) (July 2002).

116. F. Melia, T. M. McClintock, *The Astronomical Journal* **150**, 119, ISSN: 1538-3881, arXiv: 1507.08279[astro-ph,physics:hep-ph], (2023; http://arxiv.org/abs/1507.08279) (22nd Sept. 2015).

117. M. Moresco *et al.*, *Living Reviews in Relativity* **25**, 6, ISSN: 2367-3613, 1433-8351, arXiv: 2201.07241[astro-ph], (2023; http://arxiv.org/abs/2201.07241) (Dec. 2022).

118. J. Lesgourgues, *The Cosmic Linear Anisotropy Solving System (CLASS) III: Comparision with CAMB for LambdaCDM*, version: 2, 16th May 2011, arXiv: 1104.2934[astro-ph], (2024; http://arxiv.org/abs/1104.2934).

119. W. J. Percival *et al.*, *Monthly Notices of the Royal Astronomical Society* **381**, 1053–1066, ISSN: 00358711, 13652966, arXiv: 0705.3323[astro-ph], (2024; http://arxiv.org/abs/0705.3323) (28th Sept. 2007).

120. R. Lazkoz, S. Nesseris, L. Perivolaropoulos, *Journal of Cosmology and Astroparticle Physics* **2008**, 012, ISSN: 1475-7516, (2023; https://dx.doi.org/10.1088/1475-7516/2008/07/012) (July 2008).

121. D. J. Eisenstein *et al.*, *The Astrophysical Journal* **633**, 560–574, ISSN: 0004-637X, 1538-4357, arXiv: astro-ph/0501171, (2024; http://arxiv.org/abs/astro-ph/0501171) (10th Nov. 2005).

122. A. Lewis, S. Bridle, *Physical Review D* **66**, 103511, ISSN: 0556-2821, 1089-4918, arXiv: astro-ph/0205436, (2024; http://arxiv.org/abs/astro-ph/0205436) (25th Nov. 2002).

123. D. Foreman-Mackey, D. W. Hogg, D. Lang, J. Goodman, *Publications of the Astronomical Society of the Pacific* **125**, 306–312, ISSN: 00046280, 15383873, arXiv: 1202.3665[astro-ph,physics:physics,stat], (2024; http://arxiv.org/abs/1202.3665) (Mar. 2013).

124. B. Audren, J. Lesgourgues, K. Benabed, S. Prunet, *Journal of Cosmology and Astroparticle Physics* **2013**, 001–001, ISSN: 1475-7516, arXiv: 1210.7183[astro-ph], (2024; http://arxiv.org/abs/1210.7183) (1st Feb. 2013).

125. J. Lesgourgues, *The Cosmic Linear Anisotropy Solving System (CLASS) I: Overview*, 14th May 2011, arXiv: 1104.2932[astro-ph], (2024; http://arxiv.org/abs/1104.2932).

126. A. Lewis, A. Challinor, A. Lasenby, *The Astrophysical Journal* **538**, 473–476, ISSN: 0004-637X, 1538-4357, arXiv: astro-ph/9911177, (2024; http://arxiv.org/abs/astro-ph/9911177) (Aug. 2000).

127. T. Buchert, *General Relativity and Gravitation* **32**, 105–125, ISSN: 0001-7701, 1572-9532, arXiv: gr-qc/9906015, (2024; http://arxiv.org/abs/gr-qc/9906015) (Jan. 2000).

128. A. Diez-Tejedor, *Physics Letters B* **727**, 27–30, ISSN: 03702693, arXiv: 1309.4756[gr-qc], (2024; http://arxiv.org/abs/1309.4756) (Nov. 2013).

129. S. Capozziello, R. D'Agostino, R. Giambò, O. Luongo, *Physical Review D* **99**, 023532, ISSN: 2470-0010, 2470-0029, arXiv: 1810.05844[astro-ph,physics:gr-qc,physics:hep-th], (2023; http://arxiv.org/abs/1810.05844) (29th Jan. 2019).